

Spring 3-22-2019

Developing a simulation tool for evaluating in-motion detector systems (LA-UR-18-29139)

Brian Jennings

Follow this and additional works at: https://digitalrepository.unm.edu/ne_etds



Part of the [Nuclear Engineering Commons](#)

Recommended Citation

Jennings, Brian. "Developing a simulation tool for evaluating in-motion detector systems (LA-UR-18-29139)." (2019).
https://digitalrepository.unm.edu/ne_etds/84

This Thesis is brought to you for free and open access by the Engineering ETDs at UNM Digital Repository. It has been accepted for inclusion in Nuclear Engineering ETDs by an authorized administrator of UNM Digital Repository. For more information, please contact amywinter@unm.edu.

Brian Adam Matthew Jennings

Candidate

Nuclear Engineering

Department

This dissertation is approved, and it is acceptable in quality and form for publication: *Approved*

by the Dissertation Committee:

Dr. Adam Hecht, Chair

Dr. Cassiano de Oliveira , Member

Dr. James Toevs, Member

**Developing a simulation tool for
evaluating in-motion detector systems
LA-UR-18-29139**

by

Brian A. M. Jennings

B.S., Nuclear Engineering and Mechanical Engineering, Rensselaer
Polytechnic Institute, 2011

THESIS

Submitted in Partial Fulfillment of the
Requirements for the Degree of

Master of Science
Nuclear Engineering

The University of New Mexico

Albuquerque, New Mexico

May, 2019

Acknowledgments

I would like to thank my advisor, Dr. Adam Hecht for his support and guidance throughout this thesis. I would also like to thank Dr. John Rennie at Los Alamos National Laboratory for his expertise and knowledge that he provided to aid in the development of my simulation tool. To my other colleagues at Los Alamos National Laboratory, thank you for your support in acquiring equipment, collecting data, and providing guidance when needed. I would also like to thank my committee members Dr. Jim Toevs and Dr. Cassiano de Oliveira for providing feedback and input on my thesis.

This work was funded and supported by the Office of Nuclear Smuggling Detection and Deterrence (NA-213), and I would like to thank the Science and Engineering Team's Chief Scientist Dr. Luc Murphy for his support in this project.

Lastly I would like to thank my wife Audrey and the rest of my family for their support throughout my pursuit of a M.S. at UNM.

Developing a simulation tool for evaluating in-motion detector systems LA-UR-18-29139

by

Brian A. M. Jennings

B.S., Nuclear Engineering and Mechanical Engineering, Rensselaer
Polytechnic Institute, 2011

M.S., Nuclear Engineering, University of New Mexico, 2019

Abstract

Available simulation software lacks the ability to produce in-motion detector responses for detector systems that may be used to detect the illicit trafficking of nuclear materials. In this thesis, a simulation tool is developed that uses static measured data as a basis set for producing in-motion detector responses with the ability to vary many parameters in each simulated trial. Once the basis set is measured and loaded into the simulation tool, the user interface allows the user to enter variations to speed, source height, source-to-detector distance, background exposure rate, which source(s) are present, their relative strength and shielding configuration, and whether the source is moved past a fixed detector, or the detector is moved past a fixed source. The simulation tool outputs data to a standard data format, as well as a specific data format for the detector system being tested so that the system's threat identification algorithm (TIA) can be evaluated for the simulated results.

The output from the simulation tool was validated against in-motion measurements by comparing the count rate profile within an energy range region of interest (ROI) specific to the isotope being measured to see how the time-series for the simulated results matched up against the measured data. To validate the simulation as interpreted by the TIA, the results of the TIA were compared to see if the algorithm performed equally when looking at simulated data vs. measured data. The validation measurements were made with bare sources, sources behind simple shields, and sources placed in various locations inside of a “standard” car. In an attempt to better control speed and source-to-detector distance, an additional set of validation measurements were made using a motor controlled gantry that operates at a fixed speed and is mounted on a track so that there is no lateral movement.

Of the 17 drive-by measurement configurations, 10 had simulated data fall within the error bars of the measured data, with 5 of the 7 cases falling outside of this being source in vehicle trials. Source in vehicle results are expected to have the most uncertainty due to the non-uniform nature of the shielding that is encountered during a drive-by trial.

For the 8 gantry validation configurations, only 1 had agreement within the error bars between the simulated and measured count rate ROI profiles, but this was due to an unexpected background suppression that was caused by the flatbed trailer that the measurements were made on. By adjusting the measured profiles to compensate for the background suppression, 6 of the 8 configurations showed agreement between the simulated and measured results. Adding background suppression as a feature to the simulation tool will be addressed in future work.

The intended purpose of this simulation tool is to inform and reduce the effort required for a testing and evaluation campaign, so a 10-20% uncertainty in the simulated results is acceptable to provide useful information about what should or shouldn't be included in a measurement campaign. The ratio of the signal-to-noise

ratio (SNR) for the simulated results was compared to the measured results and the average value was 1.07 ± 0.03 . This SNR value is an output from proprietary TIA, and not SNR in a traditional sense. This shows that on average the TIA has an easier time identifying the simulated results than the experimental, but only by 7% which is very good. The flexibility in the tool to be able to provide simulation results quickly and reliably for a large variety of configurations reduces its accuracy to some extent, but greatly increases its value to a program that is interested in evaluating how a detector system will perform in a variety of environments and configurations.

Contents

List of Figures	ix
List of Tables	xii
Acronyms	xiii
1. Introduction	1
1.1. Motivation	1
1.2. Background	2
1.3. Literature Review	7
2. Experimental Set-up	11
2.1. Equipment Used	11
2.1.1. Spectroscopic Detection System	11
2.1.2. Exposure Rate Meter	15
2.2. Sources Used	17

Contents

2.2.1. Isotopic Sources	17
2.2.2. Special Nuclear Material & Depleted Uranium Sources	17
2.2.3. NORM Sources	18
2.3. Measurements Performed	18
2.3.1. Source Measurements	18
2.3.2. Background Variation Measurements	25
2.3.3. NORM Measurements	26
2.3.4. Verification Measurements	27
3. Simulation Methodology	31
3.1. User Inputs	31
3.1.1. Basic User Inputs	32
3.1.2. Advanced User Options	35
3.2. Running the Simulations	43
3.2.1. Initializing Variables	45
3.2.2. Multi-threading individual trials	45
3.2.3. Integrating the detector response curve	46
3.2.4. Creating the Trials	50
3.2.5. Writing the Output	50
4. Results	52

Contents

4.1. Detector Response Profile	53
4.2. Background spectrum	57
4.3. Background variation and NORM gradient	58
4.4. Simulated Spectra	60
4.5. In-Motion Comparisons	61
4.5.1. Spectral ROI comparisons	61
4.5.2. TIA Comparison	92
4.6. Assumptions and Limitations	100
5. Conclusions	103
6. Future Work	106
References	108
Appendices	112
A. N42 example file	113

List of Figures

1.1.	Handheld RID	4
1.2.	Vehicle RID	4
1.3.	Radiation Portal Monitor	5
1.4.	1-second integral profile	9
2.1.	Detector Configuration	13
2.2.	Gantry Detector Configuration	15
2.3.	Exposure Meter	16
2.4.	^{137}Cs On Tripod	19
2.5.	Profile Measurement Locations	21
2.6.	Vehicle Measurement Locations	21
2.7.	NORM Measurement Locations	26
2.8.	Gantry Cart	28
3.1.	Basic User Interface	32
3.2.	Advanced User Interface	36

List of Figures

3.3.	Geometry configuration diagram	39
3.4.	SNM Source Checked on UI	41
3.5.	Detector Reference Coordinates	44
3.6.	Solid angle geometry diagram	48
4.1.	Cubic Spline Fit	54
4.2.	^{137}Cs Profile vs. Cubic Spline Fit	55
4.3.	Integrated Response vs. Static Measurements	57
4.4.	Background dwell spectrum	58
4.5.	Background Variation CDF	59
4.6.	Simulated Trial Components	61
4.7.	Bare source drive-by comparisons	65
4.8.	Shielded source drive-by comparisons	72
4.9.	Source in vehicle drive-by comparisons	80
4.10.	^{137}Cs Source Holders	81
4.11.	Gantry in-motion comparisons	90
4.12.	Simulated ^{137}Cs spectrum comparison	92
4.13.	RSI Replay SNR Values	95
4.14.	RSI Replay SNR Ratios	97
4.15.	Correct ID % vs. Alarm Threshold	98
4.16.	RSI SNR vs. Injected SNR	99

List of Figures

4.17. Streaming Path Detector Response 101

List of Tables

2.1.	Gamma-Emitting Isotopic Sources.	17
2.2.	Drive-by Verification Measurement Test Matrix.	29
2.3.	Gantry Verification Measurement Test Matrix.	30
4.1.	Isotope ROIs	53
4.2.	Drive-by Speeds	53
4.3.	Cubic spline coefficients.	56
4.4.	RSI Replay Results.	94
4.5.	Effect of primitive used.	101

Acronyms

CDF	Cumulative Distribution Function
CON-OPS	Concept of Operations
DNDO	Domestic Nuclear Detection Office
LANL	Los Alamos National Laboratory
MCA	Multi-Channel Analyzer
NaI	Sodium Iodide
NORM	Naturally Occurring Radioactive Material
NSDD	Nuclear Smuggling Detection and Deterrence
RASE	Replicative Assessment of Spectroscopic Equipment
RDD	Radiological Dispersion Device
RID	Radionuclide Identification Device
RPM	Radiation Portal Monitor
RSI	Radiation Solutions Inc.
SMDS	Spectroscopic Mobile Detection System

Acronyms

SNM	Special Nuclear Material
SNR	Signal-to-noise ratio
TA	Technical Area
TIA	Threat Identification Algorithm
WMD	Weapon of Mass Destruction

Chapter 1

Introduction

1.1 Motivation

In order to combat the illicit trafficking of nuclear materials, understanding the detection capabilities and limitations of available detection systems is critically important. Agencies interested in detection, deterrence, and interdiction of nuclear material smuggling execute time and resource intensive testing and evaluation campaigns to understand the detection systems' capabilities and determine proper Concept of Operations (CON-OPS). Due to the time and resources required to evaluate a system, modeling and simulation solutions could present a cost savings alternative, if done correctly. There are several unique problems that need to be addressed when simulating radiation detection equipment used by these agencies. These issues include simulating an "in-motion" system where the detector response is time(position)-dependent as the source and/or detector are moving past each other, simulating the correct detector response for a given source/shielding configuration, and evaluating the various Threat Identification Algorithms (TIAs) that are included with commercially available detection systems.

Chapter 1. Introduction

The focus of this thesis is to develop a simulation tool using measured data that can be used to evaluate the capabilities and limitations of a detection system, including its TIA. The simulation tool will allow a user to vary many parameters, including the number of detectors, the detector geometry, source(s) present, their relative strengths, the speed at which the source or detector system are moving, the slope and magnitude of the background variation, and the number of trials to run for a given configuration. Chapter 3, Simulation Methodology will describe all of the parameters that can be changed by the user.

In the following sections and chapters of this thesis, a more detailed background of the problem will be given, followed by a literature review of similar work that has been conducted; the thesis will then proceed to give an overview of the scope of work for the thesis before diving into the details of the experimental set-up and then the simulation methodology; finally this thesis will end with a discussion of results, conclusions that can be drawn, and future work that can be done to enhance the simulation tool.

1.2 Background

Being able to detect nuclear smuggling is a complex and constantly evolving problem that is critical to national security. Nuclear materials that are smuggled into the United States could be used to create a weapon of mass destruction (WMD), or a radiological dispersion device (RDD). 19th United States Secretary of Defense William J. Perry issued the following statement in 2016 to describe his concern over the possibility of a nuclear weapon being detonated in a US city.

“We can hardly bear to imagine the catastrophic outcome of this hypothetical scenario—and yet we must. This example is only illustrative; the same end would result if a terror group bought or stole a nuclear bomb from North Korea or Pakistan, or stole fissile material from a reactor in one of the countries

Chapter 1. Introduction

that still has highly enriched uranium or plutonium in insufficiently guarded facilities.

The danger of a nuclear bomb being detonated in one of our cities is all too real. And yet, while this catastrophe would result in hundreds of times the casualties of 9-11, it is only dimly perceived by the public and not well understood. As a result, our present actions are not commensurate with the tragic consequences that would result from even a small-scale nuclear attack.[1]

There are agencies that work both inside the US, as well as with international partners to prevent such a nuclear nightmare from happening. Two such agencies are the Domestic Nuclear Detection Office (DNDO), and the Office of Nuclear Smuggling Detection and Deterrence (NSDD). The mission statement of DNDO is to “Prevent nuclear terrorism by continuously improving capabilities to deter, detect, respond to, and attribute attacks, in coordination with domestic and international partners[2].” The Office of NSDD “Works with international partners to strengthen capabilities to deter, detect, and investigate the smuggling of nuclear and radiological materials by providing the expertise and tools needed to respond to smuggling events[3].” These agencies use a wide variety of detector systems, some of which are gross-counting systems that measure gamma radiation without determining photon energy, and some of which are spectroscopic and determine the energy of the photons being detected in order to identify specific isotopes that are present. These detector systems can be small handheld and backpack mounted systems, medium-sized vehicle mounted systems, or large fixed location systems. Figure 1.1 shows an example of a handheld Radionuclide Identification Device (RID); Figure 1.2 shows an example of a vehicle mounted Radionuclide Identification Device (RID); Figure 1.3 shows an example of fixed location Radiation Portal Monitors (RPMs).

This thesis attempts to address the needs described above by delivering a simulation tool that can be used to predict the detector response for an in motion spectroscopic detector system, focusing only on gamma radiation. In this context, spectroscopic refers to a system that employs a multi-channel analyzer (MCA) and

Chapter 1. Introduction



Figure 1.1: Handheld Radionuclide Identification Device[4].



Figure 1.2: Vehicle Mounted Radionuclide Identification Device[5].

attempts to make an isotope identification, as opposed to a gross-counting system that simply measures total gamma counts and attempts to make an alarm determination. For detector-in-motion applications, gross-counting mobile detection systems face significant limitations due to high alarm rate caused by rapidly changing background, or alternately low sensitivity when the alarm threshold is raised to reduce



Figure 1.3: Fixed Location Radiation Portal Monitors[6].

the false alarm rate. Spectroscopic systems are anticipated to perform better than gross counting systems in the naturally varying background environments expected for in-motion applications, and some previous work performed at LANL showed the potential of using a NaI spectroscopic detector system in place of a gross counting MDS[7]. As new in-motion applications are considered, the use of modeling and simulation can help evaluate the expected performance of a given detector system without first having to undergo an extensive and time consuming test campaign. A test campaign can then be developed with advance knowledge from the simulation tool to evaluate the system for use in detector in-motion applications, such as with a spectroscopic mobile detection system (SMDS), or source in-motion applications, such as with a portal monitor.

The specific challenges to in-motion simulations that need to be addressed are the variability of the system, integrating the time-series detector response, handling the large amount of statistical noise, addressing changing environmental conditions, and evaluating a proprietary algorithm. With an in-motion system, the detectors or the source could be in-motion, and any number of parameters could be expected to vary in real-world applications such as the conveyance method (vehicle, pedestrian,

Chapter 1. Introduction

cargo, etc.), the speed, the distance and material between the source and detector(s), and the environment in which the system is operating. Once this variability is addressed, the simulated detector response needs to accurately produce a time-series detector response which is constantly changing as the source and detector approach and pass one another; the sample rate is typically on the order of one-second which makes for low count-rates and therefore large statistical uncertainty that needs to be incorporated into each of the simulated spectra. Finally, to fully evaluate a detector system, there needs to be a handshake between the output of the simulated detector response and the alarm algorithm that is used by the detector system; this algorithm is typically proprietary and therefore it may be a challenge to evaluate its performance.

Threat Identification Algorithms (TIAs) are incorporated into detection systems and process data in real time in order to make decisions about the potential presence of radiological threat materials. TIAs are often proprietary information contained within commercially available detection systems and therefore it is difficult to use simulated results to fully evaluate a detection system since the source code to incorporate the TIA into the simulation is not available. Some detection systems include a data replay tool or some other means to process the data through the TIA in an offline (not real-time) capacity. Detection systems that have this capability can be evaluated using simulated data, if the simulated output is in the same format of real data measured by the system. This thesis focuses on developing a simulation tool for a detector system that has a replay capability, the RS-700 by Radiation Solutions Inc. (RSI), and the output of the simulation tool will include both an ANSI N42[8] file as well as a RSI Survey file that can be read into the replay tool as if it were real, measured data from the detector system.

1.3 Literature Review

There has been a significant effort to improve detection capabilities, as well as gain better understanding of capabilities and limitations of current detection systems. This section will focus on discussing previous work that has been conducted, focusing specifically on developing and evaluating TIAs. The review of this other work is important in showing the niche that an in-motion simulation tool for evaluating detector systems will fill.

Since radiation detection systems are limited to a handful of detector media, there has been much focus on improving the algorithms that are employed to make alarm determinations in real-time on an item of interest. While this thesis does not attempt to develop or improve upon a specific TIA, it does have a component of evaluating the performance of a TIA and therefore it is of interest to see the methods that are employed in other works to evaluate TIAs. TIAs operate using a variety of techniques, which for spectroscopic systems include extracting peak locations from noisy/low resolution spectra using wavelet transform analysis[9][10]; comparing measured data to a library of previously measured (or simulated) spectra and using methods like fuzzy logic or maximum likelihood to determine which source is present[11][12]; or some combination of multiple techniques [13]. Wavelet transform analysis is a method that attempts to find local maxima where a specific wavelet shape fits the gamma spectrum with the greatest confidence. Different algorithms attempt to vary the width and shape of the template wavelet in order to achieve the greatest confidence for a noisy or low-resolution spectrum. Fuzzy-logic algorithms essentially make a decisions based on a set of “fuzzy rules”, or situations where the answer to an “if” statement isn’t a simple yes or no, but could also be a “maybe”. After applying a whole set of these fuzzy rules to parameters of a spectrum (peak centroid, width, area, etc.), then a confidence value is provided for the isotope that the algorithm thinks is present in the spectrum. For gross counting systems, there

Chapter 1. Introduction

has been work to attempt to reduce the number of nuisance alarms by attempting to extract information about the shape of the radiation source based on the time-dependent change in count rate[14]. This matched filtering method looks at the time-dependent change in count rate and determines if the source is a point source or distributed, and characterizes source strength and location. This method assumes that distributed sources are not threat sources so they will not contribute to nuisance alarms. For all of this work that focuses on improving TIAs, there needs to be some way to test their performance in a variety of configurations. For national or global security interests, it is essential to understand how well these TIAs perform in the presence of specific threat sources, such as Special Nuclear Material (SNM). “(SNM) is defined by Title I of the Atomic Energy Act of 1954 as plutonium, uranium-233, or uranium enriched in the isotopes uranium-233 or uranium-235, but does not include source material[15].” Since special nuclear material (SNM) sources are highly regulated and may not be readily available to individuals attempting to evaluate a TIA, much of the evaluation work is performed by using simulation and modeling techniques. The availability of a simulation tool that specifically produces in-motion detector responses would be very useful for evaluating TIA performance.

There are several widely used simulation tools, such as MCNP[®] or GADRAS, as well as other recently developed codes that attempt to provide faster and more accurate detector response spectra through libraries[16] or pre-calculated detector response functions [17][18], but all of these tools share a significant shortcoming when it comes to evaluating the performance of an in-motion system. These software tools all do a reasonable job of producing accurate spectra for a given detector system, but they can only produce static spectra; they do not have any way of producing the integrated response as the detector (or source) moves from point “a” to point “b” over a given time interval. For example, if a vehicle with a threat source moves past a detector system at 8 kph, and the detector system updates at 1-second intervals then the distance covered by that integration step (from hypothetical point “a” to “b”) is

Chapter 1. Introduction

~2.2 meters. Figure 1.4 depicts the area of the detector response profile that would be covered by a 1-second integral if the detector (or source) was moving at 8 kph. If a detector response simulation produces a 1-second spectrum at a fixed location at point “a”, “b”, or someplace in between, there could be a significant difference in detector response compared to the real case where the signal from the source on the detector is continuously changing over the 2.2 meters. This thesis develops a simulation tool that accurately produces an integrated detector response, accounting for the changing signal from point “a” to “b”. This is described in greater detail in Chapter 3, Simulation Methodology. Chapter 4, Results will provide comparisons of measured spectra, simulated spectra using a fixed location, and simulated spectra using an integrated detector response, to show how much of a difference could be seen if the source signal is not properly integrated over the change in position for a 1-second time interval.

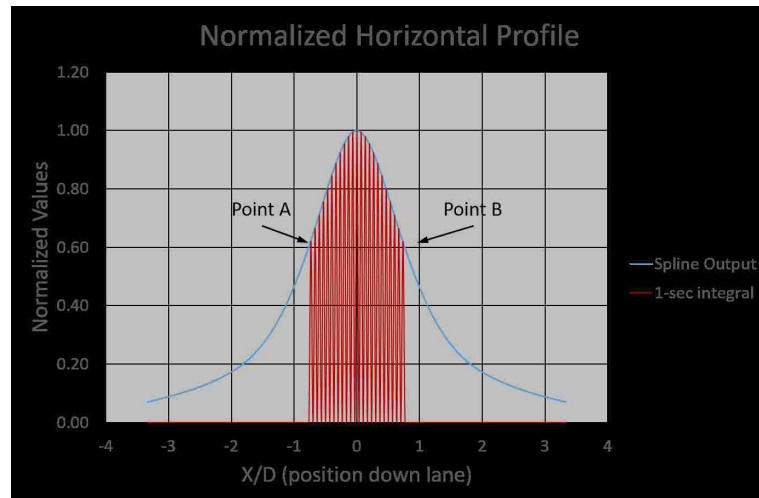


Figure 1.4: Area of detector response profile covered by 1-second when traveling at 8 kph.

One simulation tool that has been developed specifically for testing multiple TIAs, when given a “black box” replay tool is called Replicative Assessment of Spectroscopic Equipment (RASE). The RASE approach is very similar to this thesis in that it uses empirically measured source spectra, scales the signal from these spectra based

Chapter 1. Introduction

on user inputs, and then outputs the resulting detector response directly into that detector system's TIA replay "black box" [19][20]. While this tool addresses nearly all of the needs for security agencies to evaluate commercially available detector systems, it too lacks the ability to provide the time-dependent detector response for a source (or detector) in motion.

In Chapter 2, I describe the experimental setup that was used to collect the necessary data to develop the simulation tool. Chapter 3 will provide details about the simulation methodology that is used to produce an in-motion detector response. Chapter 4 presents the results, including the raw data and analysis that was done to produce the simulation tool and also comparisons between simulated results and measured results. Chapter 5 summarizes the conclusions that can be drawn from the results presented, and Chapter 6 outlines future work that should be considered.

Chapter 2

Experimental Set-up

Throughout this chapter, descriptions of measurements made with Highly Enriched Uranium (HEU), Weapons Grade Plutonium (WGPu), and Depleted Uranium (DU) are included since they were used to help develop the simulation tool, but specific results that provide any indication of the detector system's ability to detect these sources will be omitted since that information may be sensitive to programs that use the RS-700 detector system to detect the illicit trafficking of nuclear materials.

2.1 Equipment Used

2.1.1 Spectroscopic Detection System

The spectroscopic detection system that was used to collect data for this thesis was an RS-700 system which uses sodium iodide (NaI) gamma detectors. NaI detectors are inorganic crystal scintillators that are commonly used for gamma-ray spectroscopy. Scintillator detectors function by taking advantage of the prompt fluo-

Chapter 2. Experimental Set-up

rescence process in which visible light is released following the excitation of electrons caused by interaction with ionizing radiation. Scintillator media is typically encapsulated by light reflecting material on all sides except for the location where the connection to the photomultiplier tube takes place. A photomultiplier tube is a device that contains two main components, a photocathode and an electron multiplier. A photocathode converts visible light into low energy electrons, which are then multiplied in number by accelerating the electrons through a series of dynodes that each have a multiplication factor. The total number of electrons at the end of this multiplication process is proportional to the number of incident scintillation photons at the photocathode and can be collected and placed into energy bins to determine the gamma-ray energy spectrum. The light that is emitted by the scintillator is then captured and amplified by the photomultiplier tube and associated electronics are used to analyze the signal. NaI detectors have several properties that make them attractive for gamma-ray spectroscopy, including a large light output, relatively low cost, and ease of growing large crystals[21].

The RS-700 is a mobile radiation monitoring system developed by RSI that can be configured with multiple gamma and neutron detectors. For this thesis, the RS-700 system was configured with 4 NaI gamma detector modules, and since the neutron response was not in the interest of this project, no neutron detectors were included. Each gamma detector module contains one $2'' \times 4'' \times 16''$ NaI crystal attached to a photomultiplier tube and a proprietary advanced digital spectrometer module. The advanced digital spectrometer contains an analog to digital converter and stores an energy calibration curve unique to that detector which is used to linearize the outputs of individual detector modules, allowing them to be accurately summed into virtual detectors[22]. Each gamma detector outputs a 1024 channel gamma spectrum, and the controller performs automatic gain stabilization using peaks from naturally occurring isotopes so that the spectra from individual detectors can be summed together correctly. The detectors were mounted on the outside of a small

Chapter 2. Experimental Set-up

utility trailer so that there is no material shielding or obscuring the signal seen by the detectors. The arrangement of the NaI crystals, which was used for nearly all of the measurements is shown in Figure 2.1. The exception to this configuration was the cases where the reference detector module was rotated 90° to acquire the profile from a horizontal detector configuration. The lower right detector labeled “1” in the figure is the reference detector to which all of the measurements were made. The RadAssist software is a tool that comes with the RS-700 system that provides a user interface to view, collect, and record data, as well as a way to change various system settings. RadAssist was configured so that each NaI crystal was assigned to its own Virtual Detector, allowing the spectra to be captured from each crystal individually.



Figure 2.1: RS-700 NaI Mounting Configuration.

For an additional set of verification measurements, a second RS-700 system was mounted on a motor operated gantry cart that is located on a 100' track. The motor controller was programmed to maintain a constant speed of $40 \frac{cm}{sec}$ for a predetermined

Chapter 2. Experimental Set-up

distance. Using the gantry, limit switches were installed that allow automation of data collection by relaying a message to the computer which has RadAssist running and telling it when to press the “start scan” and “stop scan” buttons, ensuring that each trial covers the same distance and the source was located at the midpoint of this distance. The detector configuration is slightly different on the gantry and can be seen in Figure 2.2.

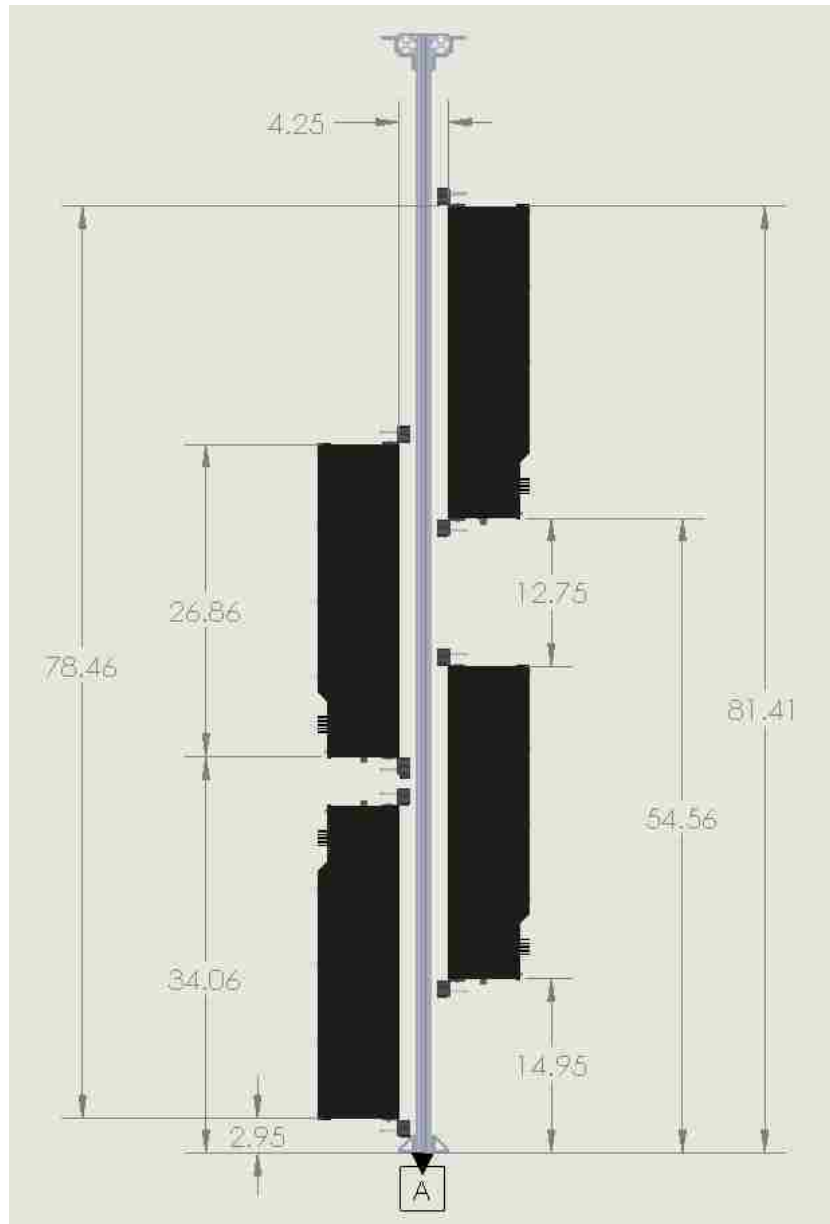


Figure 2.2: RS-700 NaI Gantry Mounting Configuration.

2.1.2 Exposure Rate Meter

To measure the exposure rate at the location where the background dwell measurements were made, a calibrated Eberline E-600 with an SHP-270 hotdog probe

Chapter 2. Experimental Set-up

was used (Figure 2.3). The E-600 with the SHP-270 probe is an energy compensated Geiger-Mueller counter that measures the exposure rate. Energy compensation is performed by using a sleeve over the probe window that flattens the energy-dependent response of the instrument to the incident radiation so that the exposure rate that is measured by the instrument is accurate for a wide range of incident photon energies. Exposure rate measurements are needed so that the user input for scaling the background level is in units of exposure rate, roentgens per hour, R/hr.



Figure 2.3: Eberline E-600 Rate meter with SHP-270 probe [23].

2.2 Sources Used

Isotopic and SNM sources that were used are listed in Table 2.1.

Table 2.1: Gamma-Emitting Isotopic Sources.

LANL Source ID	Primary Isotope	Nominal Source Strength
CS-1	^{137}Cs	250 μCi
IS200	^{137}Cs	4.137 μCi
1193-15	^{133}Ba	215 μCi
FN-591	^{133}Ba	3.035 μCi
I3-598	^{57}Co	100 μCi
1820-84-3	^{57}Co	14.22 μCi
N/A	HEU (^{235}U)	N/A
N/A	WG Pu	N/A
N/A	DU	N/A

2.2.1 Isotopic Sources

The isotopes that were chosen cover a broad range of energies and include sources that emit one or a few strongly dominant gamma rays (^{57}Co , ^{133}Ba , ^{137}Cs). The source strengths were chosen to be as large as was available for those particular isotopes so that the counting time for the cases in which the sources were farther away or behind shields would be relatively low.

2.2.2 Special Nuclear Material & Depleted Uranium Sources

While measurements with SNM and DU sources were made, and used in developing the simulation tool, the details of these sources is sensitive in nature and therefore any results that are shown from the SNM and DU sources will have some information removed in order to protect certain details. While SNM and DU sources may emit

alpha particles and neutrons, the alphas are unable to reach the active region of the detector and the neutrons are too few to impact the gamma spectra.

2.2.3 NORM Sources

Buckets containing common NORM material were used to create a gradient of increasing levels of NORM. These were necessary in order to add the ability to appropriately incorporate realistic background variation into the simulation tool for the cases in which the detectors are in motion.

2.3 Measurements Performed

All measurements, with the exception of the drive-about background variation measurements were performed at LANL Technical Area 16 (TA-16) Tumbler Road Test Bed. The measurements that were made can be broken down into several measurement types, including source measurements, background variation measurements, NORM measurements, and verification measurements. Each of these measurement types are described in greater detail in the following subsections.

2.3.1 Source Measurements

A source profile measurement is a set of static dwell measurements with low statistical uncertainty that define the shape of the detector response as the source is moved along the direction of travel. Source profile measurements were performed with a bare source placed on a tripod or placed in a source holder on a tripod as shown in Figure 2.4. With the detectors remaining stationary the source was moved to eleven positions along the direction of travel, as shown in Figure 2.5. While data

Chapter 2. Experimental Set-up

was collected with all four detectors, only the spectra from reference detector module, module 1, was analyzed for development of the simulation tool.



Figure 2.4: ^{147}Cs button source placed in foam source holder on top of tripod and aligned to reference detector module center.

Additional measurements were made with steel and high density polyethylene (HDPE) shielding, with the source positioned in the trunk, middle of vehicle, or in the footwell of a “standard” car to demonstrate the utility of the simulation tool to a specific application, and two profile measurements with different sources were made with the reference detector module rotated horizontally to give the response along the long axis of the detectors. The profile measurements with the reference detector module rotated horizontally allows flexibility of the simulation tool by providing benchmark data for the detector response when oriented this way. The steel and HDPE shielding are both cylindrical cans that fully encapsulate the source and provide shielding in all directions. The steel can is $\frac{1}{4}$ ” thick and the HDPE can is 2” thick. These materials were chosen for the shielding cases because a medium to high Z material (steel) will have predominant interaction with the gamma rays through

Chapter 2. Experimental Set-up

the photoelectric effect and for the low Z material (HDPE), the photoelectric effect will be less dominant and Compton scattering will be more important. These two interactions will change the shape of the spectrum differently and therefore will provide a better understanding of how the TIA will perform when presented with spectra that have been changed by the presence of shielding materials.

The measurements taken for the source profiles span from -5 to +5 meters along the direction of travel with measurement spacing closer together near the center of the profile to more accurately capture the region of the profile that is of greater importance. The center of the profile is of greater importance since this is the area where the signal reaching the detector from the source is greatest. For source configurations that are near the limits of detection of the system, accurately modeling the region of the profile that encompasses the point of closest approach is critical to determining whether or not the system will correctly identify the source. If the shape of this portion of the profile is not accurately captured then it will have the greatest impact on the ability of the alarm algorithm to get the correct results from the simulated trials. The measurements for sources in the “standard” vehicle and in shielded configurations were only taken at the center-line location to capture the change in the shape of the spectrum – the shape of the profile should not change. For the bare source measurements, the source on the tripod was in line with the horizontal center-line of the reference detector module, and the offset distances shown in Figure 2.5 were from the vertical center-line of the reference detector module. Figure 2.6 depicts the measurement locations for the source-in-vehicle measurements and the exact distances from the center of the reference detector module to the different sources were carefully measured and recorded. The source in vehicle measurements were performed in a 2013 Hyundai Sonata as a representative mid-sized sedan.

Chapter 2. Experimental Set-up

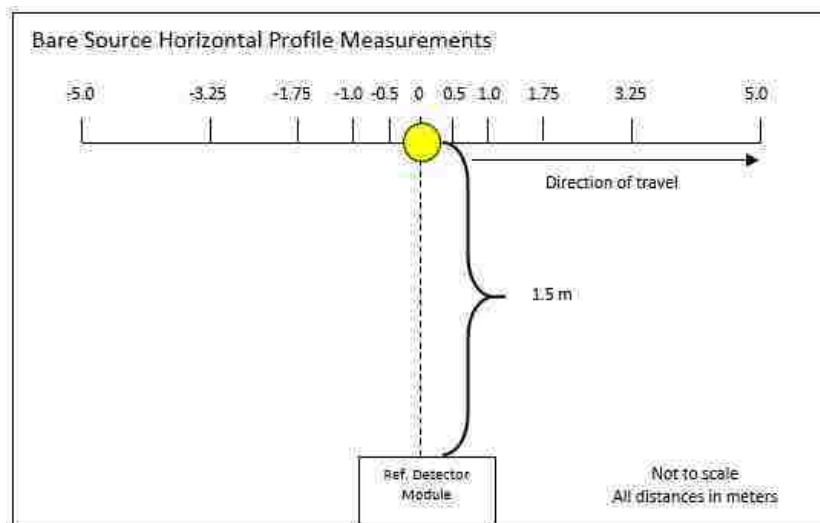


Figure 2.5: Bare Source Horizontal Profile Measurement Locations.

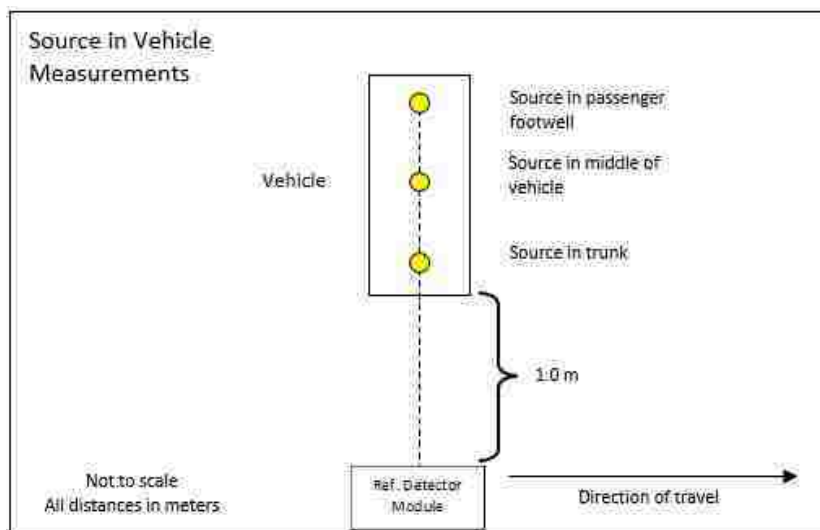


Figure 2.6: In Vehicle Source Measurement Locations.

Below are the measurement procedures that were followed to perform the source measurements.

Note: A 10 minute background measurement at the 0 m offset location was performed at the beginning and end of each day, and in between sets of measurements

Chapter 2. Experimental Set-up

to have a recent background to subtract from each profile measurement. Additionally, a long (~ 2.5 hours) background dwell measurement was captured to have a background primitive with very low statistical uncertainty.

Measurement Procedure – Bare Sources:

1. Remove all sources.
2. Record a 10 minute background spectrum with the reference detector module centered at the 0 m offset location.
3. Place the first radioactive source from Table 2.1 on the tripod at a distance of 1.5 m, with the height aligned with the vertical center of the reference detector module.
4. Record a 10 minute spectrum with the source at the 0 m offset location.
5. Calculate an estimate of counting time required to get the desired precision in Region of Interest (ROI) using the following equation:

$$t = (2B + S)/(SP)^2$$

where B is the background count rate, S is the net source count rate, and P is the desired precision ($P = (\sigma/S) \times 100\%$). Since each isotope produces photons with different energies, the ROIs are specific to each isotope in order to capture the photopeak(s) of interest.

If t is greater than 10 minutes, repeat 10 minute measurements until the sum of the measurement time is greater than or equal to t. Required precision is stricter at the locations nearest to the 0 m offset location, since these will have the greatest impact on the accuracy of the simulation. The required precisions are listed below for the different offset distances. The level of precision required at the different offset distances were chosen so that the counting times for

Chapter 2. Experimental Set-up

the cases where the source is farther away from the detector would not be substantially longer than 10 minutes with minimal sacrifice of precision.

Absolute value of offset distance (m)	Required precision (%)
0-1	1
1-2	5
>2	10

- Repeat steps 4 and 5 with the source at each measurement location displayed in Figure 2.5, aligned to the vertical center of the reference detector module.
- Repeat steps 1 & 2.
- Repeat steps 3-7 for each of the remaining sources listed in Table 2.1.
- With the ^{137}Cs source from Table 2.1, center source on the tripod to the horizontal and vertical center of a different NaI crystal, 1.5 meters away.
- Record a 10 minute spectrum.
- Repeat steps 9 and 10 for the 2 remaining NaI crystals.
- Repeats steps 9-11 with the WGPu source from Table 2.1
- Repeat steps 1 & 2.

Measurement Procedure – Shielded Sources:

- Remove all sources.
- Record a 10 minute background spectrum with the reference detector module centered at the 0 m offset location.
- Place the first radioactive source from Table 2.1 on the tripod at a distance of 1.5 m, inside the $\frac{1}{4}$ " steel can, with the height aligned with the vertical center of the reference detector module.

Chapter 2. Experimental Set-up

4. Record a 10 minute spectrum.
5. Calculate counting time required to get the desired precision in Region of Interest (ROI) using the following equation:

$$t = (2B + S)/(SP)^2$$

where B is the background count rate, S is the source only count rate, and P is the desired precision. The ROIs will be determined for each isotope to capture the peak(s) of interest.

If t is greater 10 minutes, repeat 10 minute measurements until the sum of the measurement time is greater than or equal to t. Required precision for this measurement is 1%.

6. Replace the $\frac{1}{4}$ " steel can with the 2" HDPE can.
7. Repeat steps 4 and 5.
8. Repeat steps 3-7 for each of the remaining sources listed in Table 2.1.
9. Repeat steps 1 & 2.

Measurement Procedure – Sources in Vehicle:

1. Remove all sources.
2. Record a 10 minute background spectrum at the 0 m offset location.
3. Insert a radioactive source from Table 2.1 into the trunk of the standard vehicle.
4. Record a 10 minute spectrum with the source aligned to the horizontal center of the reference detector module.
5. If source signal cannot be seen above background, move to step 12.

Chapter 2. Experimental Set-up

6. Calculate counting time required to get the desired precision in Region of Interest (ROI) using the following equation:

$$t = (2B + S)/(SP)^2$$

where B is the background count rate, S is the source only count rate, and P is the desired precision. The ROIs will be determined for each isotope to capture the peak(s) of interest.

7. If the source signal can be seen, but t is greater than 10 minutes for a precision of 1%, repeat 10 minute measurements until the sum of the measurement time is greater than or equal to t.
8. Move source to the middle of the vehicle.
9. Repeat steps 4-7.
10. Move source to the footwell of the vehicle.
11. Repeat steps 4-7.
12. Repeat steps 3-11 for each of the other sources listed in Table 2.1.
13. Repeat steps 1-2.

2.3.2 Background Variation Measurements

Drive-about background variation measurements were made in the Coronado Mall parking lot in Albuquerque, NM. The data were collected by driving up and down the parking lot aisles at a fixed speed, once while the parking lot was empty and once after the mall had opened so the parking lot was partially full. These data were used to generate a distribution of the rate of change in background radiation levels that is seen in a real world situation. Previous work performed at LANL showed that the

Coronado Mall parking lot provides a distribution of background radiation variation that is comparable to the distribution of background variation that is found in an urban environment in the Albuquerque, NM area[24][25].

2.3.3 NORM Measurements

Background variation profiles were obtained by taking a series of static measurements in the presence of an increasing gradient of NORM buckets. The magnitude of the NORM gradient was chosen to increase the count rate in the ROI about the 1460 keV peak by approximately the same magnitude as the maximum background variation seen in the drive-about data. The fill amount and spacing of the NORM buckets was selected to provide a smooth increase in the count rate in the ROI about the 1460 keV peak over a 10 meter span along the direction of travel. Figure 2.7 depicts the NORM gradient setup, with the measurement locations at the 1 meter intervals from 0 to 10 meters shown along the bottom of the diagram.

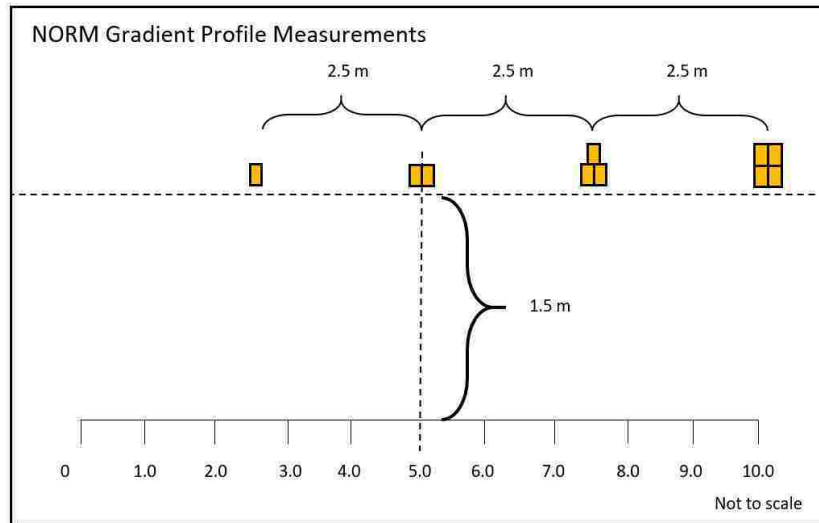


Figure 2.7: NORM Gradient Measurement Locations.

Measurement Procedure:

1. Remove all sources, including buckets of NORM.
2. Perform a 10 minute background at the 0 m offset location.
3. Measure exposure rate with calibrated exposure rate meter at the 0 m offset location.
4. Place the 1st type of NORM buckets in an arrangement similar to that shown schematically in Figure 2.7.
5. Record a spectrum for 10 minutes with the horizontal center of the reference detector module at each of the measurement locations.
6. At 0 m offset, directly in front of location with 4 NORM buckets, measure exposure rate due to NORM using calibrated exposure rate meter.

2.3.4 Verification Measurements

A set of drive-by measurements was taken to be benchmarked against the simulated drive-by spectra of the same configuration to verify the simulation results. Table 2.2 shows the matrix of verification measurements that were performed, and the procedure used is below. Drive-by speeds and source locations/configurations were arbitrarily chosen to have variety in several of the parameters that can be changed by the user interface of the simulation tool. Engine speed, rather than vehicle speed is listed because for the slowest speeds, the speedometer needle would not come off the 0 mph mark and the operator was only able to maintain the correct speed by monitoring the tachometer. Engine speeds of 600 RPM, 900 RPM, and 1200 RPM correspond to speeds of 4.9 kph, 7.9 kph, and 10.2 kph, respectively.

Chapter 2. Experimental Set-up

In order to reduce uncertainty in both speed and source-to-detector distance, an additional set of measurements were made using a second detector system that is mounted on on a motorized gantry cart (Figure 2.8). These measurements are listed in Table 2.3 and the associated measurement procedure follows the table. These measurements were chosen after the simulation tool was developed and the shielding and distances were chosen so that they would be more challenging cases for the TIA to correctly identify.

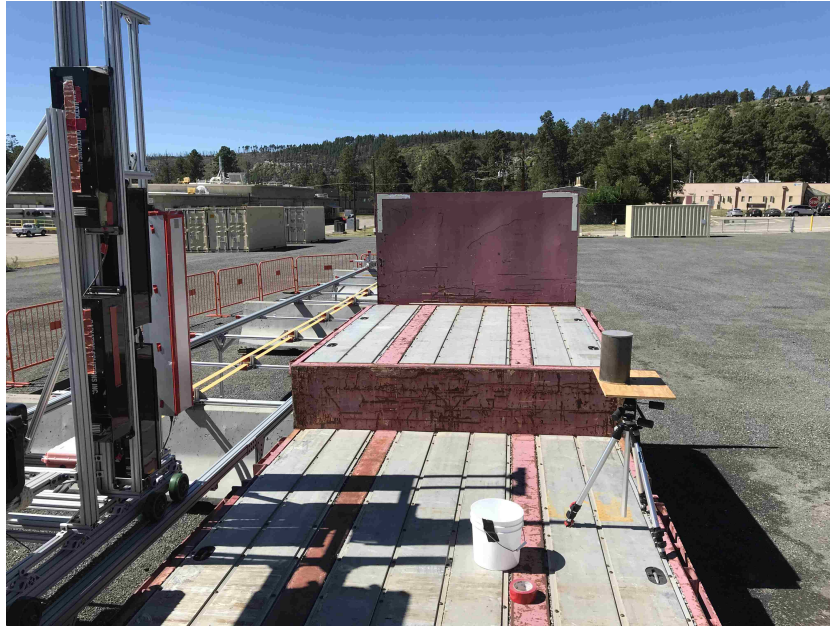


Figure 2.8: Gantry measurement setup.

Table 2.2: Drive-by Verification Measurement Test Matrix.

Source	Source Location	Engine Speed (RPM)	Vehicle Speed (kph)	source-to-detector distance (cm)
HEU	Trunk	600	4.9 ± 0.2	138
HEU	Middle of Car	1200	10.2 ± 0.7	309
HEU	Bare	600	4.9 ± 0.2	150
HEU	$\frac{1}{4}$ " Steel	600	4.9 ± 0.2	150
HEU	2" HDPE	600	4.9 ± 0.2	150
WGPu	Trunk	600	4.9 ± 0.2	134
WGPu	Foot Well	600	4.9 ± 0.2	404
WGPu	Bare	1200	10.2 ± 0.7	150
WGPu	$\frac{1}{4}$ " Steel	600	4.9 ± 0.2	150
WGPu	2" HDPE	600	4.9 ± 0.2	150
DU	$\frac{1}{4}$ " Steel	600	4.9 ± 0.2	150
DU	2" HDPE	600	4.9 ± 0.2	150
CS-1	Trunk	600	4.9 ± 0.2	149
CS-1	Middle of Car	600	4.9 ± 0.2	310
CS-1	Foot Well	600	4.9 ± 0.2	399
I3-598	Bare	600	4.9 ± 0.2	150
1193-15	$\frac{1}{4}$ " Steel	900	7.9 ± 0.2	150

Measurement Procedure:

1. Place a source from Table 2.2 in location specified by test matrix.
2. Maintaining constant engine speed in first gear as specified by test matrix drive detector system past source located in specified configuration.
3. Press "start scan" and start the stopwatch when detector reaches the -10 m location.
4. Press "stop scan" and stop the stopwatch when detector reaches the +10 m location.
5. Record time of trial.

Chapter 2. *Experimental Set-up*

6. Repeat steps 1-5 for each configuration listed in Table 2.2.

Table 2.3: Gantry Verification Measurement Test Matrix.

Source	Source configuration	Speed	Source-to-detector Distance
IS200	$\frac{1}{4}$ " Steel	40 cm/sec	230 cm
IS200	2" HDPE	40 cm/sec	230 cm
1820-84-3	$\frac{1}{4}$ " Steel	40 cm/sec	230 cm
1820-84-3	2" HDPE	40 cm/sec	230 cm
1820-84-3	Bare	40 cm/sec	40 cm
FN-591	$\frac{1}{4}$ " Steel	40 cm/sec	150 cm
FN-591	2" HDPE	40 cm/sec	150 cm
FN-591	Bare	40 cm/sec	230 cm

Measurement Procedure:

1. Place a source from Table 2.3 in location & configuration specified by test matrix.
2. Start the automated data collection script.
3. Press "motion 1" to start a trial from west to east.
4. Press "motion 2" to start a trial from east to west.
5. Repeat steps 3 and 4 until 10 trials are complete.
6. Stop automatic data collection script.
7. Repeat steps 1-6 for each configuration listed in Table 2.3.

Chapter 3

Simulation Methodology

The overall simulation process is straightforward: first user inputs are modified to create the desired trial configuration, and then these user inputs are used to produce simulated results which can be viewed in a spectral analysis software such as PeakEasy, or can be read into the RSI RadAssist replay tool to be analyzed by the RadAssist TIA. The simulation tool was developed using the C++ programming language.

3.1 User Inputs

The user inputs can be broken down into two categories: those modifiable from the basic user interface (UI), and those that can only be modified by an advanced user. These will be described below as basic user inputs and advanced user inputs with units and/or limits denoted in square brackets.

3.1.1 Basic User Inputs

When the application is launched, the UI (Figure 3.1) will allow the operator to change several parameters that will change the simulation results. These inputs are listed below, with a description of how they impact the simulation. Whenever the application is launched, the settings on the basic UI are reset to default values.

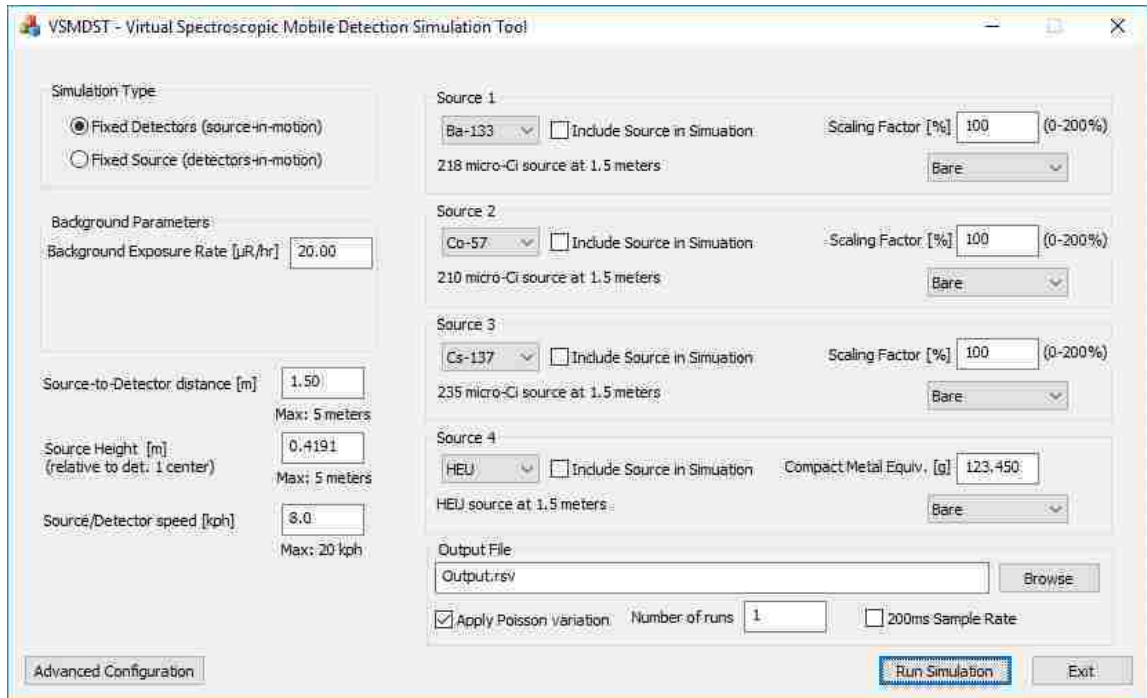


Figure 3.1: Basic User Interface.

- Simulation Type:** [*Fixed Detectors(source-in-motion)* / *Fixed Source (detectors-in-motion)*] This parameter will allow the operator to switch between a scenario where the detectors are in a fixed location and a source is passed by the detectors, and a scenario where the source is in a fixed location and the detectors pass by the source. When the detectors are in motion background variation will be applied to the simulation, but when the detectors are fixed, the background will remain constant (with statistical variation).

Chapter 3. Simulation Methodology

- **Background Exposure Rate:** [$\mu R/hr$] This parameter will allow the user to adjust the background exposure rate, which will apply a scaling factor to the background spectrum that is included in the scenario. The background spectrum may be changed within the advanced UI.
- **Sample Gradient from Distribution**[*checked/unchecked*] This checkbox is only visible when the simulation type is “Fixed Source”, and when checked will sample from the background variation distribution. When unchecked, the background gradient input field will become visible.
- **Background Gradient:** [$0.5-99.5\%$] This parameter that is only visible when the “Sample Gradient from Distribution” box is unchecked allows the user to select the percentile of background gradient to apply to a detector-in-motion simulation. This option will not be available for a source-in-motion simulation. The application of the background gradient will be described in greater detail later in this document.
- **Source-to-Detector Distance:** [$0-5\text{ meters}$] This parameter will change the distance at which the source passes the plane on which the face of the detector lies.
- **Source Height:** [$-5\text{ to }+5\text{ meters}$] This parameter changes the height (relative to the center of detector 1) that the source passes by the detector array. The default value is set to halfway between the center of detector 1 and detector 2. If there is only 1 detector present, then the default value will be 0.0 m.
- **Source/Detector Speed:** [$0-20\text{ kph}$] This parameter changes the speed at which the source is moved past the detectors or at which the detectors move past the source, depending on which simulation type is selected.
- **Source 1-4 options:** The following parameters are modifiable for each of the 4 sources that can be included in a trial.

- **Source Label:** [*dropdown list*] The advanced configuration UI allows for up to 25 different sources to be loaded into the simulation tool and within the basic UI, up to 4 of those can be included into any one simulation trial. This dropdown list allows the user to select what the 4 sources that can be included in the simulation trial will be.
 - **Include Source in Simulation:** [*Checked/Unchecked*] If checked, this source is included in the simulation trial, scaled according to the scaling factor or mass. If unchecked, this source’s spectrum will be left out of the simulated trials.
 - **Scaling Factor:** [*0-200%*] This option will only be available for a non-SNM source, and it will allow the user to change the relative strength of the source primitive that is included in a particular trial. A scaling factor of 100% corresponds to the measured source primitive that is loaded into the simulation tool.
 - **Compact Metal Equiv.:** [*grams*] This option will replace the “Scaling Factor” for an SNM source, and it will allow the user to change the relative strength of the source primitive that is included in a particular trial. The default value will be the value entered in the advanced UI for the particular source, and scaling of the source will be proportional to $M^{\frac{2}{3}}$, where M is mass¹.
 - **Configuration:** [*dropdown list*] This option allows the user to choose which of the source configurations to include in the simulation. The advanced UI allows up to 10 different configurations to be added per source (1 bare spectrum + 9 shielding configurations).
- **Output File:** [*text input*] This parameter allows the user to specify the path

¹SNM sources will be scaled this way since the high density of the material provides self-shielding, the gamma ray emissions will scale with the change in surface area, which for a sphere is proportional to $M^{\frac{2}{3}}$

and filename that the output files will be written to. A filename with no path will write the output to the same directory that contains the executable (.exe).

- **Apply Poisson variation:** [*checked/unchecked*] This option will apply statistical variation to the spectra so that each trial produced is not identical; when unchecked every single background spectrum sample is identical (with some variation from one detector to the next), and all trials run from -10 m to +10 m with no variation in starting and ending location.
- **Number of trials:** [*integer value*] This is the number of trials to be run for the chosen configuration.
- **200 ms Output:** [*checked/unchecked*] This option writes the output at a 200 ms sample rate instead of the default one-second sample rate.
- **Advanced Configuration:** [*button*] When pressed, this prompts the user for a password and if entered correctly, launches the advanced UI (Figure 3.2).
- **Run Simulation:** [*button*] When pressed, this executes the simulation the desired number of times.
- **Exit:** [*button*] When pressed, this closes the UI and exits the program.

3.1.2 Advanced User Options

These options can have a significant impact on the simulation results and should only be modified by an advanced user, which is why a password is required to launch the advanced UI (Figure 3.2). These will only be modified to change things such as the available source primitives² and detector configurations. They are listed and

²A primitive is a background subtracted spectrum with low statistical uncertainty that is sampled from to create simulated trials.

Chapter 3. Simulation Methodology

described in detail below. Changes to these settings are saved to a configuration file located in the same directory as the executable, and they can be retained without needing to modify the advanced UI during subsequent instances of running the application. This file is a binary file that is not man-readable and if none are present, then default values and sources that are packed into the executable are the only options that will be available.

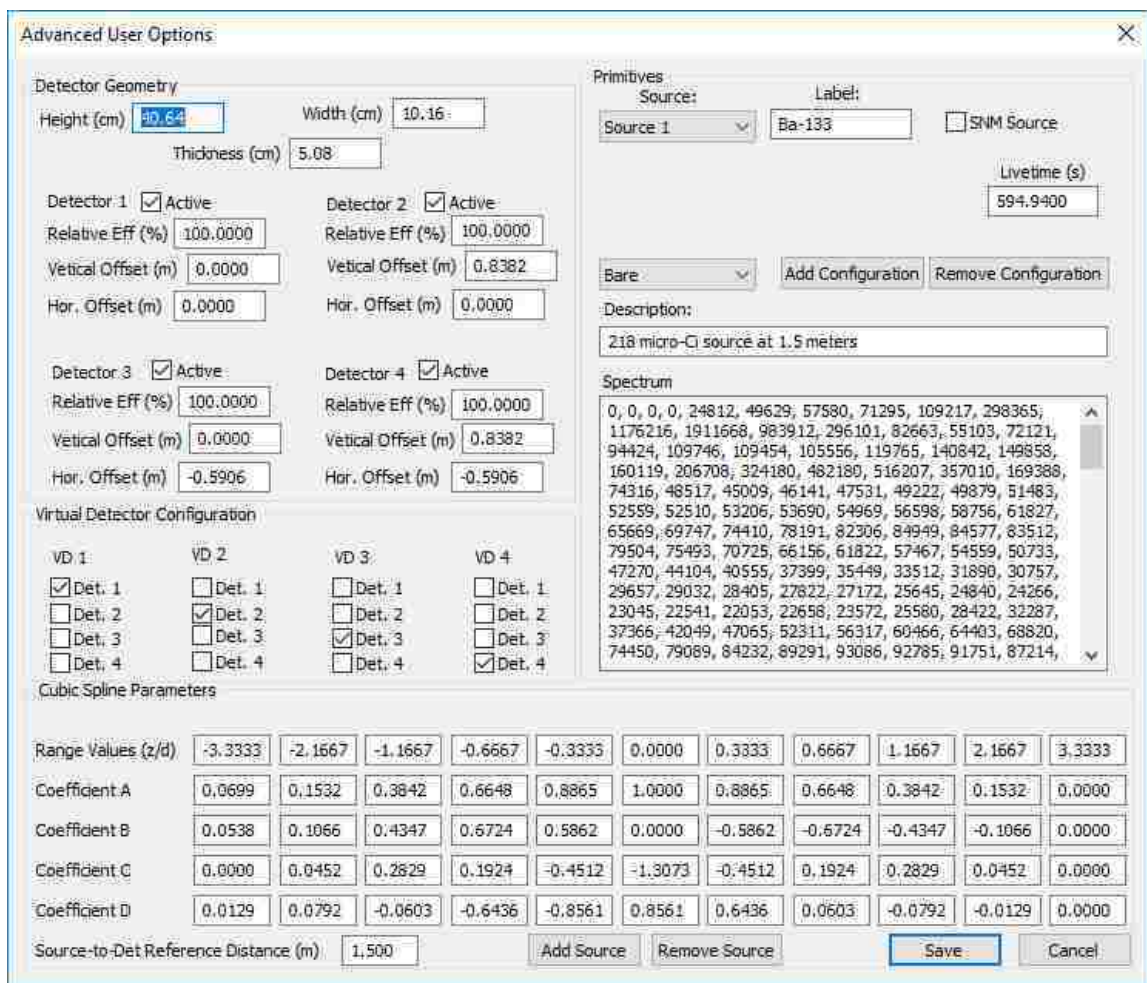


Figure 3.2: Advanced User Interface.

- **Detector Geometry:** This section allows the user to define the layout of the detector array. Detector 1 will always be the reference detector and therefore

Chapter 3. Simulation Methodology

must be included in the simulation and must be located with a vertical and horizontal offset of 0.00 meters. The following parameters are used to change detector geometry. Figure 3.3 is included to provide a reference as to how these parameters will impact the layout of the detector array.

- **Height:** [*centimeters*] Applied to all detectors in array, this parameter sets the height that will be used in the surface area portion of the solid angle calculations.
- **Width:** [*centimeters*] Applied to all detectors in array, this parameter sets the width that will be used in the surface area portion of the solid angle calculations.
- **Thickness:** [*centimeters*] Applied to all detectors in array, this parameter sets the thickness that can be included if solid angle calculations are modified to include streaming into the sides and top/bottom of the detector crystals.
- **Detector 1-4 Active:** [*checked/unchecked*] This parameter determines whether or not the detector is included in the simulation. The detector 1 check box cannot be unchecked.
- **Detector 1-4 Relative Eff:** [%] This parameter will allow for tuning of individual detectors within the detector array by multiplying the signal for each detector by the relative efficiency term. Since the spectra that are loaded into the simulation tool are measured from detector 1, this parameter allows realistic variation between the detector crystals if there are differences in efficiency on the real system.
- **Detector 1-4 Vertical Offset:** [*meters*] This parameter is used to set the vertical distance between the center of detector 1 and the center of the other detectors in the array. The value for detector 1 cannot be changed from 0.00 since this is the reference detector.

Chapter 3. *Simulation Methodology*

- **Detector 1-4 Hor. Offset:** [*meters*] This parameter is used to set the horizontal distance between the center of detector 1 and the center of the other detectors in the array. The value for detector 1 cannot be changed from 0.00 since this is the reference detector.

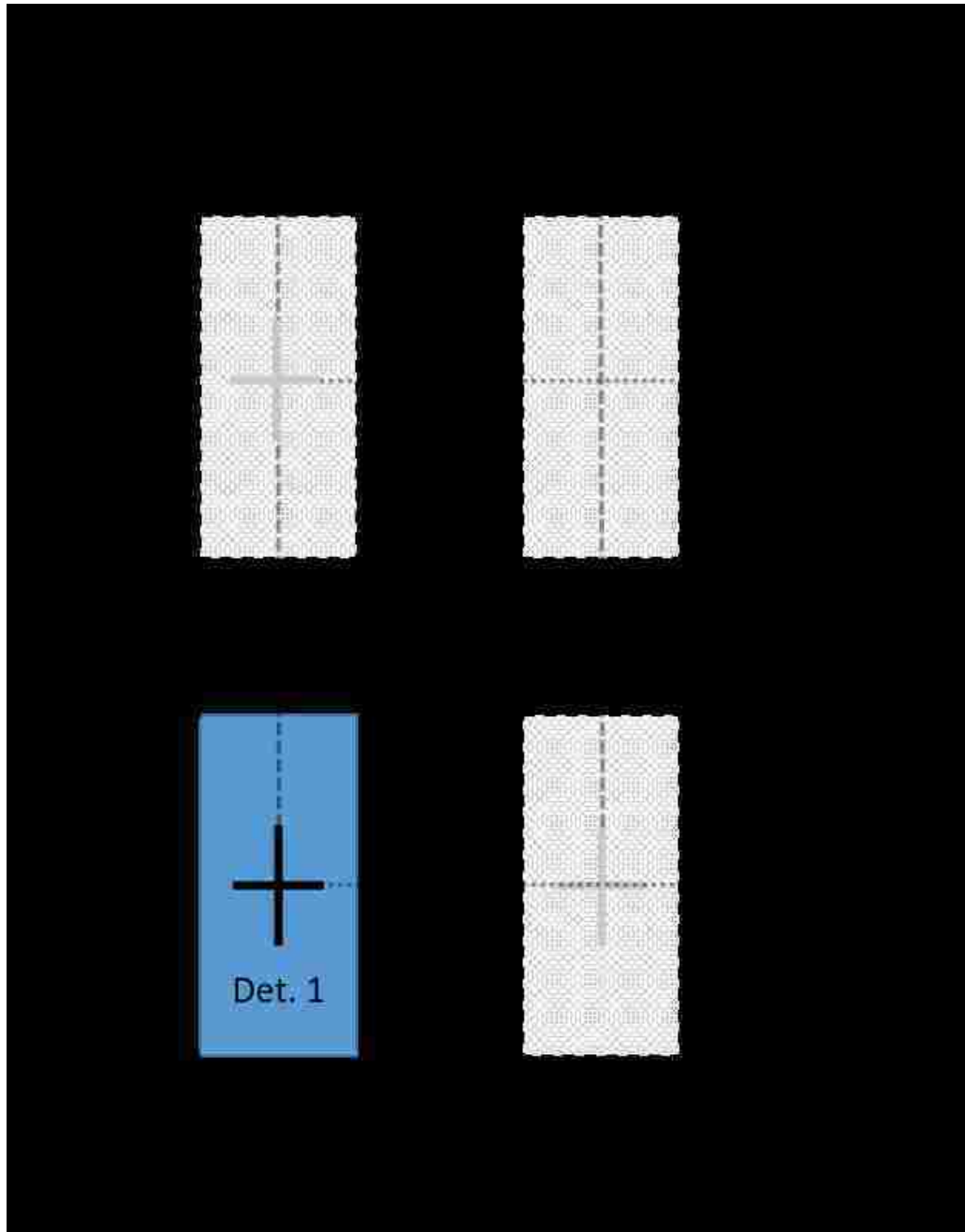


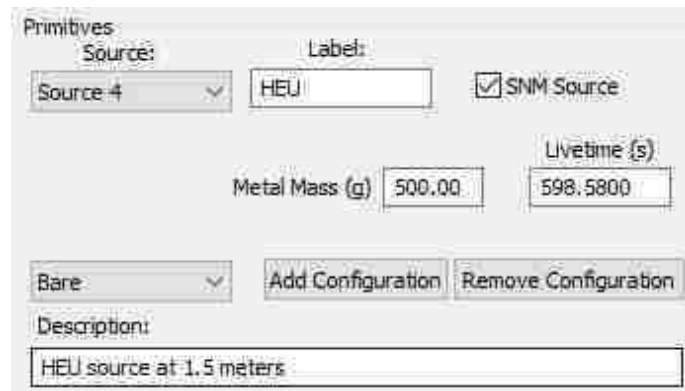
Figure 3.3: Diagram of geometry configuration (horizontal and vertical offsets can be positive or negative from the reference detector).

- **Virtual Detector Configuration:** [*check boxes*] These check boxes are used to define which of the physical detectors are combined into the different virtual detectors. There are 4 virtual detectors and these can contain the summed spectra from any combination of the 4 simulated detectors.
- **Cubic Spline Parameters:** These are the parameters that will be used for the cubic spline interpolation to be used in the integrating function of the simulation. Refer to Section 3.2.3 for details on how the cubic spline interpolation is integrated for each simulated timestep.
 - **Range Values (x/d):** [*decimal entry boxes*] These are the locations along the direction of travel at which the profile measurements were made, divided by the reference source-to-detector distance at which they were measured (d).
 - **Coefficient A:** [*decimal entry boxes*] These are the A coefficients for the 3rd order polynomials that define the cubic spline interpolation.
 - **Coefficient B:** [*decimal entry boxes*] These are the B coefficients for the 3rd order polynomials that define the cubic spline interpolation.
 - **Coefficient C:** [*decimal entry boxes*] These are the C coefficients for the 3rd order polynomials that define the cubic spline interpolation.
 - **Coefficient D:** [*decimal entry boxes*] These are the D coefficients for the 3rd order polynomials that define the cubic spline interpolation.
 - **Source-to-Det Reference Distance:** [*meters*] This is the source-to-detector distance that was used for the profile measurements used to determine the coefficients for the cubic spline interpolation (distance at closest approach).
- **Primitives:** The background subtracted source primitives will be loaded here, with their energy calibration, as well as a label and description that will be

Chapter 3. Simulation Methodology

displayed on the UI to identify which source primitives are present when the simulation tool is launched.

- **Source:** [*dropdown list*] This is a dropdown list that allows the user to switch between the different sources that are loaded into the simulation tool. Switching between sources will update all of the related fields with data for that particular source. If “Background” is selected, the only fields that can be edited are the livetime, spectrum, and exposure rate.
- **Label:** [*text input*] This is the name of the source that is displayed on the basic UI. It should be a short identifier that is unique to that source.
- **SNM Source:** [*checked/unchecked*] When checked, this makes the “Metal Mass” field visible and indicates that this source should be scaled by change in mass.
- **Metal mass:** [*grams*] For an SNM source, this is the compact metal equivalent for that source. Figure 3.4 shows the input that is visible when the SNM Source option is checked.



The screenshot shows a configuration window titled "Primitives". It contains several fields and controls:

- Source:** A dropdown menu currently showing "Source 4".
- Label:** A text input field containing "HEU".
- SNM Source:** A checked checkbox.
- Metal Mass (g):** A text input field containing "500.00".
- Livetime (s):** A text input field containing "598.5800".
- Bare:** A dropdown menu.
- Buttons:** "Add Configuration" and "Remove Configuration".
- Description:** A text area containing "HEU source at 1.5 meters".

Figure 3.4: Metal mass option visible when SNM Source option is checked.

- **Exposure Rate:** [$\mu R/hr$] If the source selected is “Background”, then this option is visible and is the exposure rate that was measured at the location where the background was measured. This value is used to scale the

background appropriately when the background exposure rate is changed on the basic UI.

- **Livetime:** [*seconds*] This is the livetime in seconds for the background subtracted source spectrum that is loaded into the simulation tool.
 - **Configuration:** [*dropdown list*] This dropdown list allows the user to toggle between the source configurations for the specific source. The Livetime, Description, and Spectrum fields are unique to each configuration within the source³.
 - **Description:** [*text input*] This parameter allows the user to provide a specific description for the selected source configuration and this will be displayed on the basic UI when the user toggles between different configurations.
 - **Spectrum:** [*1024 comma-separated values*] This box contains the spectrum for the selected configuration. It must contain 1024 values separated by a comma, which corresponds to the total counts in each channel for the background subtracted spectrum.
 - **Add Configuration:** [*button*] When pressed, this button adds a new configuration to the source. The spectrum, description, and livetime for the new configuration will be empty and must be filled in by the user. The maximum number of configurations for a given source is 10.
 - **Remove Configuration:** [*button*] When pressed, this button removes the selected configuration from the source. The bare source configuration cannot be removed.
- **Add Source:** [*button*] When pressed, this button adds a new source to the available sources. All fields will be blank and must be filled in by the user.

³Configurations are different measurements that were made with the same source, but are configured in such a way as to modify the shape of their spectrum (behind shielding material, in a vehicle, in front of something that provides backscatter, etc.)

The maximum number of sources that can be included in the simulation tool is 25. This limit was chosen to limit the memory allocation of application and could be increased in later versions of the application if desired.

- **Remove Source:** [*button*] When pressed, this button removes the selected source from the available sources. The background cannot be removed (but it can be changed), and at a minimum there must be four sources to fill the four source locations on the basic UI.
- **Save:** [*button*] When pressed, this button saves all changes that were made in the advanced UI and then closes the advanced UI, returning to the basic UI.
- **Cancel:** [*button*] When pressed, this button discards all changes that were made in the advanced UI and then closes the advanced UI, returning to the basic UI.

3.2 Running the Simulations

This section describes how the simulation tool operates when the “Run Simulation” button is pressed. Once pressed, the simulation tool creates the desired number of trials, using the user defined parameters to configure the trials. The following sections describe the process in detail. Throughout this thesis, the x direction will refer to the direction of travel, the z direction will refer to the direction normal to the face of the detector, and the y direction will represent the vertical direction, as depicted in Figure 3.5.

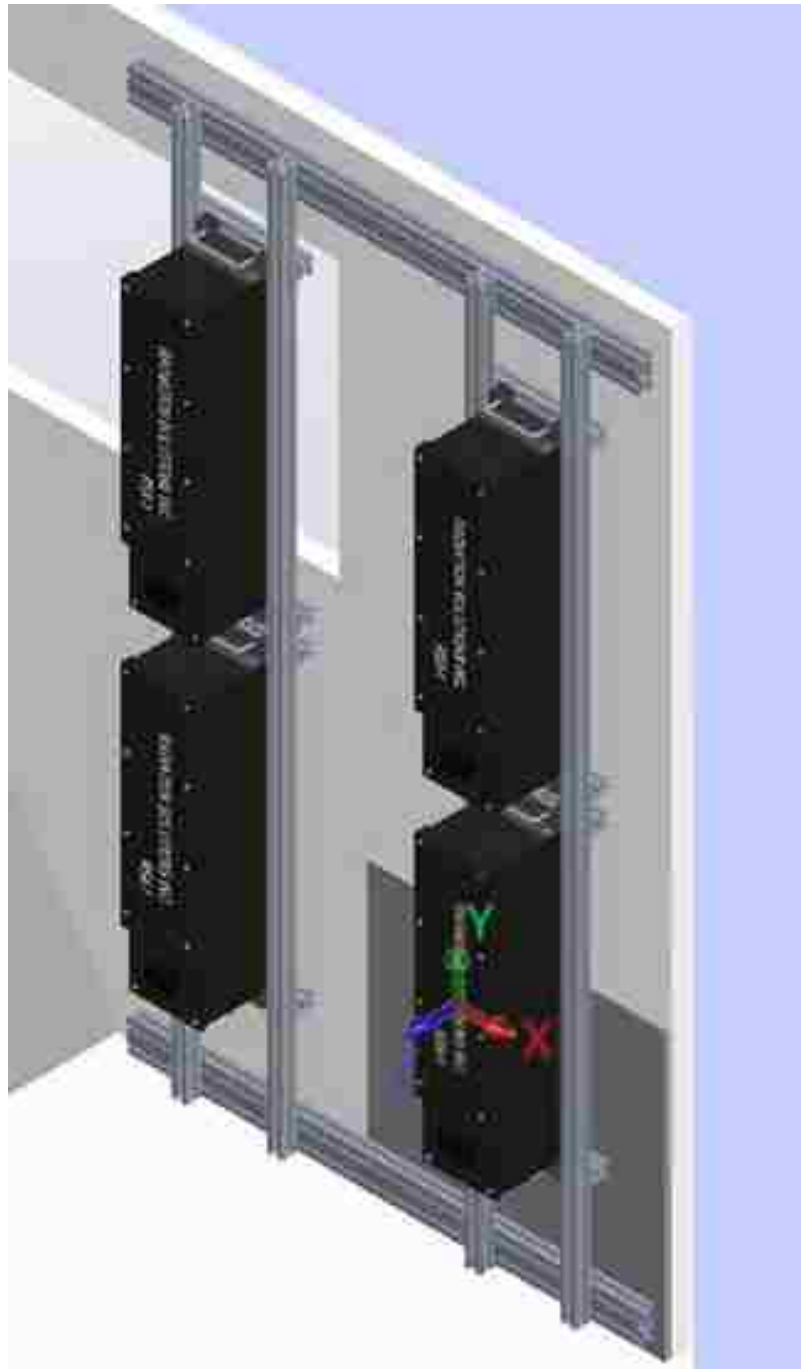


Figure 3.5: Reference coordinate system used.

3.2.1 Initializing Variables

When the “Run Simulation” button is pressed, all inputs to the UI are locked until all of the simulations are completed. All of the variables that are applied to the global scope of the simulation configuration are initialized. The global scope here refers to variables that remain constant for all trials that are to be performed for a given configuration. This includes reading all of the user inputs from both the basic UI and the advanced UI into corresponding variables defined inside the software. It is more efficient to set these variables once, on a global scale, than it is to set them for each trial that is created. During this step, the individual source primitives are combined into a single source primitive that will be used for the simulation trials; if the “include source” parameter is checked, then that source is included in the combined primitive and scaled according to the scaling factor parameter.

3.2.2 Multi-threading individual trials

Once the global parameters are set, individual trials are created. In order to do this as efficiently as possible, the simulation tool will query the computer for the number of processors available and then divide the total number of trials equally among the available processors. For each simulation trial, on each processor, the following steps are executed in series to create a single, unique trial. Trial numbering is determined by a counter internal to each processor; for example, in a 100 trial simulation with 4 processors, processor #1 will create trials 0-24, processor #2 will create trials 25-49, processor #3 will create trials 50-74, and processor #4 will create trials 75-99.

3.2.3 Integrating the detector response curve

For each of the individual trials, the starting and ending locations will be randomly selected if the “Apply Poisson variation” checkbox is selected on the basic UI, and will be fixed at -10 m and +10 m if the checkbox is unchecked. When randomly selected, they are chosen to fall within the ranges: $[-10-2dx] < x_{start} < [-10-dx]$, and $[10 + dx] < x_{end} < [10 + 2dx]$; where dx is the distance traveled (meters) in one timestep (200 ms or 1 s) based on the speed defined by the user. A distance of roughly 10 meters from the source location was chosen to be a good distance for many anticipated applications. This distance should be far enough from the source that there is not a lot (if any) signal from the source already impacting the detector, but not so far away that the background would be expected to be all that different. The exact starting and ending locations are determined by using a uniform random number generator that outputs a value between zero and one, and is then multiplied by dx . The range for the starting/ending locations is chosen so that no matter what speed is selected, there will be at least one integration step that encompasses the peak where the source signal is greatest. Once the starting and ending locations are determined, then the location of the timestep (200 ms or 1 s) intervals are defined.

Once the timestep interval locations are defined, an integrated detector response multiplication factor for each detector in the array is calculated at those locations, denoted by ϵ in Equation 3.4. The integration is performed using the extended trapezoidal rule, which integrates the cubic spline interpolation multiplied by the solid angle ratio from “a” to “b”, which are consecutive timestep interval locations. The extended trapezoidal rule is implemented as the function $qtrap(f(x), a, b, epsilon)$ [26] which is essentially an extension of the trapezoidal rule that breaks up the distance from a to b into smaller and smaller subsections and applies the trapezoidal rule to each of those subsections until the overall error term reaches the input epsilon value. The trapezoidal rule and extended trapezoidal rule are shown in Equation 3.1 and

Chapter 3. Simulation Methodology

Equation 3.2, respectively[26].

$$\int_{x_0}^{x_1} f(x)dx = h\left[\frac{1}{2}f_0 + \frac{1}{2}f_1\right] + O(h^3 f'') \quad (3.1)$$

$$\int_{x_0}^{x_{N-1}} f(x)dx = h\left[\frac{1}{2}f_0 + f_1 + f_2 + \dots + f_{N-2} + \frac{1}{2}f_{N-1}\right] + O\left(\frac{(b-a)^3 f''}{N^2}\right) \quad (3.2)$$

where h is the step size between N abscissa points, f_N is the function $f(x)$ evaluated at the N^{th} abscissa point and O is the error term.

The solid angle calculations performed are for “A solid angle subtended by a rectangle at an arbitrary point” [27] and are used to calculate the solid angle for the front face of each detector to a point source. It was decided that the sides, top, and bottom of the detectors would not be included in the simulation because detector response profile was being over predicted when correcting the measurements from the other three detectors in the array using the solid angle ratio. This is discussed further in Section 4.6, Assumptions and Limitations. The solid angle calculation is shown in Equation 3.3 and is valid for the geometry depicted in Figure 3.6.

$$\begin{aligned} \Omega = & \arctan \frac{(x_2 - x_p)(y_2 - y_p)}{z_p[(x_2 - x_p)^2 + (y_2 - y_p)^2 + z_p^2]^{\frac{1}{2}}} \\ & - \arctan \frac{(x_1 - x_p)(y_2 - y_p)}{z_p[(x_1 - x_p)^2 + (y_2 - y_p)^2 + z_p^2]^{\frac{1}{2}}} \\ & - \arctan \frac{(x_2 - x_p)(y_1 - y_p)}{z_p[(x_2 - x_p)^2 + (y_1 - y_p)^2 + z_p^2]^{\frac{1}{2}}} \\ & + \arctan \frac{(x_1 - x_p)(y_1 - y_p)}{z_p[(x_1 - x_p)^2 + (y_1 - y_p)^2 + z_p^2]^{\frac{1}{2}}} \end{aligned} \quad (3.3)$$

The equation that is evaluated using the trapezoidal rule is shown in Equation 3.4, where $g(x)$ is the cubic spline interpolation and $\frac{\Omega}{\Omega_0}$ is the ratio of the solid angle for a

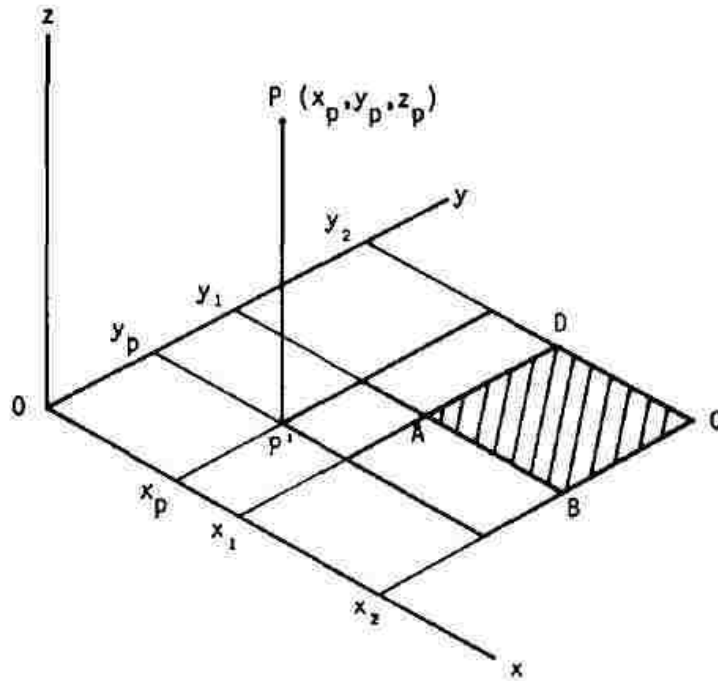


Figure 3.6: Geometry for Equation 3.3 for the solid angle subtended by the shaded rectangle ABCD at the point P. (from [27])

given detector to the solid angle that the measured profile was made. For instance, in a 4 detector system if the cubic spline measurements were made to the center of one of the detectors, then when the simulated source is passed by the center of the detector array, the solid angle ratio will account for the difference between the solid angle at the center of the detector and the solid angle at the center of the detector array. The integrated values for the individual detectors are then multiplied by the user input for relative detector efficiency to scale the detector response appropriately. The math behind the cubic spline interpolation and interpolating the background gradient are presented below.

$$\epsilon = \int_a^b g(x) \frac{\Omega}{\Omega_0} dx / (b - a) \quad (3.4)$$

Cubic Spline Interpolation: The equation for the cubic spline is defined in the advanced user inputs and describes the detector response function for a source passing along in the x/d direction. “d” is the source-to-detector distance (1.5 m) that the source profiles were measured at. The reason that the cubic spline is along the x/d instead of simply down the x direction is that it will allow the detector response to fall on the correct portion of the curve when the source-to-detector distance in the simulation is not the same. A cubic spline is a set of third order polynomials that pass through the measured data points and polynomial coefficients are determined by setting the second derivative to zero at the ends of each polynomial.[28] The cubic spline equation that will be used is:

$$Y = a + b(x - X(i)) + c(x - X(i))^2 + d(x - X(i))^3 \quad (3.5)$$

where the arrays for a, b, c, d, and X(i) are defined in the advanced user inputs.

Background Gradient Interpolation: For “detector-in-motion” simulations, the amount of background gradient will either be randomly sampled from distribution of measured background variation, or will be defined by the user. If randomly sampled, each trial will pull a different value from the distribution. Once the amount of background variation is determined, the background variation will be applied from -5 meters to +5 meters and will then remain at the new background level for the remainder of the trial. The background gradient will be applied as a linear function over 10 meters with the increase (or decrease) in count rate coming from a NORM primitive that was measured using common NORM materials.

3.2.4 Creating the Trials

For each trial, 15 seconds of purely background data are added to the front and back end of each run to allow the TIA to be able to see data with no impact from the source before making alarm decisions. These spectra are created simply by using the scaled background primitive, and applying Poisson statistics to each channel in the spectra. In the region between the starting and ending locations, the previously scaled and summed source primitive is added to the appropriately scaled background primitive, and the Poisson statistics are applied to each channel. If this is a detector-in-motion simulation, then the appropriate background gradient will be applied as well, prior to applying the Poisson statistics. The background gradient sampling methodology is described below.

3.2.5 Writing the Output

In order to feed the output into the replay tool for the RSI system, the output needs to be written to a survey file, with file extension `.rsv`. This is a binary file which needs to be written using the functions supplied by RSI in a header file. The functions will take the individual detector spectra and combine them into spectra for Virtual Detectors, which are defined in the user inputs. From there, the functions package the spectra, along with date and time information into the appropriate memory locations and write the file. The output filenames and locations are defined by the user, and an `_XX.rsv` is appended to each filename, where the `XX` is the trial number. The files will be written to the output directory as defined by the user inputs. The tool will also output an `.n42` file with the same data, so that it can be easily read by software such as PeakEasy. An `.n42` file is a standard data format that is used for the output of radiation measurement instruments that are used for

Chapter 3. Simulation Methodology

homeland security applications[8]. The .n42 file will group the output spectra as time-series data for the four virtual detectors. An example .n42 file is included in Appendix A.

Chapter 4

Results

The purpose of this thesis is to provide a spectroscopic in-motion simulation tool for the RSI RS-700 detector system that provides the ability to evaluate how well the detector system (and its TIA) will perform when attempting to detect the illicit trafficking of nuclear material. The results presented in this chapter consist of the data and analysis of the raw measured data that was used to create the simulation tool, followed by an evaluation of how well the output of the simulation tool matches the verification measurements. The output comparisons are presented in two parts, first the time-series spectra are compared and then the results of the RSI TIA are compared.

For all of the analysis of both measured and simulated data, a unique region of interest (ROI) was chosen for each source to include the photopeak(s) of interest. The ROIs used are shown in Table 4.1.

Table 4.1: Isotope specific ROIs used in analysis.

Primary Isotope	ROI Range (KeV)	Number of Channels
^{137}Cs	528-777	83
^{133}Ba	249-456	69
^{57}Co	99-177	26
HEU (^{235}U)	138-225	29
WGPu	285-492	69
DU	915-1095	60

For the in-motion validation measurements, the time it took to traverse the 20 meter test lane was used to determine the speed for each of the different engine speeds used. Table 4.2 shows these speeds. These parameters are used to determine the detector response profile.

Table 4.2: Drive-by speeds used.

Engine Speed (RPM)	Speed (kph)
600	4.9 ± 0.2
900	7.9 ± 0.2
1200	10.2 ± 0.7

4.1 Detector Response Profile

The detector response profile was created by making 11 long dwell measurements at various positions along the X-axis, at 1.5 meters in the Z direction with each of the six sources. The X-axis is defined as the direction of travel, the Y-axis is the vertical position, and the Z-axis is the direction normal to the face of the detectors, as shown in shown in Figure 3.5. For each of these measurements, the count rate in the source specific ROI was normalized to the measurement made at the center position (0.0 m in the X direction). Since the measurement locations in the positive and negative X directions were the same distance from 0, the detector response was expected to be symmetric and therefore the net count rate in the ROI for the

Chapter 4. Results

location in the positive X direction was averaged with the corresponding location in the negative X direction. This symmetric detector response was used to fit the cubic spline interpolation. Figure 4.1 shows the cubic spline interpolation overlaid on the normalized average ROI count rates for all six sources with the blue data points showing the output of the cubic spline equation and the red data points are the normalized average ROI count rates. While this work was done with a configuration that provides symmetric responses in the positive and negative X direction, if there were detector housing or other structural material that would skew the profile, the cubic spline interpolation provides the flexibility to account for this.

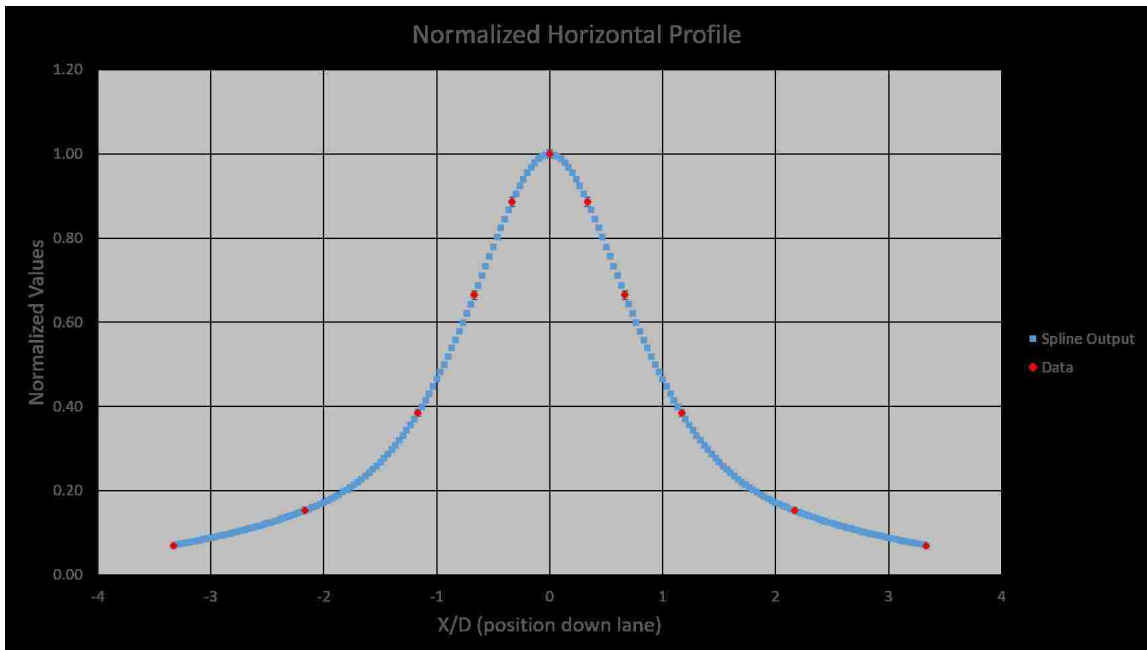


Figure 4.1: Cubic spline interpolation fit to measured data points.

The cubic spline interpolation from the average of all six sources was then checked against each individual source profile to verify that the cubic spline was valid for all of the isotopes measured. Figure 4.2 shows the cubic spline interpolation compared to the measured data from the ^{137}Cs source. The data points displayed include both the actual measured data as well as the two point averages to make the profile sym-

Chapter 4. Results

metric. The cubic spline interpolation fits the measured data by applying piecewise 3rd order polynomials between each of the measured data points. Table 4.3 shows the coefficients to solve Equation 3.5 that were determined from the measured data. A macro-enabled excel workbook was downloaded with predefined functions to solve for the coefficients[29].

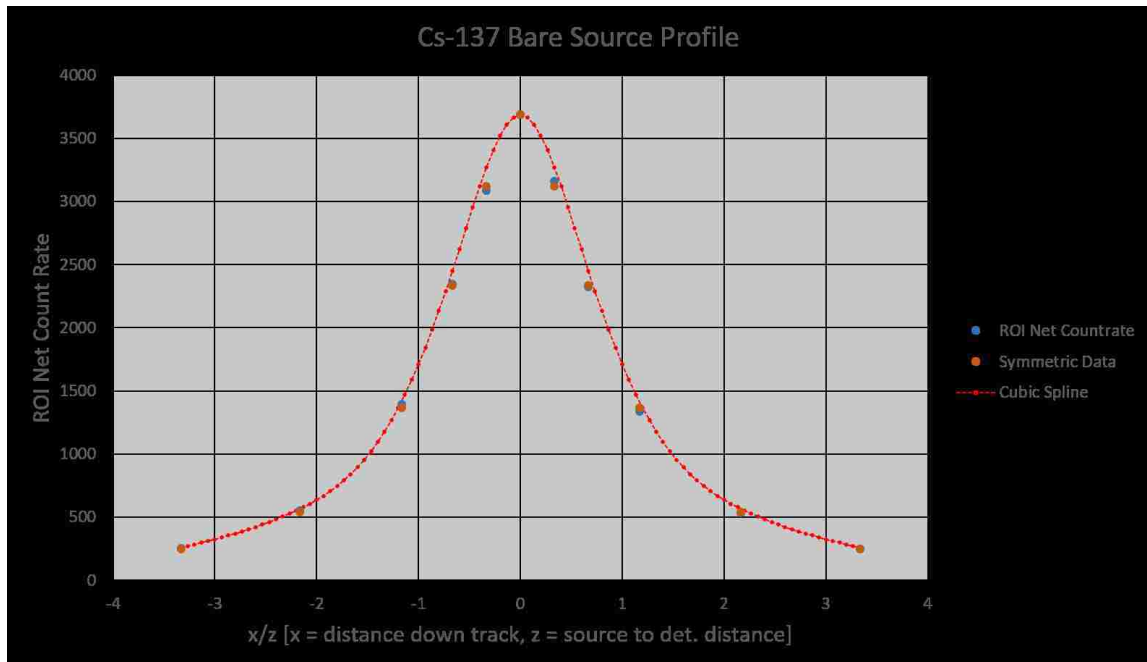


Figure 4.2: Cubic spline interpolation fit to ^{137}Cs source profile. Data points for both data sets are present at all locations but overlapping at several locations that appear to only have data for “Symmetric Data”. Error bars are present for both data sets as well but too small to be visible on the plot.

Table 4.3: Cubic spline coefficients.

X(i)	coeff a	coeff b	coeff c	coeff d
-3.333	0.069	0.053	0	0.012
-2.166	0.153	0.106	0.045	0.079
-1.166	0.384	0.434	0.282	-0.060
-0.666	0.664	0.672	0.192	-0.643
-0.333	0.886	0.586	-0.451	-0.856
0	1	0	-1.307	0.856
0.333	0.886	-0.586	-0.451	0.643
0.666	0.664	-0.672	0.192	0.060
1.166	0.384	-0.434	0.282	-0.079
2.166	0.153	-0.106	0.045	-0.012

Figure 4.3 shows the importance of using an integrated detector response for in-motion simulations. At 15 kph, a one second time interval represents a distance of ~ 4.2 meters. The plot was made by allowing the simulation tool to randomly define the starting point and the location of each one second interval. The red line represents the relative detector response obtained by integrating along the detector response curve between each one second interval; the data point locations represent the end point of the one second time interval. The blue line shows what the detector response would be if a one second dwell measurement were simulated at each of these locations and the white line shows what the detector response would be if a one second dwell were simulated at the midpoint between each location. The blue line grossly overestimates the integrated detector response and the white line underestimates the response. Section 4.5 will demonstrate how the integrated response compares to measured data.

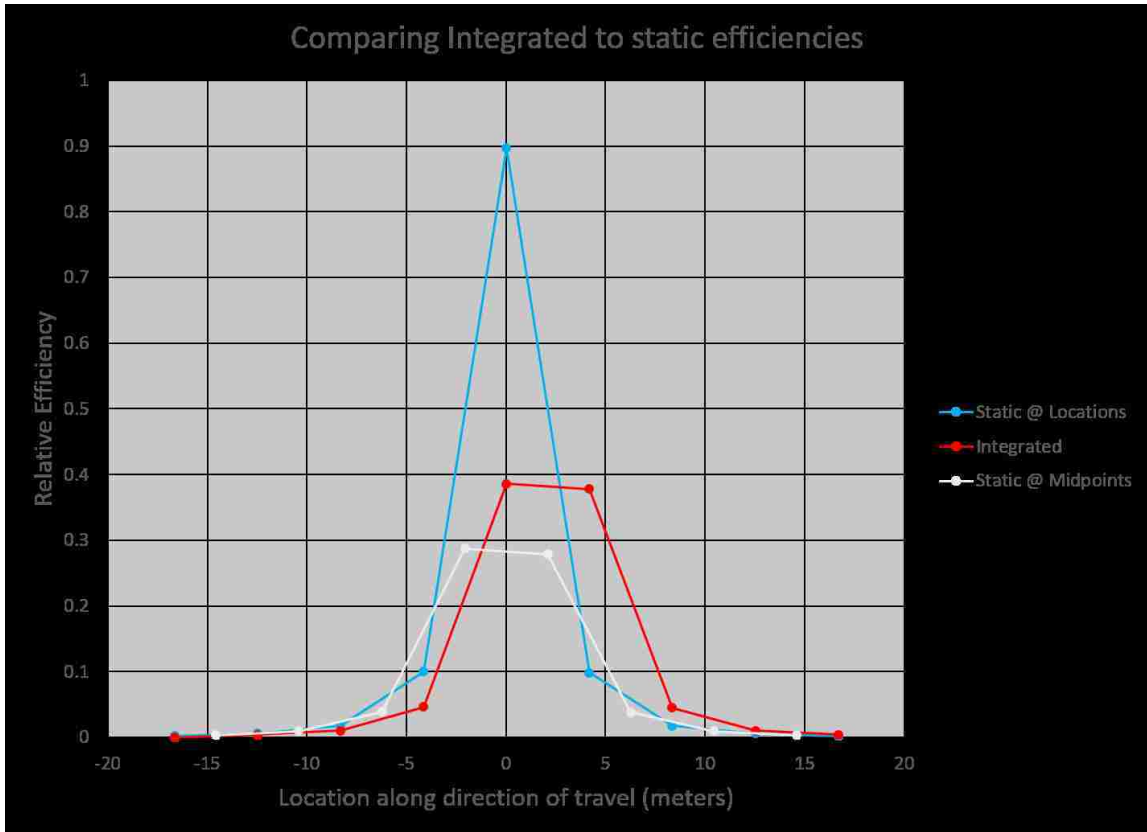


Figure 4.3: Relative efficiency comparison between using an integrated response versus using static measurement locations.

4.2 Background spectrum

In order to reduce the statistical uncertainty in the background spectrum that is used as the background primitive in the simulation tool, a 2.5 hour background dwell measurement was captured at the location that was measured, and found to have an exposure rate of $22.6 \mu\text{R/hr}$. Figure 4.4 shows the background dwell measurement is a very smooth spectrum with very little statistical noise across the entire energy range.

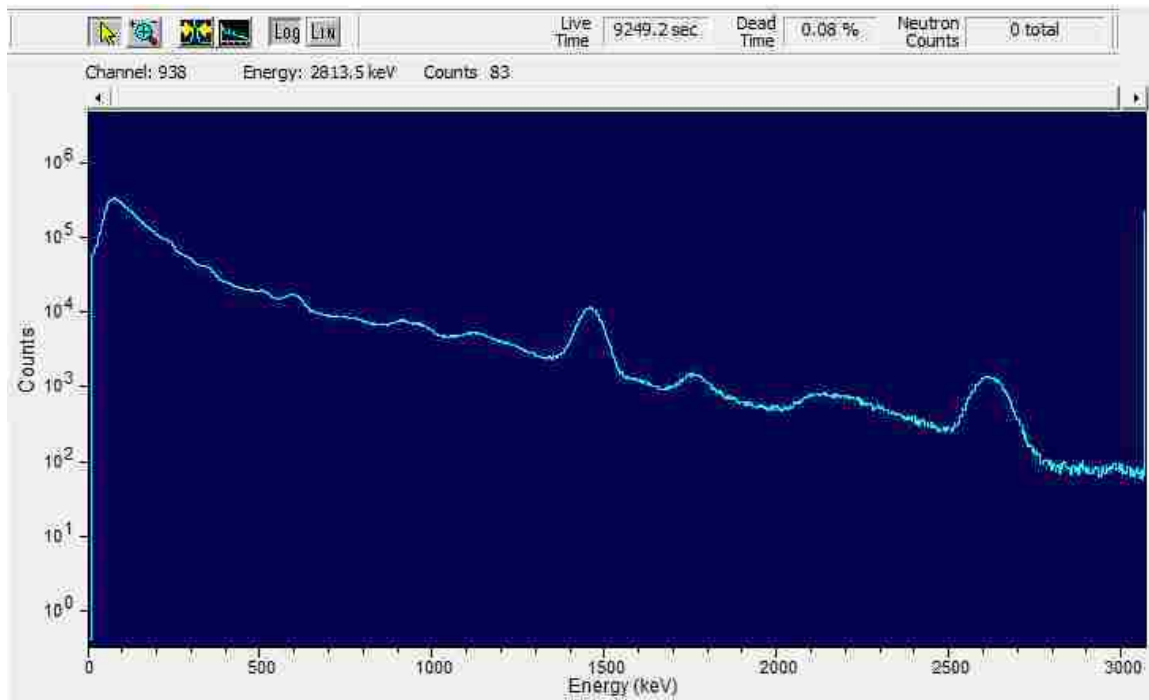


Figure 4.4: Long dwell background spectrum.

4.3 Background variation and NORM gradient

Approximately 3 hours of drive-about data were collected at the Coronado Mall parking lot in Albuquerque, NM, for a total of 54,462 200 millisecond data points. These were analyzed by performing a one second average (5 data points) and then comparing it to a one second average 10 meters away. To determine the 10 meter difference, the average speed from the drive-about data collection was assumed to be 1.36 meters per second (m/s) and therefore the first data point in each of the one second average was separated by a time of 7.4 seconds. The 1.36 m/s number was determined by having the driver maintain the same speed as was used for the 600 RPM in-motion validation measurements, where the time to perform each 20 meter trial was measured and recorded. Figure 4.5 shows the cumulative distribution function (CDF) as the red line overlaid on top of the measured data. For the distribution,

Chapter 4. Results

the average value for the change in background radiation over a 10 meter interval was 0.00016 cps/10 m, near zero as expected, and the standard deviation was 10.369 cps/10 m.

The NORM gradient that was engineered at LANL's TA-16 Tumbler Road Test Bed provided an increase of 17 counts per second on the reference detector module. An increase of 17 counts per second over 10 meters corresponds to $\sim 93^{\text{rd}}$ percentile in the drive-about data collected at the Coronado Mall parking lot. The engineered NORM gradient caused an increase in the background exposure rate of $0.81 \mu\text{R}/\text{hr}$. The spectrum for the engineered NORM gradient was background subtracted and loaded into the simulation tool as as another primitive that is scaled according to the NORM gradient percentile that is chosen for each simulated trial.

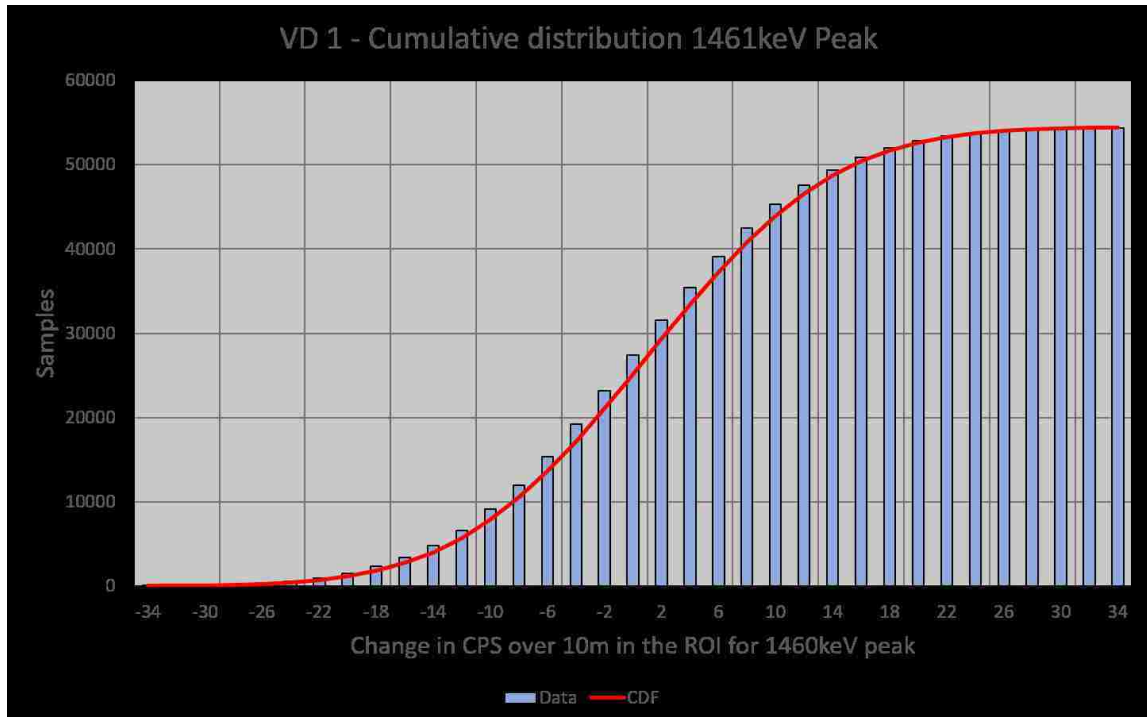
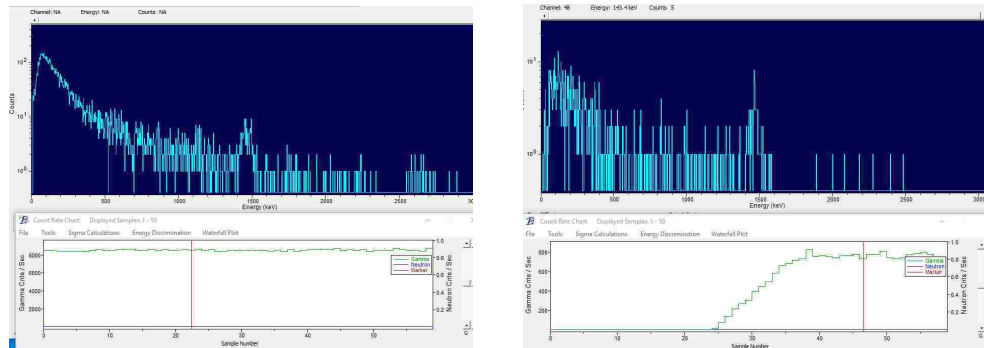


Figure 4.5: Background variation cumulative distribution for virtual detector 1.

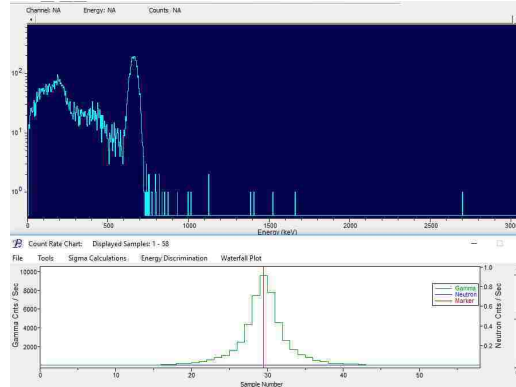
4.4 Simulated Spectra

The simulated spectra that are produced by the simulation tool are a combination of three separate components. Those components are the background component, the source component, and the background gradient component (if applicable). Since the individual components are loaded into the simulation tool from measurements that were made with the specific detector that is being simulated, the shape of the spectra that are produced as the output match the measured data very well. Figure 4.6 depicts simulation output for the three components that make up a single simulation trial. Figure 4.64.6.a shows the background component, with the upper portion of the image displaying a single one second spectrum out of the ~ 60 samples that make up the drive-by trial; the lower portion of the figure shows the gross counts for all 59 samples in this trial. The background component remains constant (with statistical variation) throughout the entire trial. Figure 4.64.6.b shows the background gradient component of the trial; with the lower portion that shows gross counts as a function of sample number showing no counts for the first ~ 25 samples and then a steady increase over the center portion of the trial, and then the last portion of the trial maintains a constant level of contribution from the background gradient component. Figure 4.64.6.c shows the effect of adding a ^{137}Cs source to a drive-by trial. The lower portion of the image shows the gross counts contribution as a function of sample number, while the upper portion of the image shows the full energy spectrum of the source component that is added for the sample which has the largest source contribution.

Chapter 4. Results



(4.6.a) Background component of simulated trial. (4.6.b) Background gradient component of simulated trial.



(4.6.c) Source component of simulated trial.

Figure 4.6: Components that are combined to make a single simulated drive-by trial.

4.5 In-Motion Comparisons

4.5.1 Spectral ROI comparisons

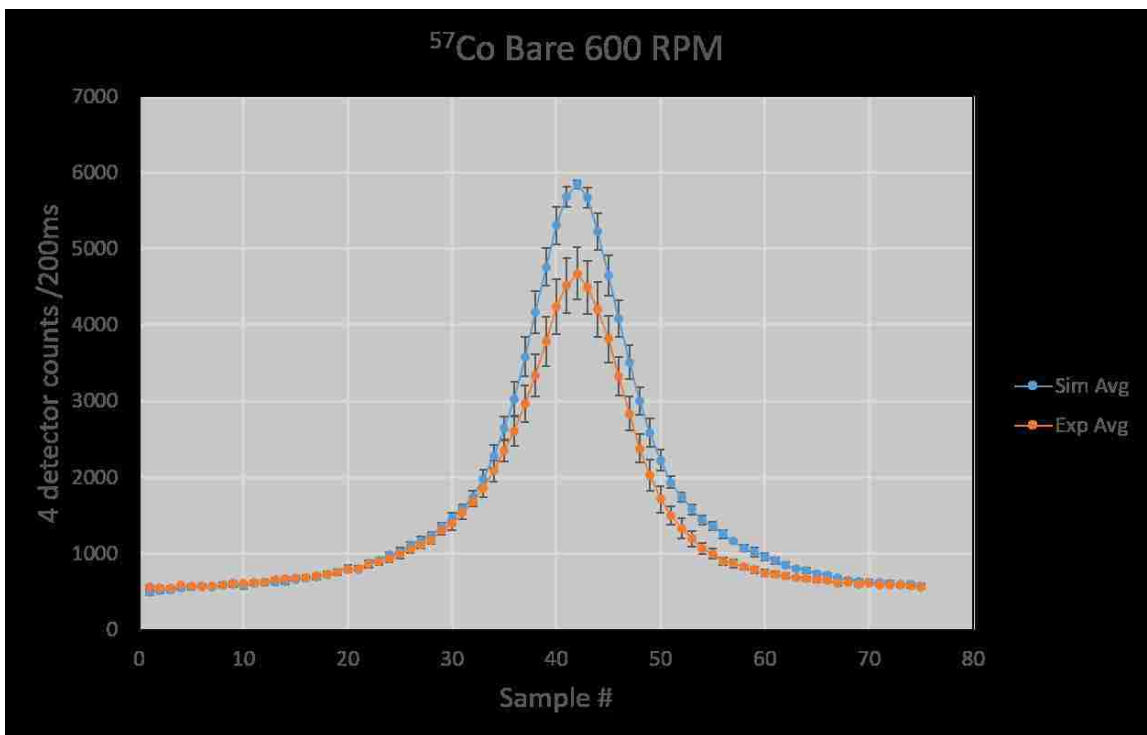
Figures 4.7, 4.8, and 4.9 show comparisons of the simulated data to the in-motion validation measurements from Table 2.2. Figure 4.11 shows comparisons of the simulated data to the in-motion validation gantry measurements from Table 2.3. The plots represent the time-series count rate in the source specific ROI from the four detector system. For the plots with SNM or DU sources, the count rate values were

Chapter 4. Results

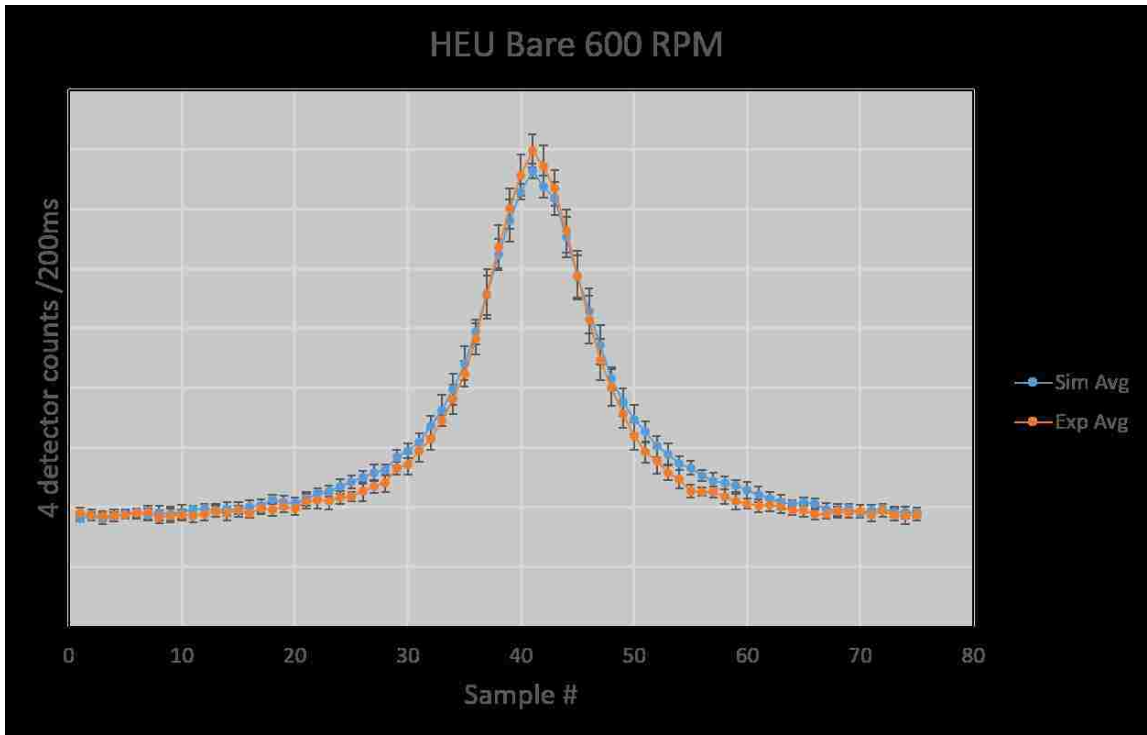
removed so that no information regarding the size of these sources can be inferred from this thesis, but the y-axis scale for simulated and measured values are the same. The blue lines in the plots represent the average count rate in the ROI for 10 simulated trials, while the orange line shows the average count rate in the same ROI for 10 in-motion measurements. The error bars represent one standard deviation for the 10 trials of either simulated or measured data for that particular sample number. Since there is some variation between the starting location for each trial and between the simulated and measured trials, each trial was aligned so that the sample with the greatest count rate in the ROI was at the same sample number. The simulated results were considered to be in agreement if the error bars for data points near the peak of the profile overlap. It is important to consider differences in areas of the profile outside of the peak, but since the signal to noise ratio is expected to be lower in these regions, they are less important to the analysis and identification capability of the TIA. Significant deviations in the regions outside of the peak of the profile will be noted and investigated further at a later time.

Figure 4.7 shows the comparisons for the bare source validation measurements. Of the three bare source drive-by trials, two of the cases agree very well and have overlapping error bars in the peak region of the profile.

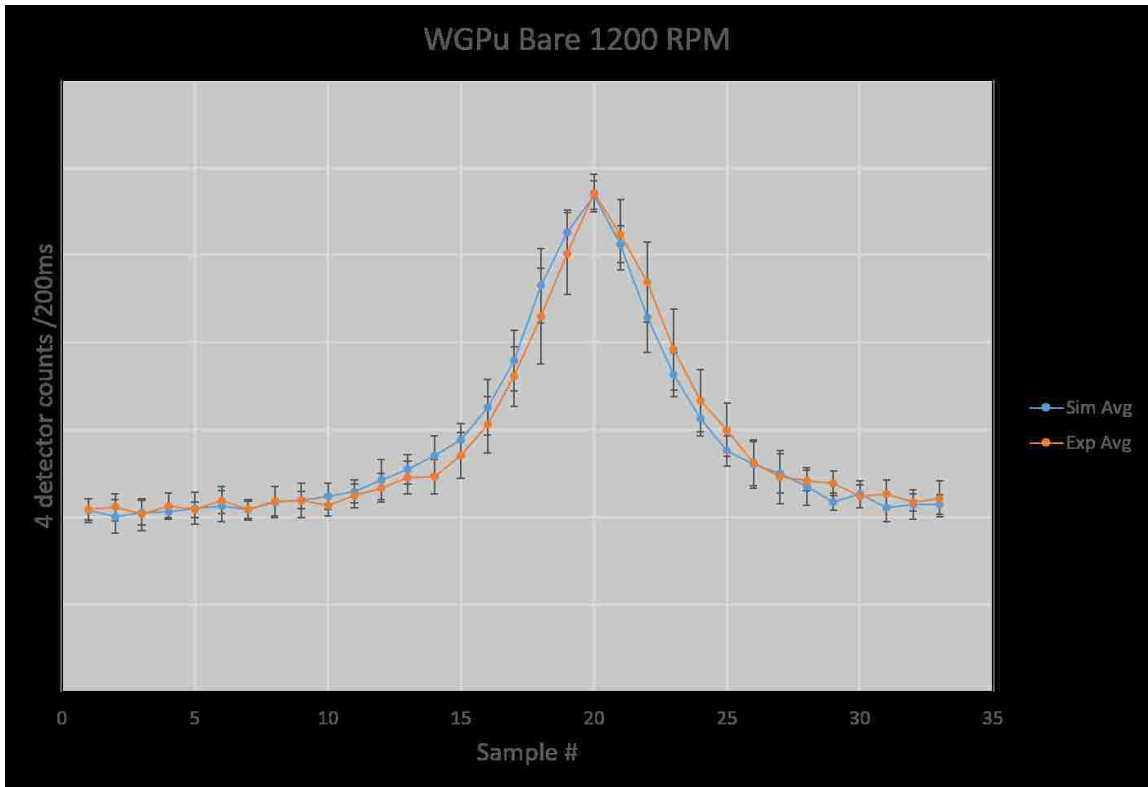
Chapter 4. Results



(4.7.a) ^{57}Co with simulated vs. measured. For this configuration the simulated count rate profile for the four detector system was larger than the measured data, falling outside of the error bars at the peak of the profile.



(4.7.b) HEU with simulated vs. measured. For this configuration the simulated count rate profile agreed with the measured count rate profile very well, with the data points around the peak of the profile having overlapping error bars. The measured profile for the HEU source is slightly narrower than for the measured profile because the HEU source does not emit photons uniformly in all directions and the source was pointed perpendicular to the direction of travel. This results in the count rate for the measured profile falling off quicker when the detector system is not directly aligned with the source.

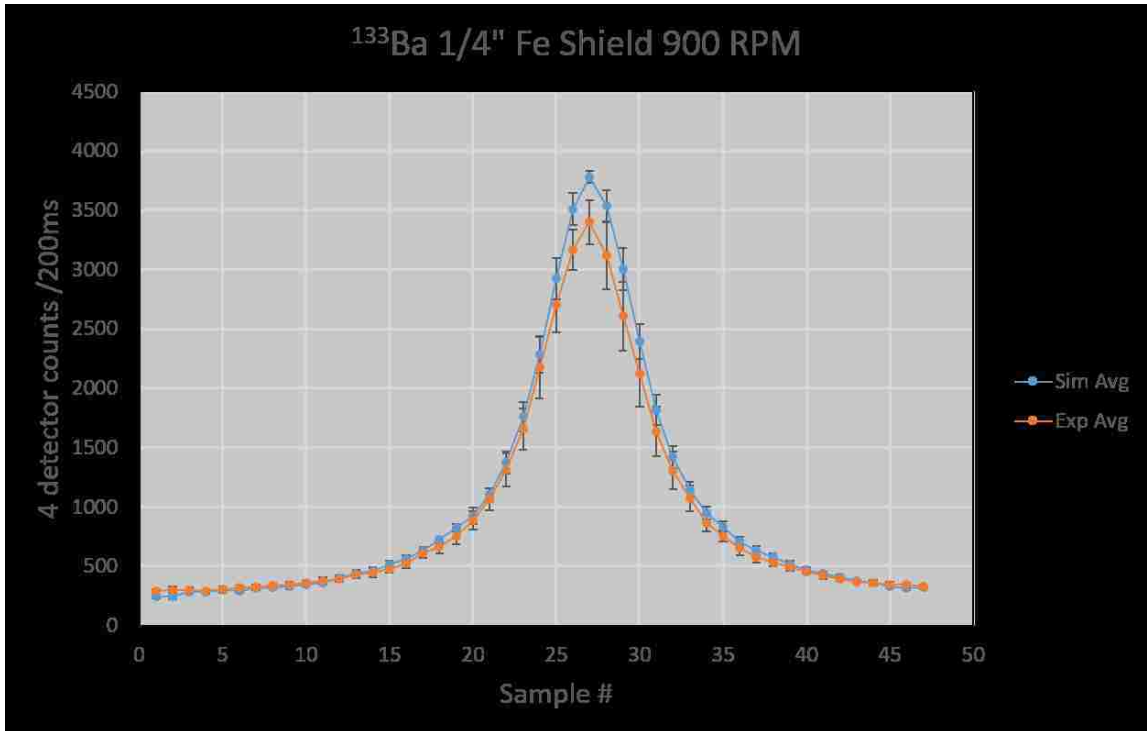


(4.7.c) WGPU with simulated vs. measured. For this configuration the simulated count rate profile agreed with the measured count rate profile very well, all of the data points in the trial having overlapping error bars. At a speed of 1200 RPM, there are fewer one second samples needed to span the ~ 20 meter trial distance than the 600 RPM speed that most trials were performed at, which is seen along the x-axis of the plot.

Figure 4.7: Drive-by comparisons of bare source measurements to simulated drive-by trials.

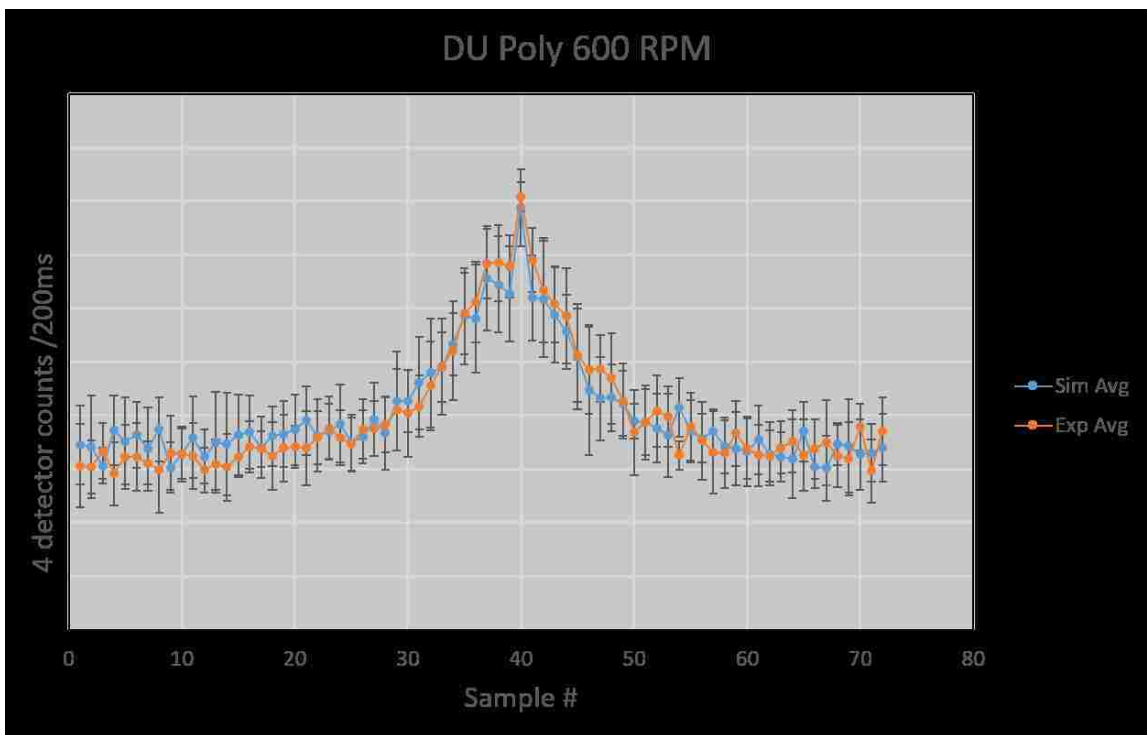
Chapter 4. Results

Figure 4.8 shows the ROI count rate profiles comparing the simulated results to the measured data for the cases in which the source was placed behind a shield. Of the 7 cases in which the source was placed behind either a steel or HDPE shield, 6 of the simulated cases were in good agreement with the measured results.

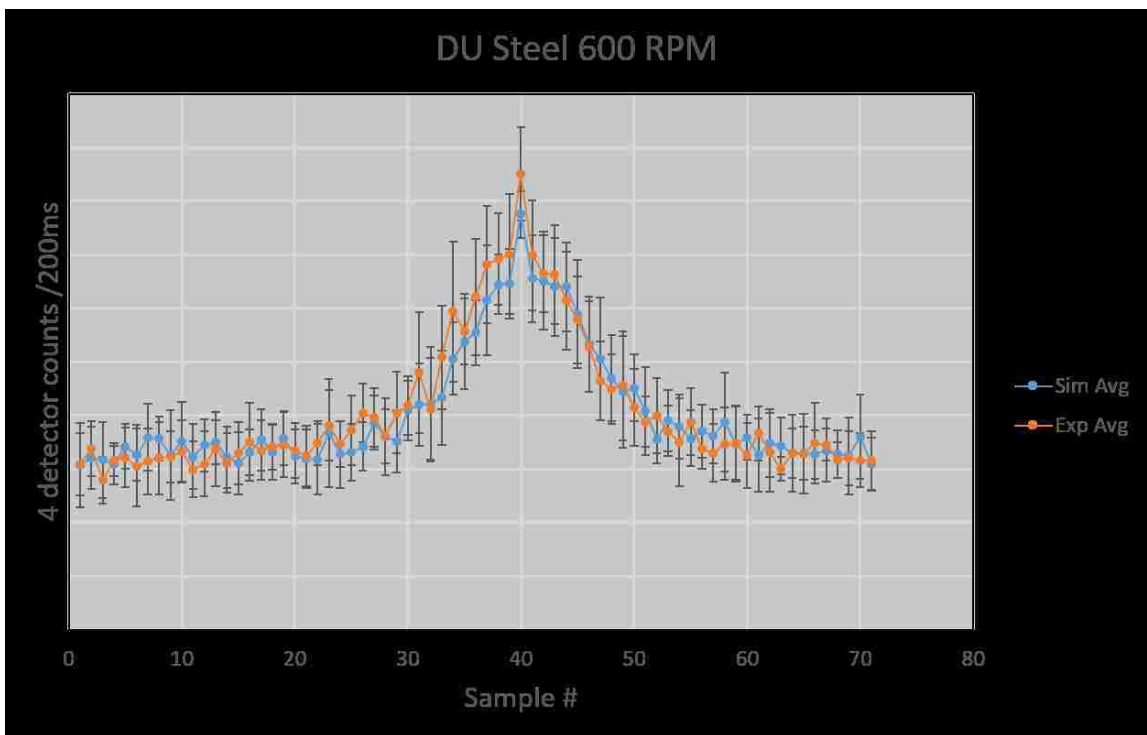


(4.8.a) ^{133}Ba behind $\frac{1}{4}$ " steel shield with simulated vs. measured. for this configuration the simulated results overestimate the source signal for this trial and fall outside of the one sigma error bars. At a speed of 900 RPM, there are fewer one second samples needed to cover the ~ 20 meter trial distance than the 600 RPM speed that most trials were performed at, which is seen along the x-axis of the plot.

Chapter 4. Results

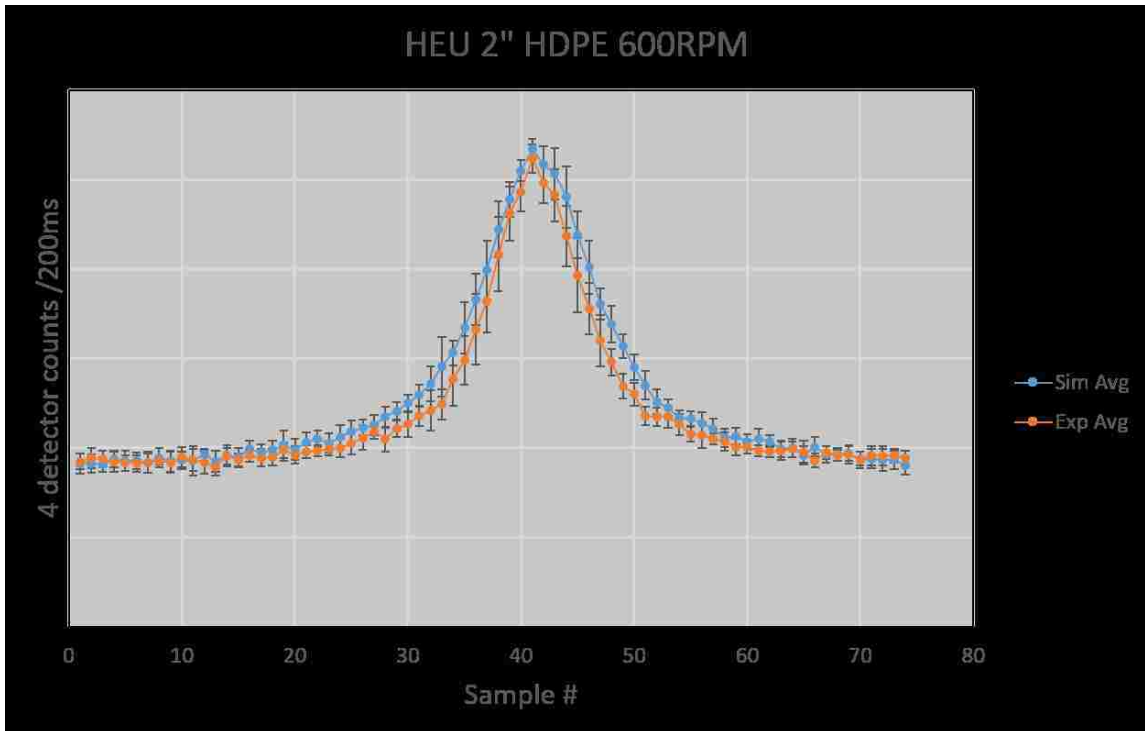


(4.8.b) DU behind 2" HDPE shield with simulated vs. measured. For this configuration the simulated count rate profile agreed with the measured count rate profile very well, all of the data points in the trial having overlapping error bars.

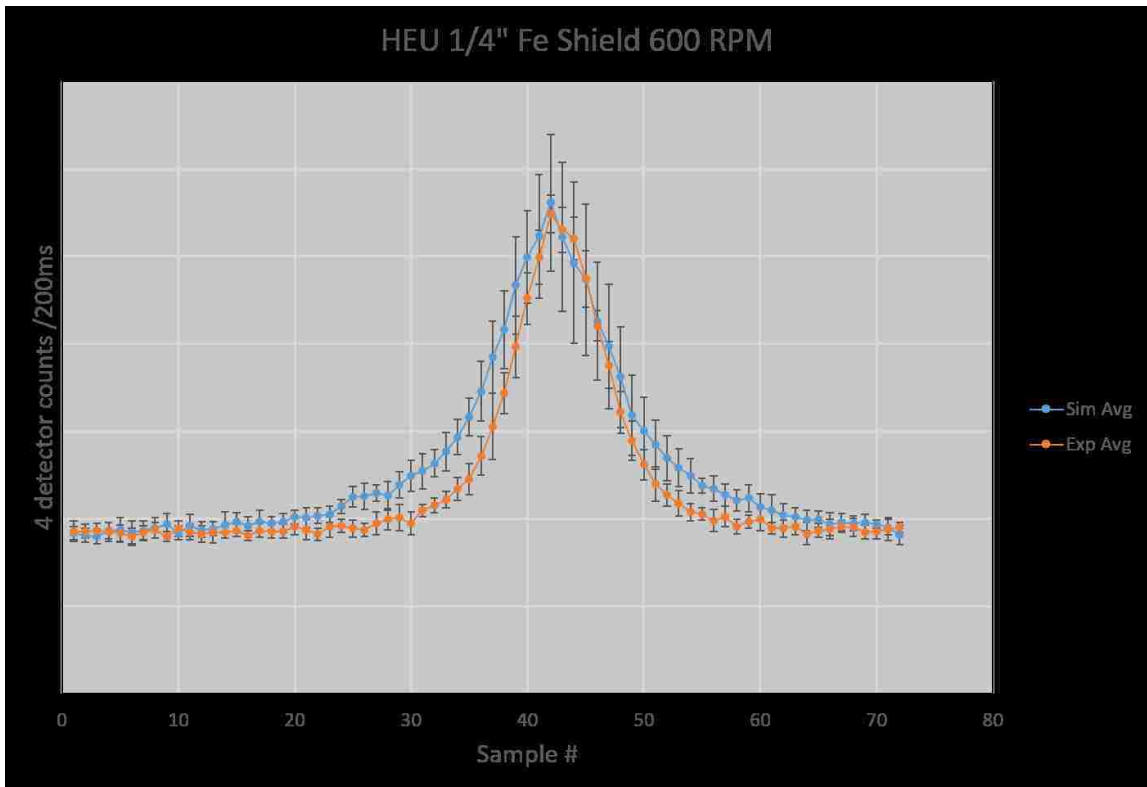


(4.8.c) DU behind $\frac{1}{4}$ " steel shield with simulated vs. measured. For this configuration the simulated count rate profile agreed with the measured count rate profile very well, all of the data points in the trial having overlapping error bars.

Chapter 4. Results

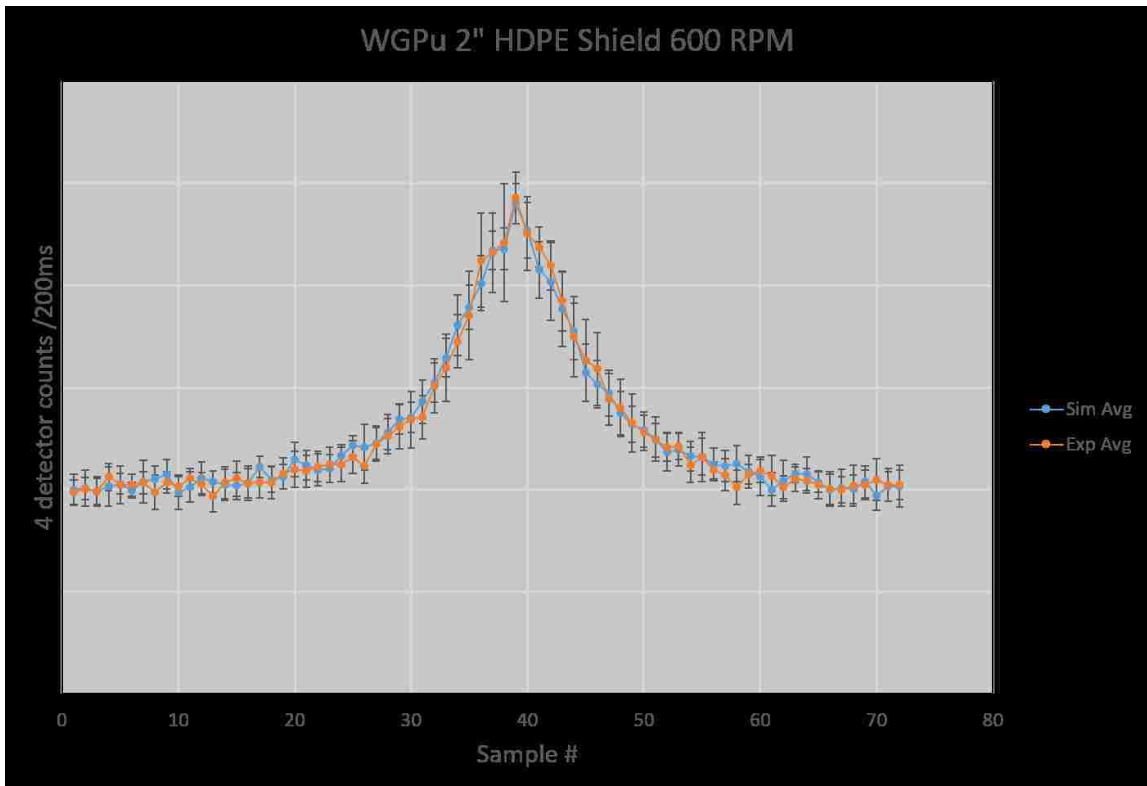


(4.8.d) HEU behind 2" HDPE shield with simulated vs. measured. For this configuration the simulated count rate profile agreed with the measured count rate profile very well, the data points around the peak of the profile have overlapping error bars. The measured profile for the HEU source is slightly narrower than for the measured profile because the HEU source does not emit photons uniformly in all directions and the source was pointed perpendicular to the direction of travel. This results in the count rate for the measured profile falling off more quickly when the detector system is not directly aligned with the source.

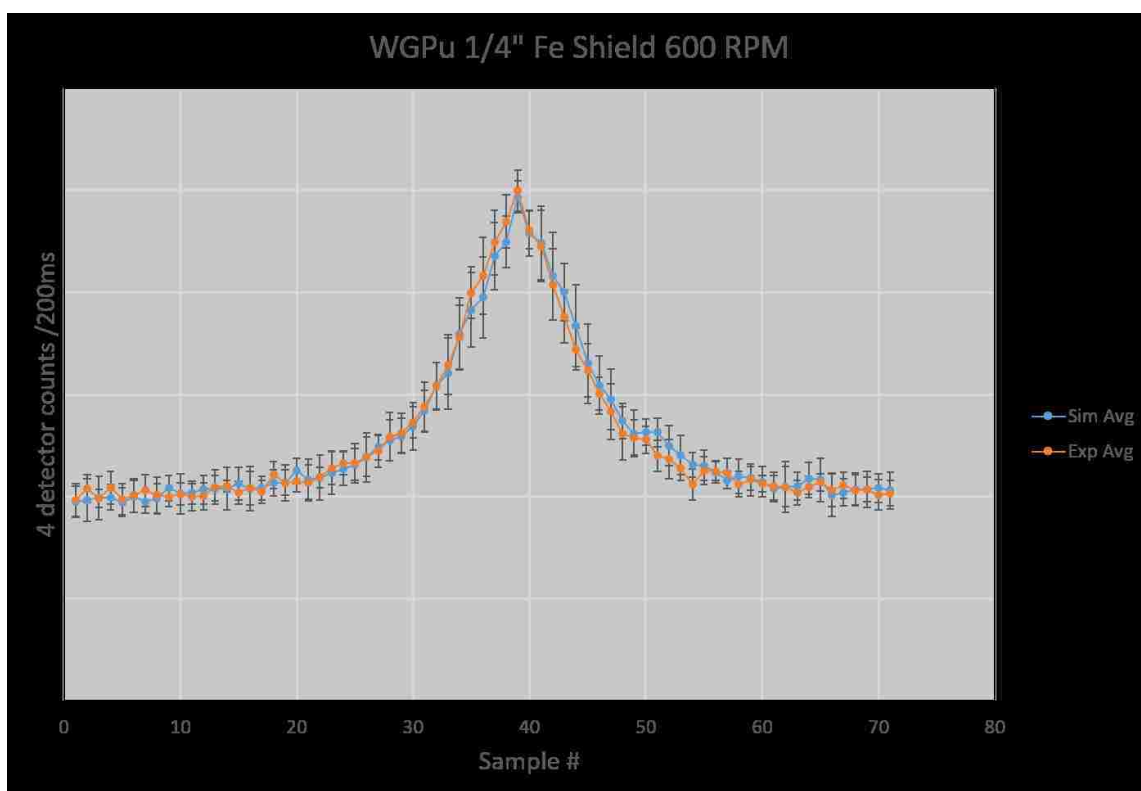


(4.8.e) HEU behind $\frac{1}{4}$ " steel shield with simulated vs. measured. For this configuration the simulated count rate profile agreed with the measured count rate profile very well, the data points around the peak of the profile have overlapping error bars. The measured profile for the HEU source is slightly narrower than for the measured profile because the HEU source does not emit photons uniformly in all directions and the source was pointed perpendicular to the direction of travel. This results in the count rate for the measured profile falling off quicker when the detector system is not directly aligned with the source.

Chapter 4. Results



(4.8.f) WGPu behind 2" HDPE shield with simulated vs. measured. For this configuration the simulated count rate profile agreed with the measured count rate profile very well, all of the data points in the trial having overlapping error bars.



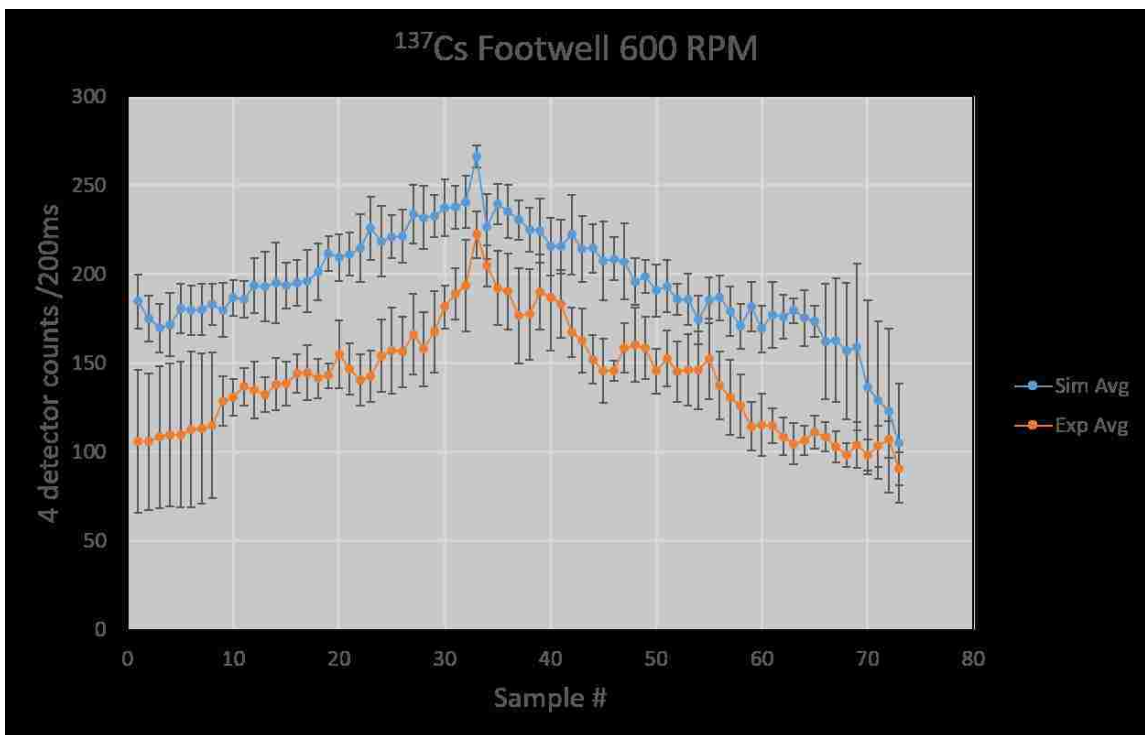
(4.8.g) WGPu behind $\frac{1}{4}$ " steel shield with simulated vs. measured. For this configuration the simulated count rate profile agreed with the measured count rate profile very well, all of the data points in the trial having overlapping error bars.

Figure 4.8: Drive-by comparisons of shielded source measurements versus simulated drive-by trials.

Chapter 4. Results

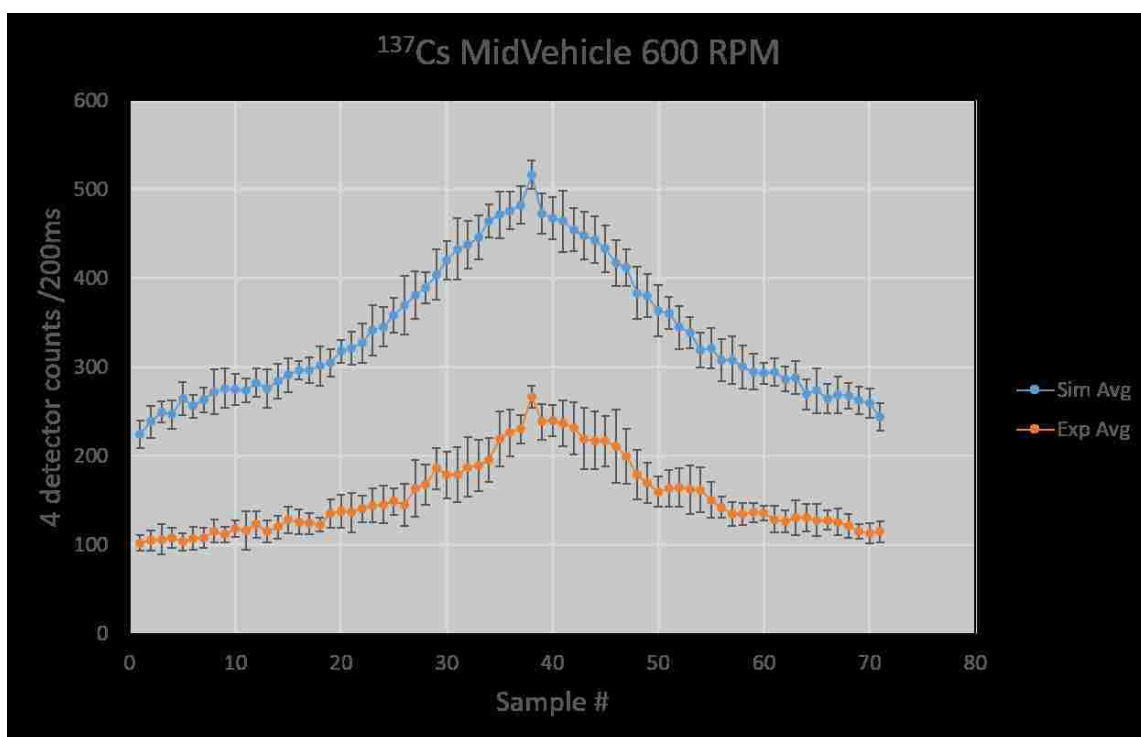
Figure 4.9 shows the cases where the source was placed inside of the “standard vehicle”. Quotation marks around standard vehicle are used here because these results are specific to the 2013 Hyundai Sonata that was used for the measurements and it is expected that differences in design will provide unique shielding and streaming paths across nearly all mid-sized sedans. It is hoped that the differences will be small enough that the results from this specific vehicle will be similar enough to provide an estimate on the detection performance of the RS-700 system against all mid-sized sedans. Work has not yet been done to characterize the detector response profile for a variety of mid-sized sedans to understand the range of shielding that can be seen among various vehicles of a similar size. This is discussed in Chapter 6, Future Work.

For the source in vehicle measurements, the source could not be placed 1.5 meters from the center of the reference detector, and therefore the ratio of the solid angle in the measurement configuration to the solid angle at 1.5 meters from the center of the detector was used to correct the source primitive before it was loaded into the simulation tool. This is done so that the source primitive differs from the bare source measurement only by the shielding from the vehicle and not from the change in solid angle between the source and detector. When the simulated trials were created, the correct source-to-detector distance and vertical height were entered on the UI to match the configuration in which the drive-by validation measurements were made. The source-in-vehicle primitive measurements were performed on a different day than the drive-by measurements, and it was assumed that the source location and positioning of the “standard vehicle” were consistent between the two sets of measurements. The distances were not explicitly measured, so it is an additional source of uncertainty that could be a reason for some of the discrepancies between the simulated and measured trials. 5 of the 7 source-in-vehicle drive-by trials had the simulated results outside of error bars of the measured results, as presented in Figure 4.9.



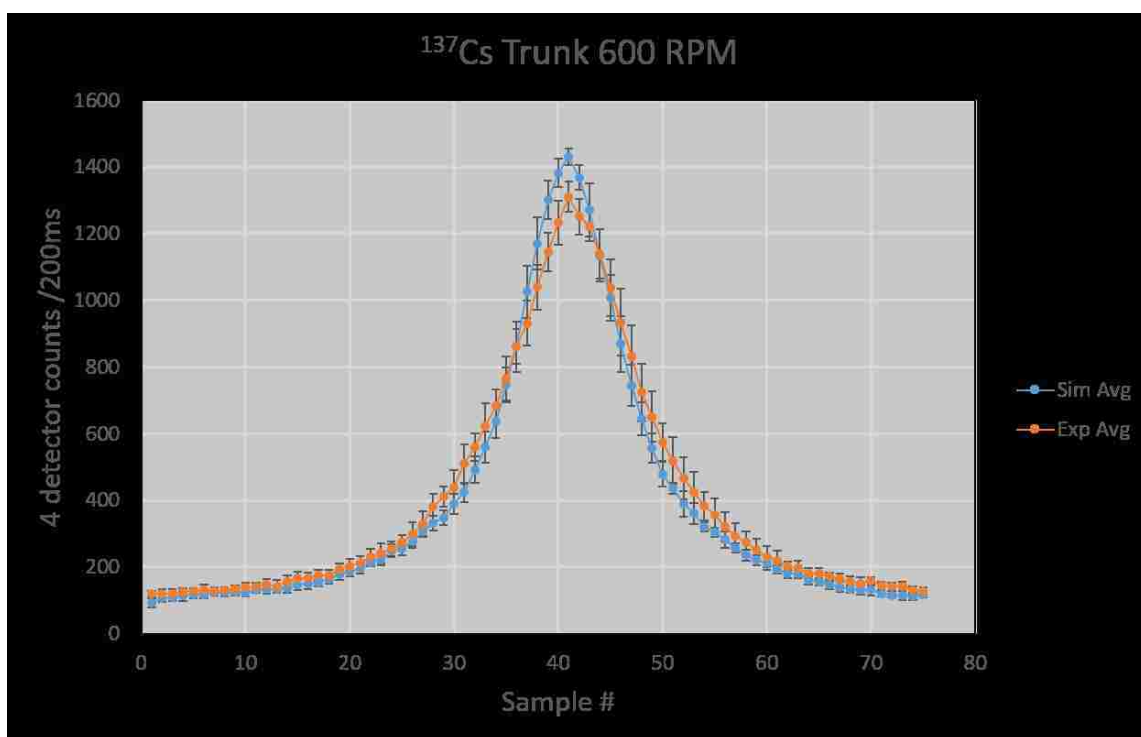
(4.9.a) ¹³⁷Cs placed in footwell with simulated vs. measured. The simulated trials over predict the detector response for all of the data points within the trials. An explanation for this is provided in the following paragraphs.

Chapter 4. Results

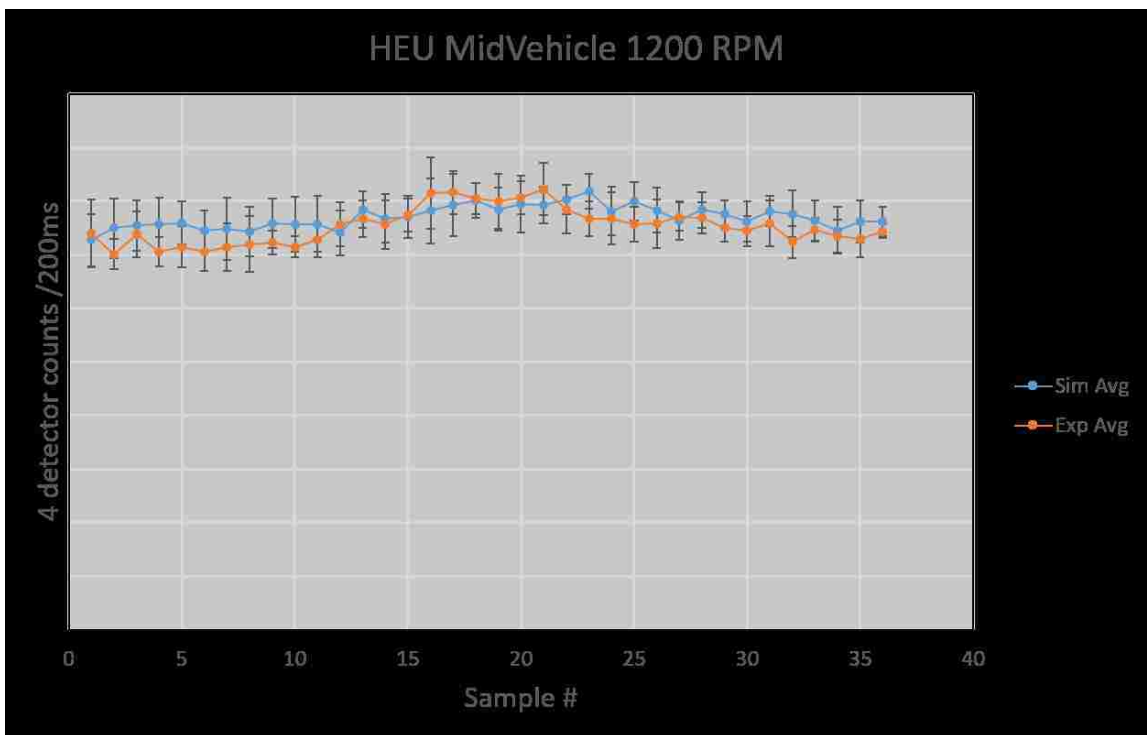


(4.9.b) ^{137}Cs placed mid-vehicle with simulated vs. measured. The simulated trials over predict the detector response for all of the data points within the trials. An explanation for this is provided in the following paragraphs.

Chapter 4. Results

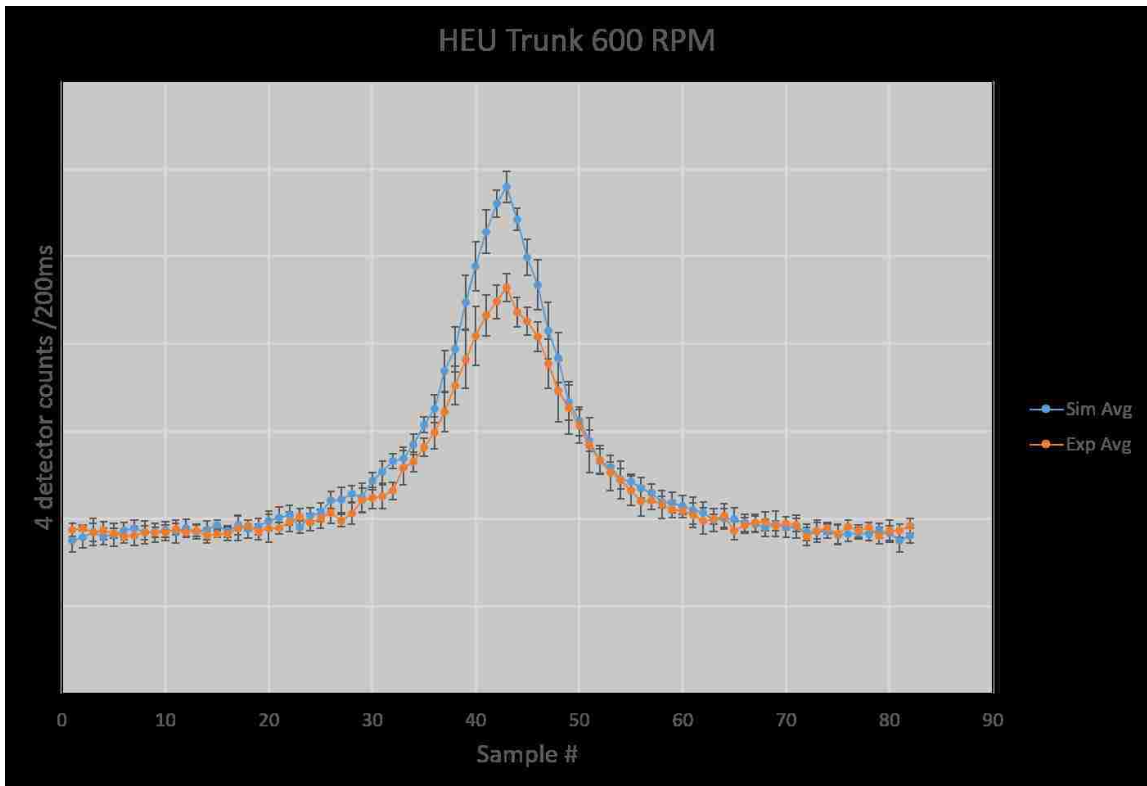


(4.9.c) ^{137}Cs in trunk with simulated vs. measured. For this configuration, the simulated trials match the measured data well, but slightly over-predict the detector response at the central peak of the profile.



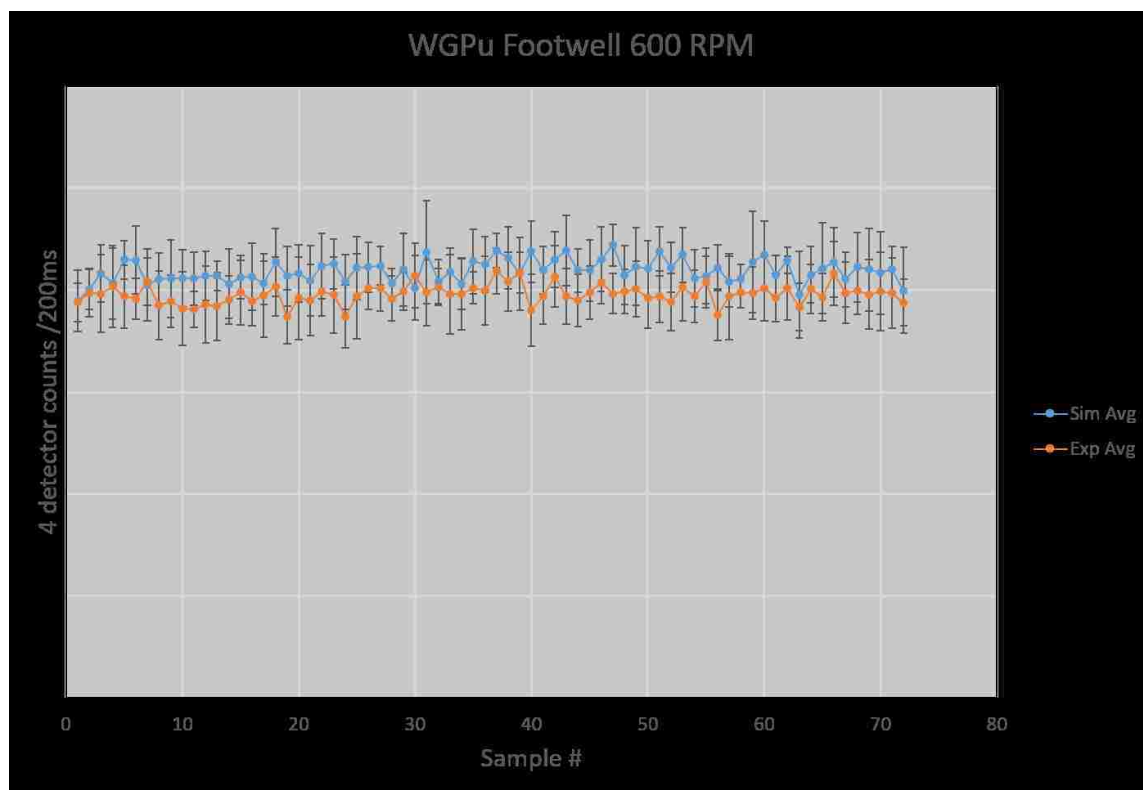
(4.9.d) HEU placed mid-vehicle with simulated vs. measured. For this configuration, the source signal is barely seen above the background, but the simulated data matches the measured data very well, with all of the data points having overlapping error bars.

Chapter 4. Results

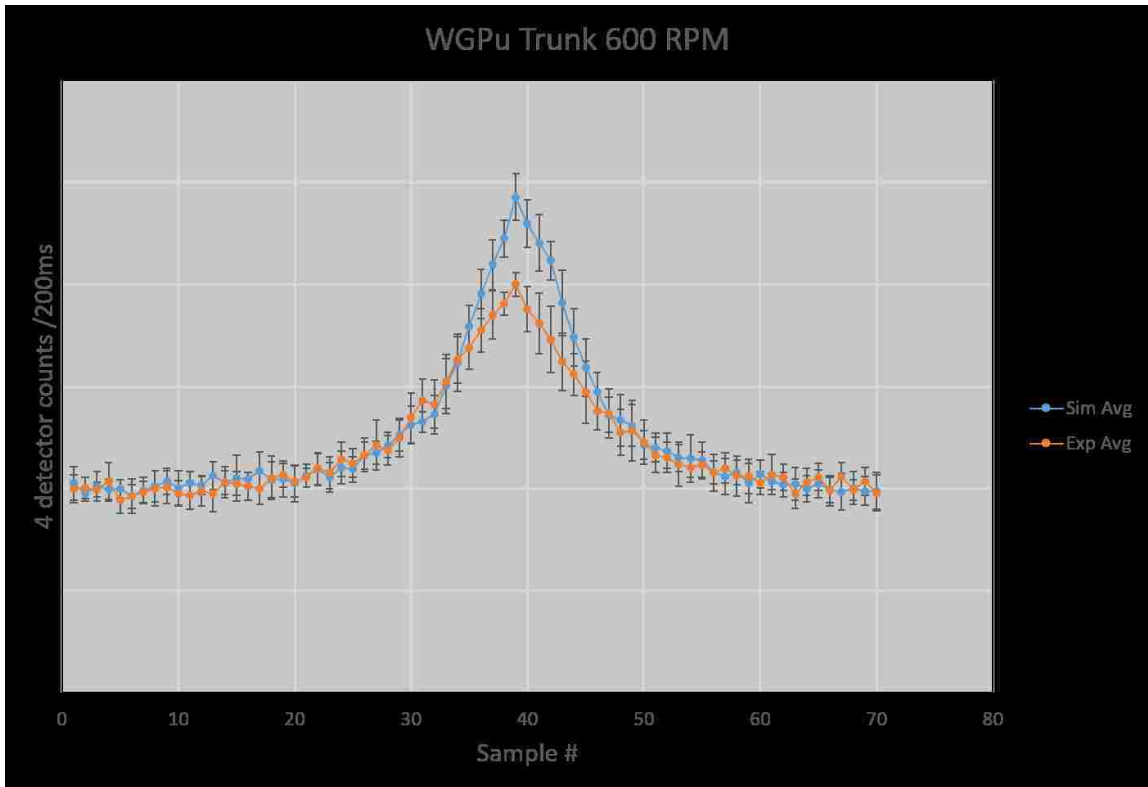


(4.9.e) HEU placed in trunk with simulated vs. measured. For this configuration, the peak of the profile is significantly over-predicted by the simulation output and does not agree with the measured data.

Chapter 4. Results



(4.9.f) WGPu placed in footwell with simulated vs. measured. For this configuration it is hard to tell if there is any contribution from the source, or if the profile is only displaying the background radiation. The simulated results agree with the measured results very well and all data points have overlapping error bars, though this is almost a null result as there is no clear peak, only background.

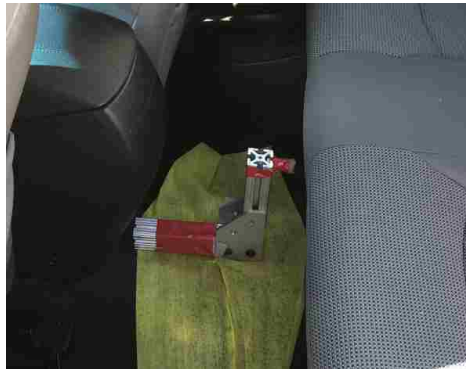


(4.9.g) WGPu in trunk with simulated vs. measured. For this configuration, the peak of the profile is over-predicted by the simulation output and does not agree with the measured data.

Figure 4.9: Drive-by comparisons of sources located in a vehicle measurements to simulated drive-by trials.

Chapter 4. Results

Figures 4.94.9.b and 4.94.9.a show a large discrepancy between the drive by measurements and the drive by simulations; which is explained by a change that was made to the source holder for the ^{137}Cs source between the time of the dwell measurements for the source-in-vehicle primitive and the source-in-vehicle drive-by. Figure 4.10 shows the two source holders that were used. The taller source holder (Figure 4.104.10.a) likely placed the source in a position that allowed less shielding material between the source and the reference detector module, which is the reason for the much higher predicted count rate due to the source located in the middle of the vehicle and in the footwell. The change to the shorter holder was made to fit the source and holder inside of the shields that were used, and this change was overlooked when the drive-by verification measurements were being made. It is likely that the results would have been much closer if the taller source holder was used for the in-motion measurements inside the vehicle.



(4.10.a) Taller source holder used for source-in-vehicle basis set measurements.



(4.10.b) Shorter source holder used for source-in-vehicle in-motion validation measurements.

Figure 4.10: Two different source holders used for ^{137}Cs measurements.

There were several reasons for performing an additional set of verification mea-

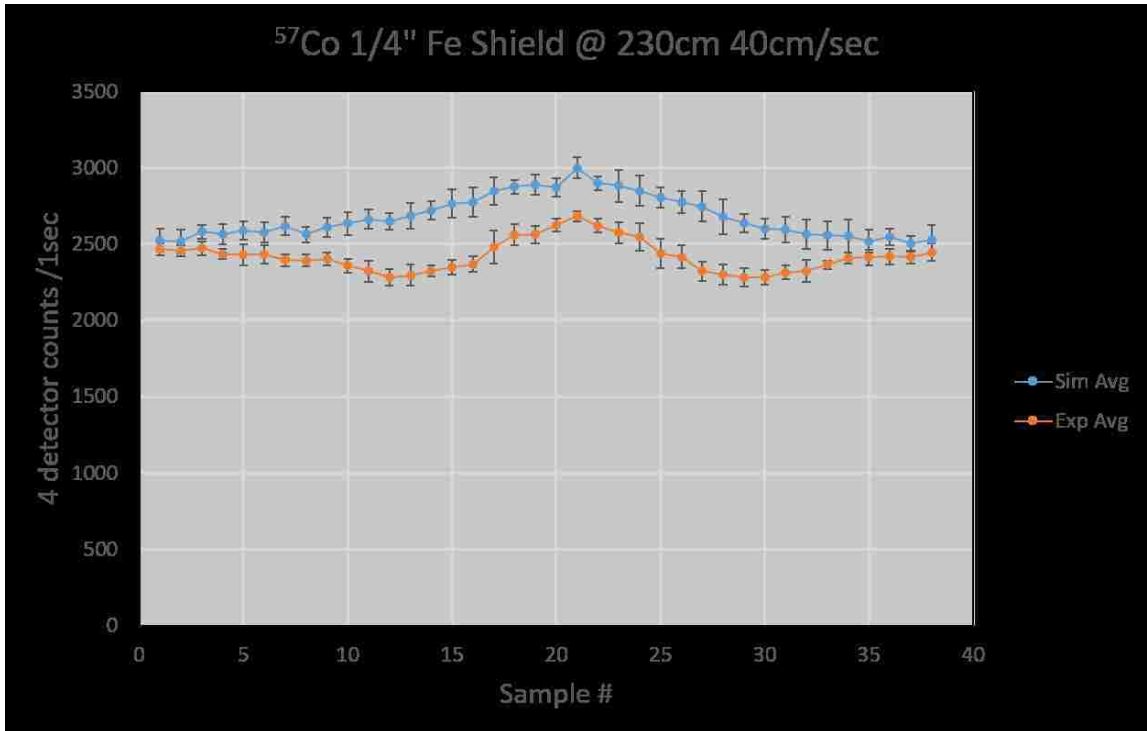
Chapter 4. Results

measurements using a second RS-700 detector system mounted on the gantry located at LANL's TA-16 Tumbler Road Test Bed. First, the gantry set-up has a programmable drive motor that maintains a constant speed throughout the entire area in which a scan is taking place. The gantry also prevents lateral movement in the detector system and therefore the source-to-detector distance remains constant for each of the 10 trials in a given configuration. By using a different RS-700 system, good agreement with the simulation results are not only valid for the system that was used to make the basis set of measurements. And lastly, a second set of sources with much lower activity were used so that the scaling capability of the simulation tool could be verified. To create the simulated results, the detector configuration was changed to match the configuration on the gantry, but the source primitives and cubic spline parameters were kept the same. The scaling factors for the sources were set by taking the activity of the gantry sources and dividing them by the activity of the basis set sources. For example, the scaling factor to reproduce the source IS200 was $\frac{4.137 \mu Ci}{250 \mu Ci} \times 100\% = 1.65\%$. Figure 4.11 shows the simulated vs. measured results for the measurements made on the gantry. The measured results all show a slight dip before increasing when approaching the source. This slight dip is likely due to background suppression caused by the flatbed trailer that is parked parallel to the gantry track in order to provide a level surface at the same height as the gantry cart. The simulated results were set to randomly sample the background variation CDF.

Of the 8 gantry verification measurements, only one of the configurations showed the simulated results in agreement within error bars of the measured results. However, if the background suppression is accounted for by adding an offset to the measured count rate values that is equal to the suppression that is seen, then the simulated results are in agreement with measured results 5 out of 8 times, but still over-predict the response profile. To get the amount of background suppression adjustment, the average of the lowest two consecutive data points was subtracted from the average of the first two data points for the measured trials. This method

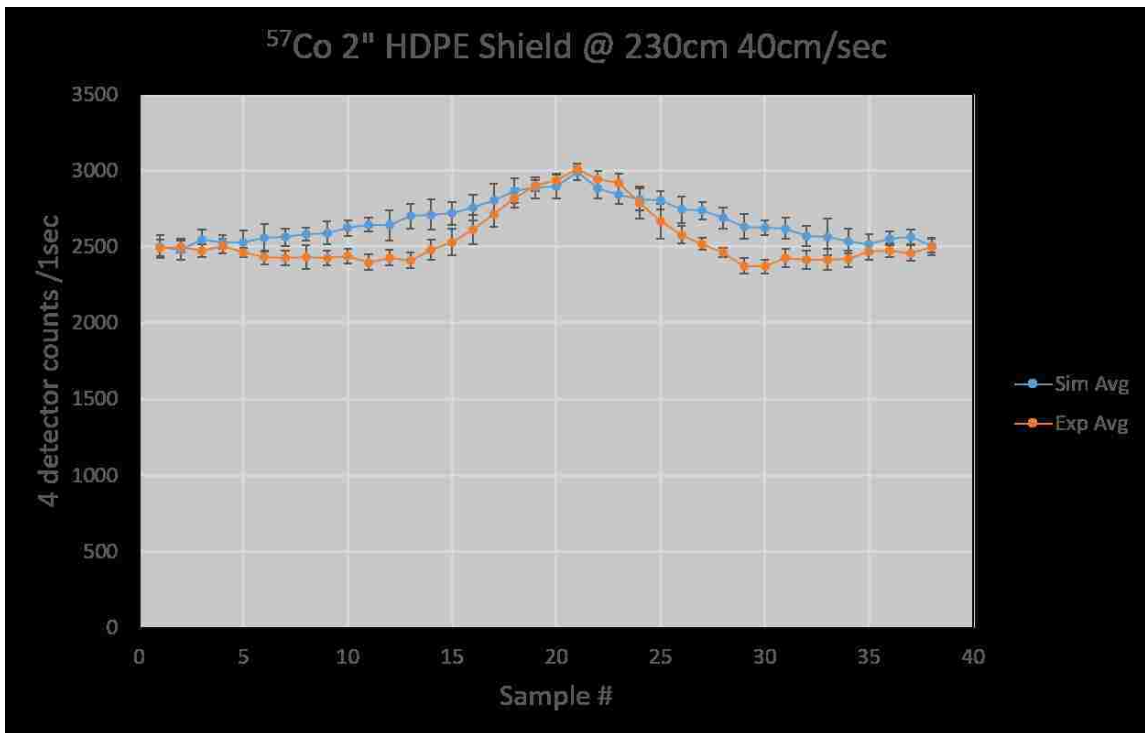
Chapter 4. Results

of determining the suppression is likely estimating a lower value for the background suppression because the two data points that are used for the greatest amount of suppression are likely seeing some photons from the source. Additional measurements should be made to characterize the background suppression seen on the gantry set-up.

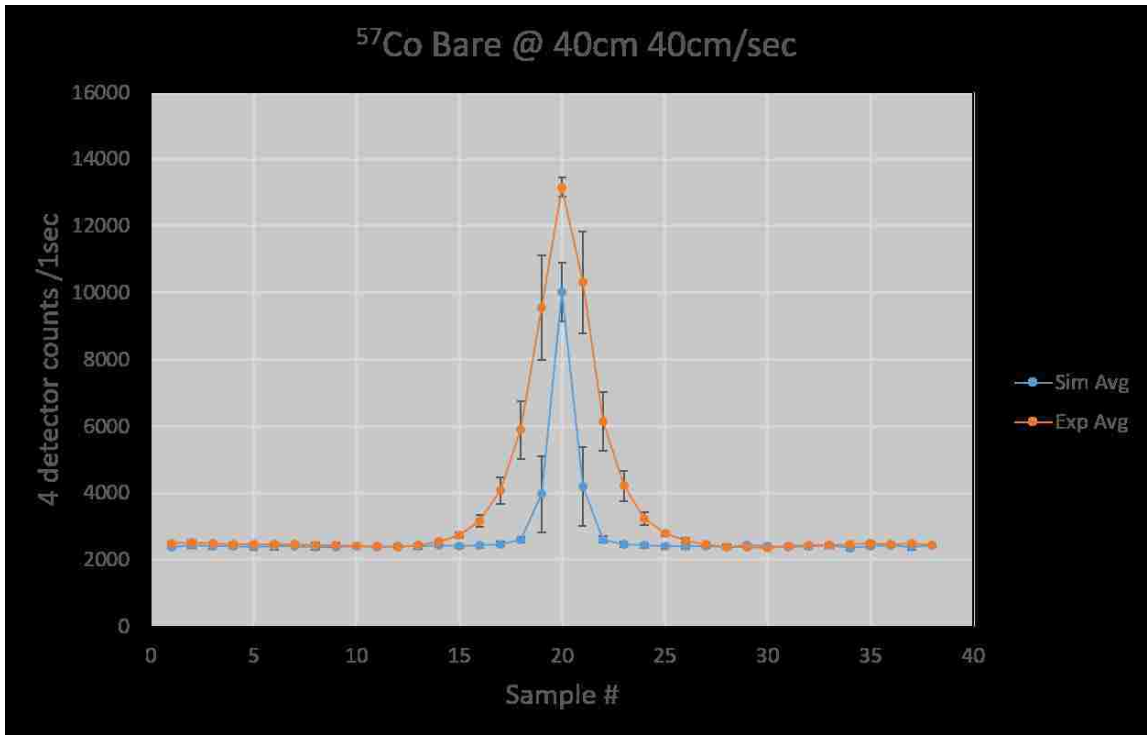


(4.11.a) ^{57}Co behind $\frac{1}{4}$ " steel shield on the gantry, comparing simulated results vs. measured results. Simulated results over-predict the detector response profile when the background suppression effects are not accounted for.

Chapter 4. Results

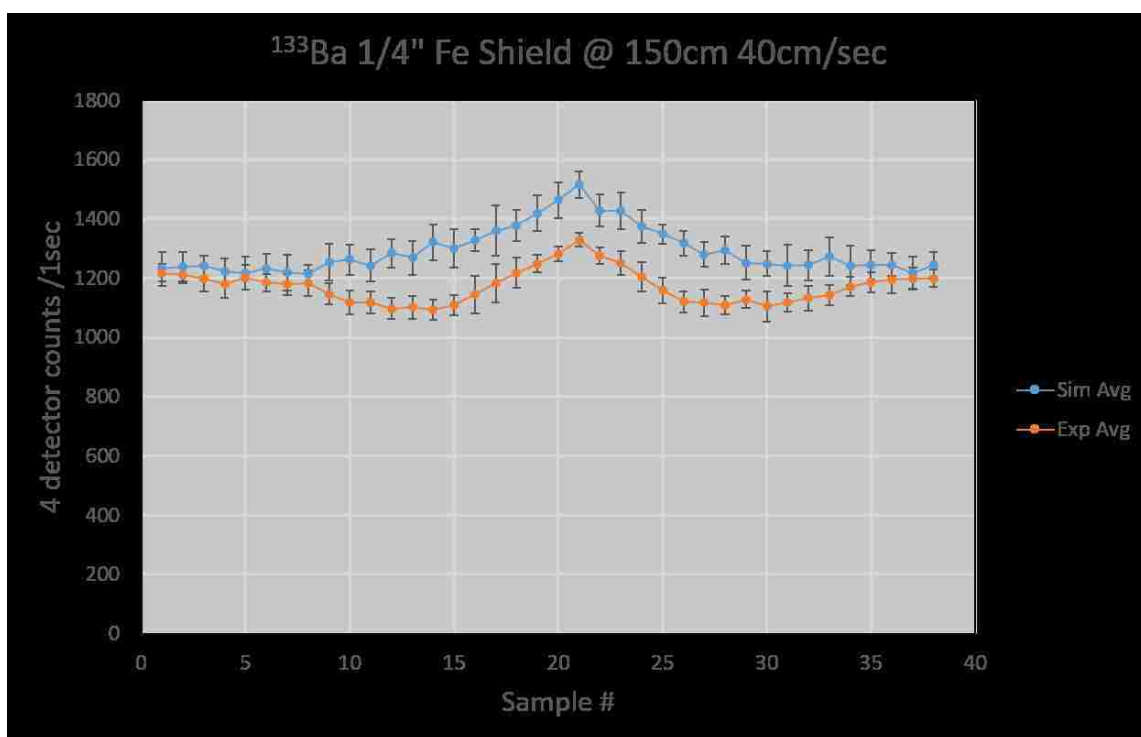


(4.11.b) ^{57}Co behind 2" HDPE shield on gantry, comparing simulated results vs. measured results. Simulated results are in agreement with measured results at the peak of the profile, but have a much wider shape than the experimental data, which could be caused by suppression in the background signal on the measured data.



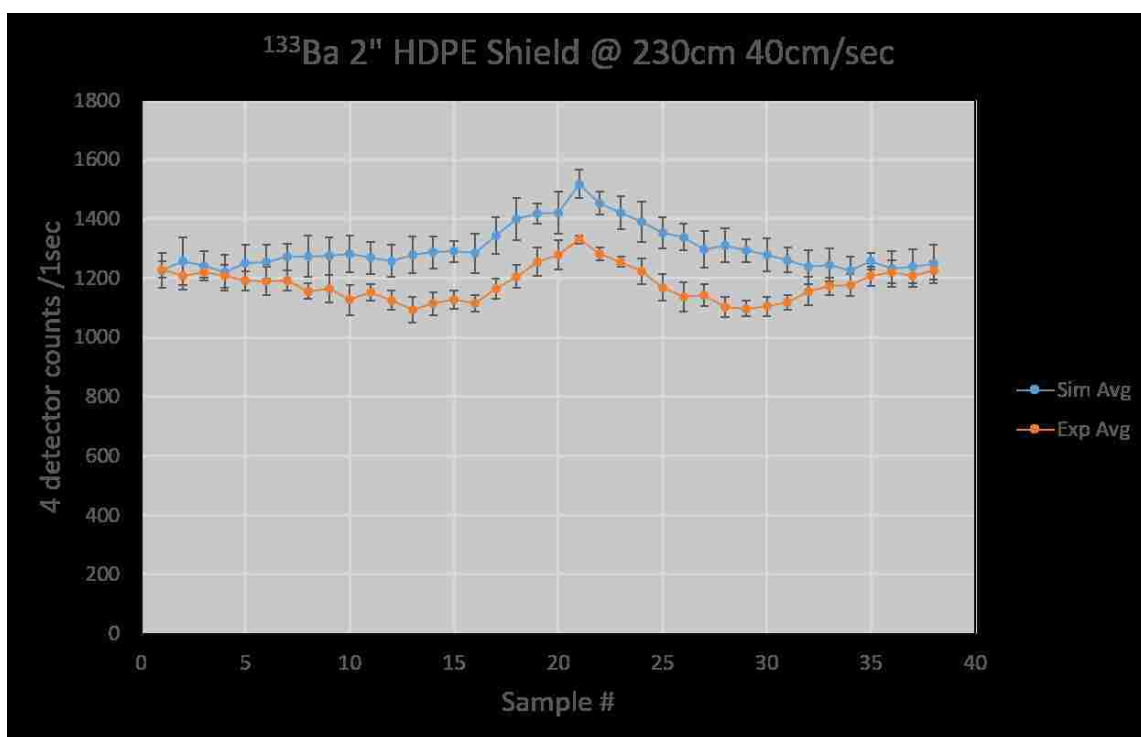
(4.11.c) ^{57}Co bare source on gantry, comparing simulated results vs. measured results. For this configuration the simulated results are significantly lower than the measured results. We suspect that this is because the source is located at a distance of only 40cm and there is a significant contribution of the signal seen by the detector that is coming in through the side of the detector. Since the simulated trials do not include the sides of the detector in the solid angle calculations, they under-predict the detector response for configurations that have a small source-to-detector distance.

Chapter 4. Results



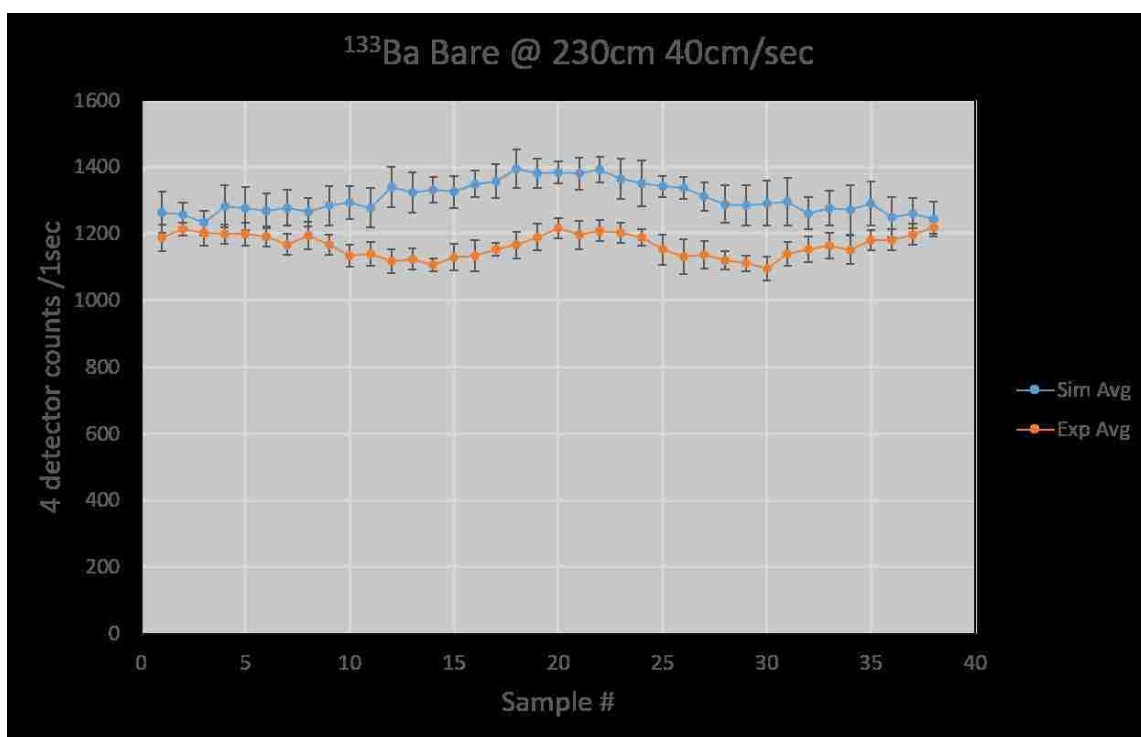
(4.11.d) ^{133}Ba behind $\frac{1}{4}$ " steel shield on gantry, comparing simulated results vs. measured results. Simulated results over-predict the detector response profile when the background suppression effects are not accounted for.

Chapter 4. Results



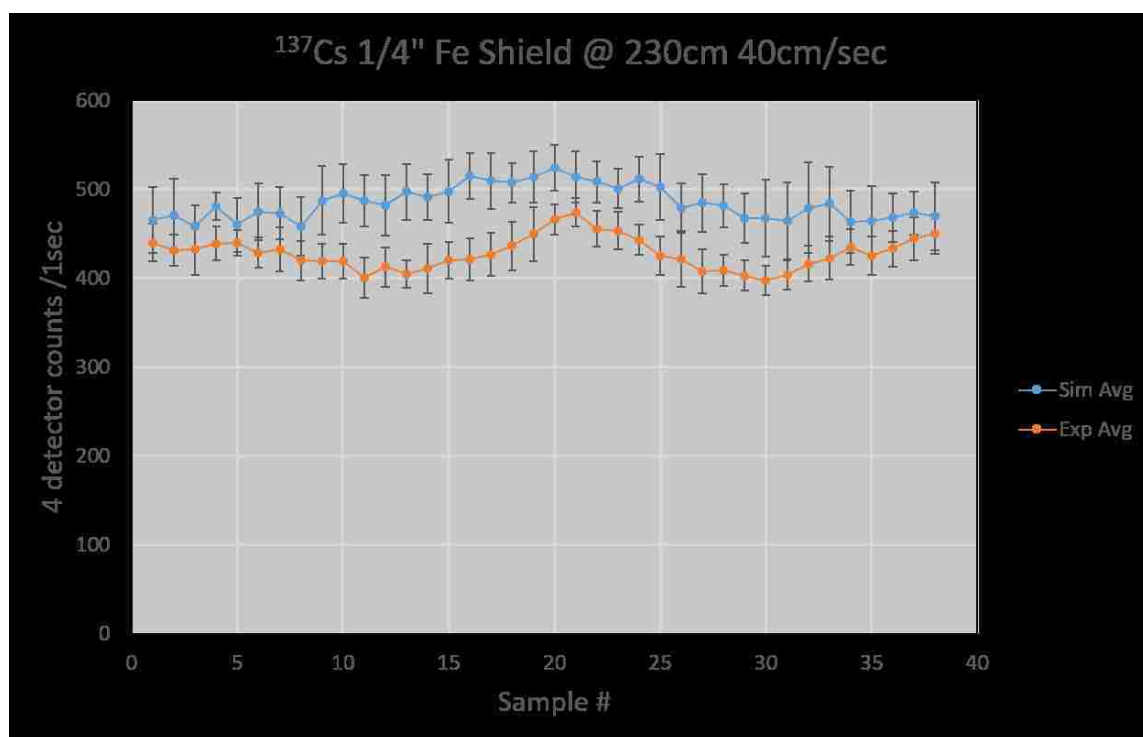
(4.11.e) ^{133}Ba behind 2" HDPE shield on gantry, comparing simulated results vs. measured results. Simulated results over-predict the detector response profile when the background suppression effects are not accounted for.

Chapter 4. Results

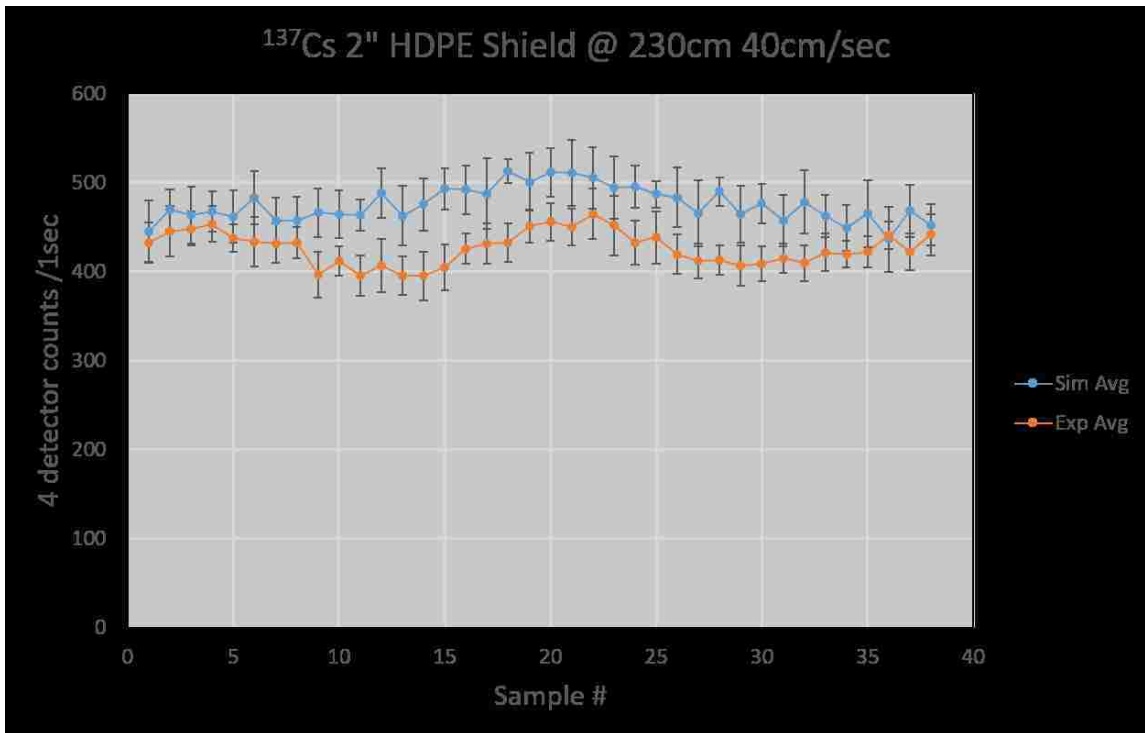


(4.11.f) ^{133}Ba bare source on gantry, comparing simulated results vs. measured results. Simulated results over-predict the detector response profile when the background suppression effects are not accounted for.

Chapter 4. Results



(4.11.g) ^{137}Cs behind $\frac{1}{4}$ " steel shield on gantry, comparing simulated results vs. measured results. Simulated results over-predict the detector response profile when the background suppression effects are not accounted for.

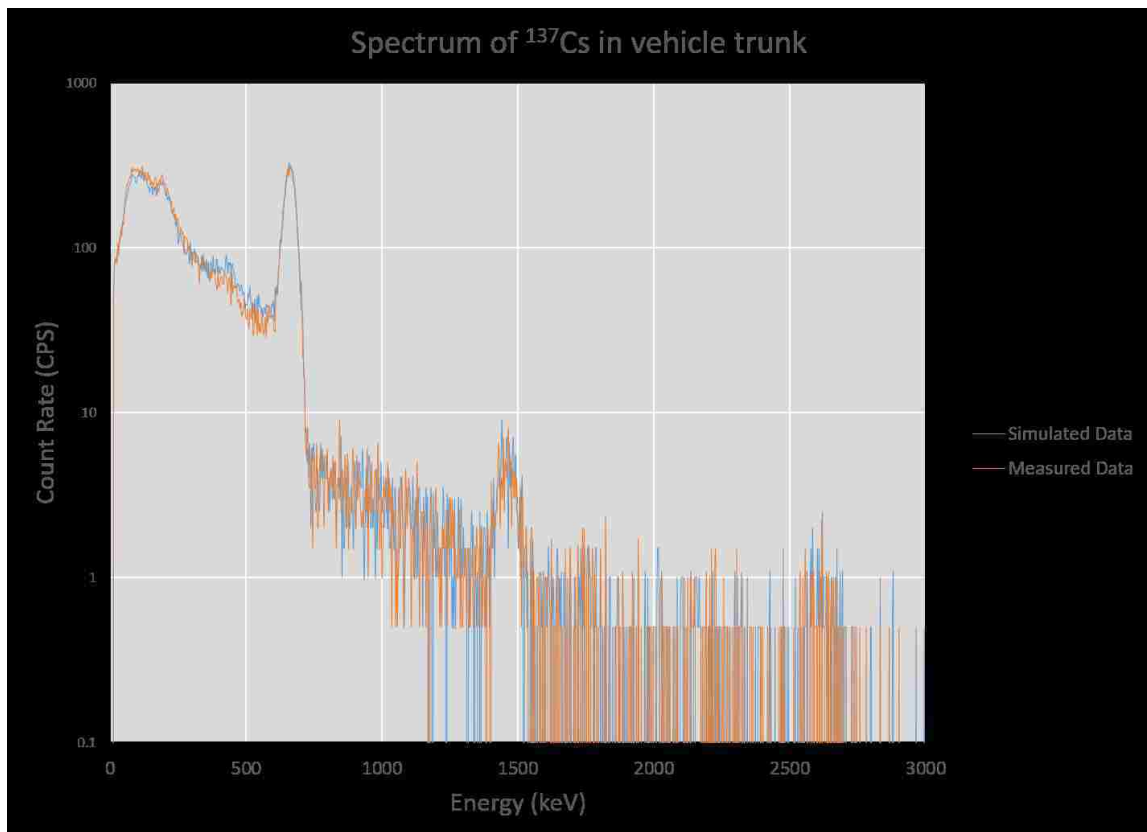


(4.11.h) ^{137}Cs behind 2" HDPE shield on gantry, comparing simulated results vs. measured results. Simulated results over-predict the detector response profile when the background suppression effects are not accounted for.

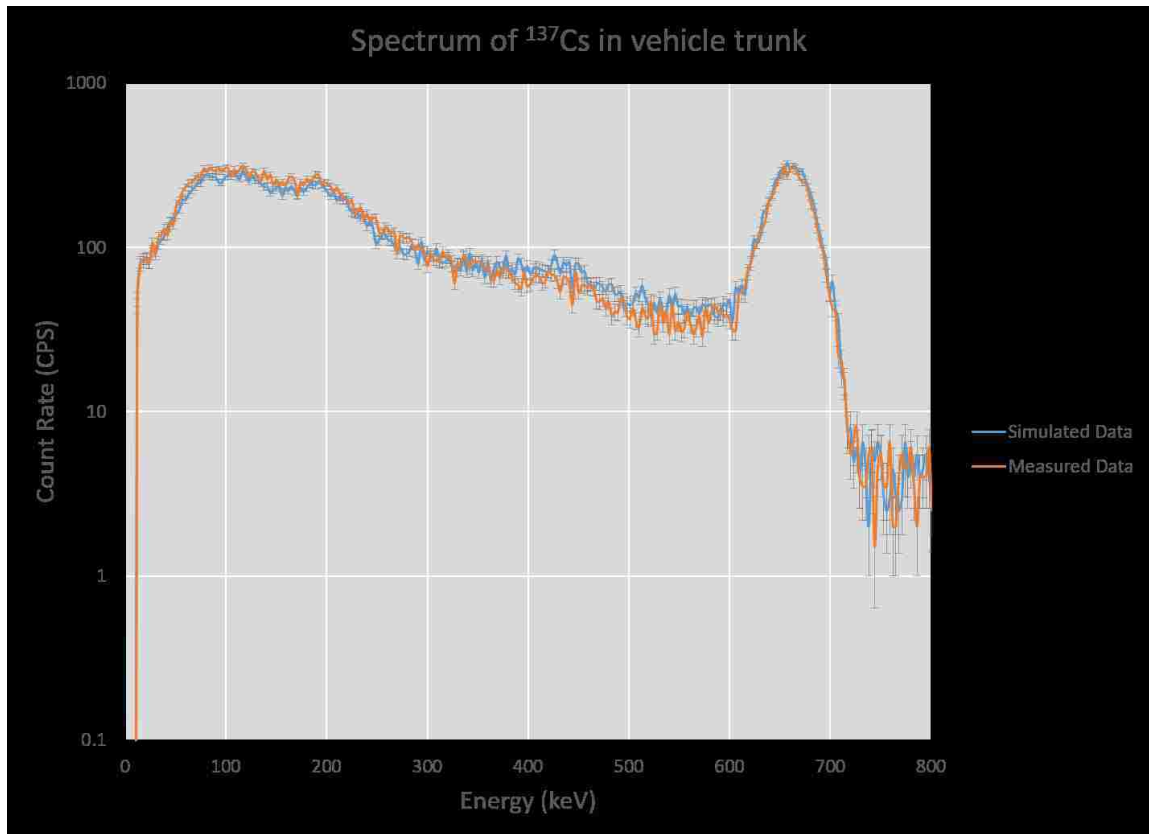
Figure 4.11: In-motion gantry comparisons of source measurements to simulated trials.

Chapter 4. Results

While the count rate profile in the ROI is important to compare for validation of the simulated detector response, it is also important to compare the shapes of the entire measured and simulated spectra. Since the details of the RSI TIA are proprietary information, it is not known how much of an impact shape of the full energy spectrum will have on the TIAs ability to identify specific isotopes. For the drive-by trial with the ^{137}Cs located in the trunk, the full energy spectra of the simulated and measured trials were compared for the sample that had the greatest count rate in the ROI. The spectrum for a ^{137}Cs source that is placed into the trunk of a vehicle is shown in Figure 4.12.a and Figure 4.12.b shows the portion of the spectrum that contains the photopeak and Compton continuum. It can be seen that the simulated output very closely matches the spectrum that was measured.



(4.12.a) ^{137}Cs simulated vs. measured full energy spectrum.



(4.12.b) ^{137}Cs simulated vs. measured spectrum 0-800keV with one-sigma error bars.

Figure 4.12: Spectrum at point of shortest distance for ^{137}Cs placed in the trunk of a vehicle.

4.5.2 TIA Comparison

RSI's RadAssist software contains a TIA that analyzes spectra and assigns a signal-to-noise ratio (SNR) value to each isotope that it suspects is present in each spectrum, which is used as an indicator of how confident the algorithm is in its identification. The SNR value assigned by the proprietary algorithm is compared with the traditional measurement of SNR in Figure 4.16 to understand what the TIA means by SNR, and appears close to a traditional sense of a signal-to-noise ratio. For every isotope in the library, the user can define an alarm threshold. If the SNR for a given

Chapter 4. Results

measurement exceeds the threshold, then that isotope is displayed on the RadAssist UI. By adjusting the threshold for each isotope, the user can optimize sensitivity and false alarm rate for each isotope. Since RSI's algorithm is proprietary information the author of this paper cannot make any definitive statements about how the SNR value is calculated, but because of the replay capability of the RadAssist software, the SNR values from the validation measurements can be compared to the SNR values of the simulated trials. Table 4.4 shows the number of trials (out of 10) where the isotope was correctly identified, as well as the corresponding SNR values for both the simulated trials and measured trials. The results include both drive-by verification measurements as well as gantry verification measurements and the alarm thresholds that were chosen are the default settings recommended by RSI. In many of the configurations, 10 correctly identified out of 10 does not help discern the differences between the TIA's handling of simulated vs. real data. Changing thresholds changes the number identified correctly in both simulations and measurements, and are investigated later in this section. These results are depicted graphically in Figure 4.13 with the configuration numbers corresponding to the order of the configurations listed in Table 4.4. By removing the uncertainty in the source-to-detector distance and in the speed, the SNR values from the gantry validation measurements generally show better agreement between the simulated and measured results. The SNR values for trials with SNM or DU sources are not included in this thesis since it may be sensitive to show how well a specific detection system performs against these sources.

Table 4.4: RSI Replay Results.

#	Configuration	Simulated Correct ID	Simulated SNR	Measured Correct ID	Measured SNR
1	^{133}Ba Fe 900RPM	10	22.5 ± 0.7	10	20.4 ± 0.9
2	^{57}Co Bare 600RPM	10	46.4 ± 0.3	10	43.0 ± 0.8
3	^{137}Cs Footwell 600RPM	10	14.6 ± 0.6	10	11.5 ± 0.7
4	^{137}Cs MidVehicle 600RPM	10	25.0 ± 0.3	10	14.3 ± 0.5
5	^{137}Cs Trunk 600RPM	10	37.5 ± 0.3	10	36.7 ± 0.8
6	1820-84-3 Fe 230cm	10	10.1 ± 0.4	10	8.9 ± 0.3
7	1820-84-3 HDPE 230cm	10	10.1 ± 0.5	10	12.2 ± 0.3
8	1820-84-3 Bare 40cm	10	33.8 ± 0.6	10	43.4 ± 0.6
9	FN-591 Fe 150cm	4	3.0 ± 0.4	2	3.1 ± 0.7
10	FN-591 HDPE 150cm	5	3.5 ± 0.6	3	4.0 ± 0.5
11	FN-591 Bare 230cm	5	4.5 ± 0.9	2	4.3 ± 0.4
12	IS200 Fe 230cm	10	6.2 ± 0.5	10	5.9 ± 0.6
13	IS200 HDPE 230cm	10	6.0 ± 0.7	10	6.1 ± 0.8

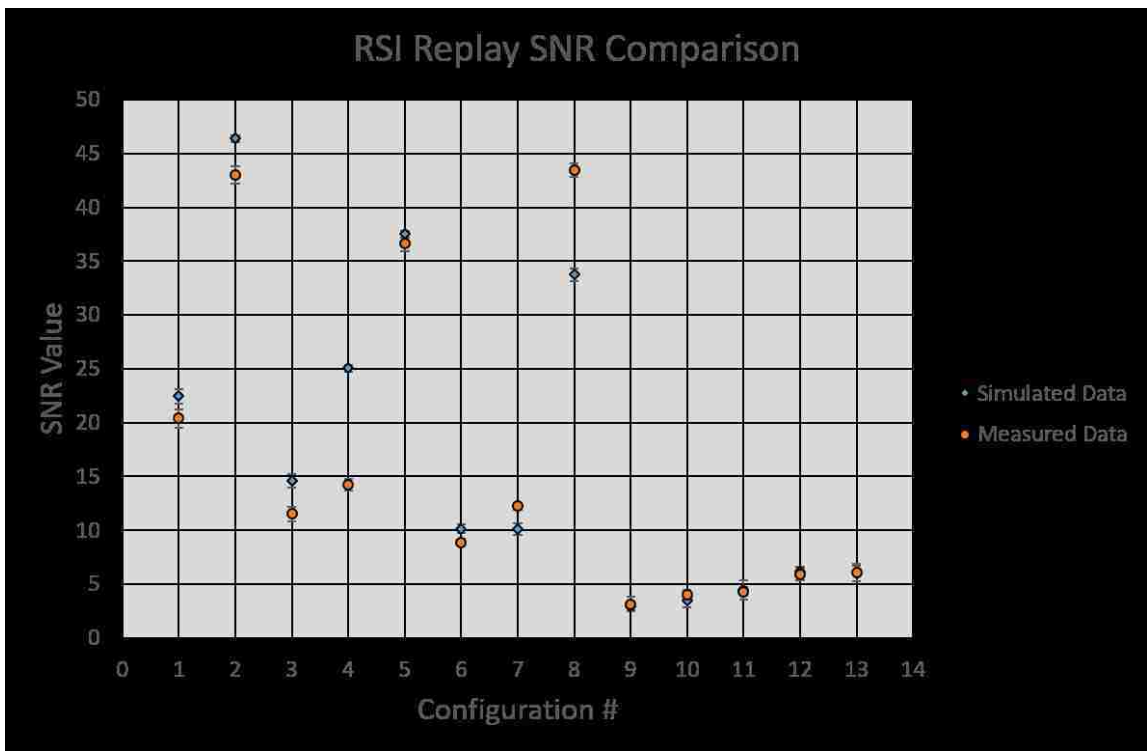


Figure 4.13: Comparison of SNR values.

Chapter 4. Results

In order to determine whether or not the output of the TIA between the simulated and measured data were acceptable, the ratio for the SNR of the simulated data to the measured data were calculated and deemed acceptable if the value of that ratio was within 20% of 1.0. Figure 4.14 shows the value of these ratios and also includes the configurations in which SNM or DU sources were present. The SNM and DU results can be included here because the ratio of the simulated to measured SNR value does not give any information about how well the TIA was able to identify a particular source, it simply compares the TIA's confidence in the simulated result to its confidence in the measured result. 19 out of 23 trials have a ratio of SNRs that is within 20% of 1.0. For the 23 configurations displayed in Figure 4.14, the average ratio of simulated SNR to measured SNR is 1.07 ± 0.03 which should correspond with the TIA correctly identifying the simulated results more often than the experimental results, but it is well within the acceptable value of 20%. If the configurations for ^{137}Cs located mid-vehicle and in the footwell are removed due to the known measurement error that was incurred by using the wrong source holder, the average ratio of simulated SNR to measured SNR drops to 1.03 ± 0.03 .

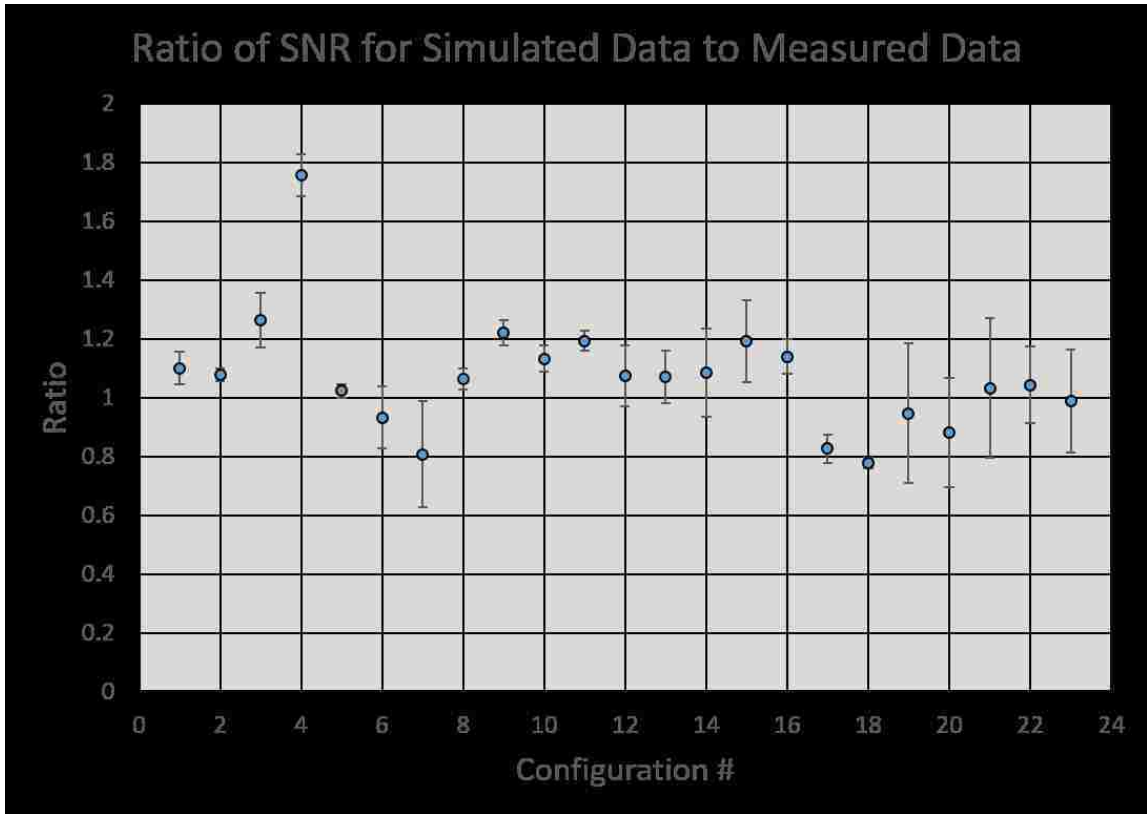


Figure 4.14: Ratio of the SNR from simulated results to the SNR from measured data.

Since many of the test configurations used in this report had an RSI algorithm output SNR value that was significantly higher than the alarm threshold on the RadAssist software, purely stating the correct number of isotope identifications out of the 10 trials is not a useful comparison to evaluate how well the simulated data matches the measured data. Figure 4.15 shows the percent of correct identifications as a function of alarm threshold for both the simulated and measured trials. This plot is not intended to evaluate the performance of the RSI system, only as an overall measure of how well the simulated data fed to the TIA gives the same results as measured data fed to the TIA. Since the plot shows 25 different configurations with varying source strengths and isotopes, the plot shows that for a large range of SNR values, the simulated results continue to track well with the measured data.

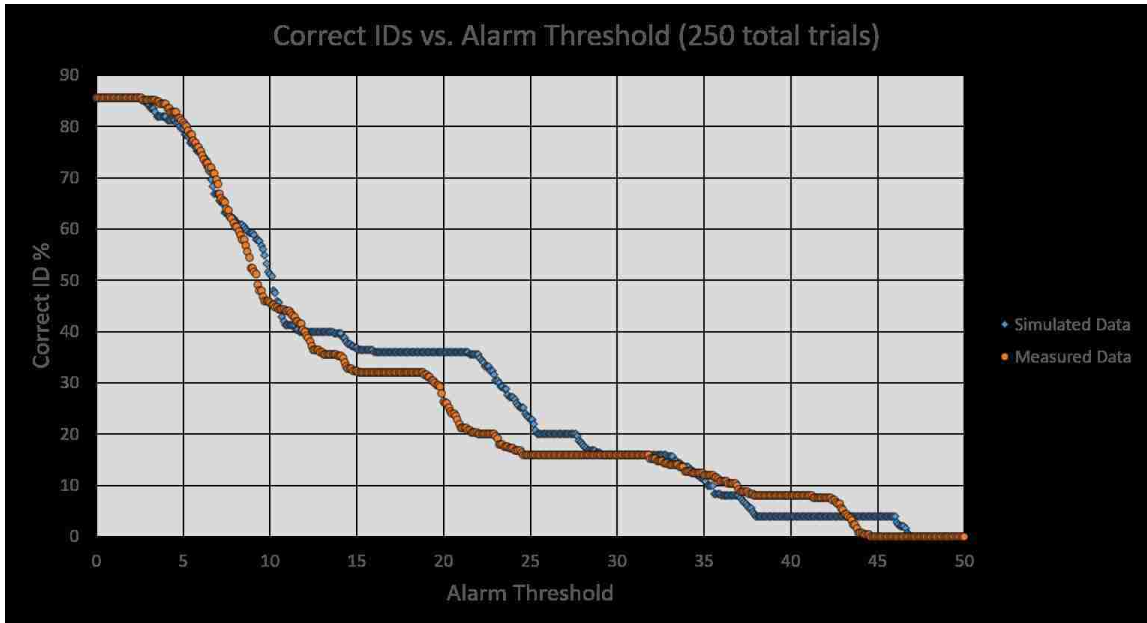


Figure 4.15: Percent of correct identification for all 250 trials; simulated results vs. measured results.

An example of how the RadAssit alarm algorithm could be evaluated is shown in Figure 4.16 where the injected source strength (plotted as injected SNR) is plotted versus the RSI output SNR. For this plot, the simulation tool was used to scale the ^{137}Cs primitive to 7 different source strengths, and all other parameters were kept fixed. The detector configuration was also changed so that only one detector was included in the simulation. 10 simulated trials for each source strength were created and fed into the RadAssit software. The alarm algorithm has the ability to make alarm decisions using multiple integration times for each one second sample update, but for this analysis the algorithm was limited to a one second integration time to make the comparison between injected SNR and RSI output SNR. The vertical error bars on the figure represent one standard deviation for the 10 trial average RSI output SNR, and the horizontal error bars account for two sources of uncertainty in the injected SNR. Since the simulation tool randomly selects the starting location for each trial, the one second integral of the detector response profile that encompasses

Chapter 4. Results

the center of the response profile will vary slightly between each trial, which is the first source of uncertainty. The second source of uncertainty comes from the Poisson variation that is applied randomly to each channel in the spectrum for each trial. As expected, an increasing injected SNR corresponds to an increasing RSI calculated SNR value. A plot like this could be useful for determining the minimum detectable quantity of a specific isotope in a specific configuration. For a pre-defined alarm threshold, with all parameters in the configuration except source strength fixed, a linear trendline fitted to this plot could be used to determine what injected SNR would produce an RSI calculated SNR that is greater than the alarm threshold.

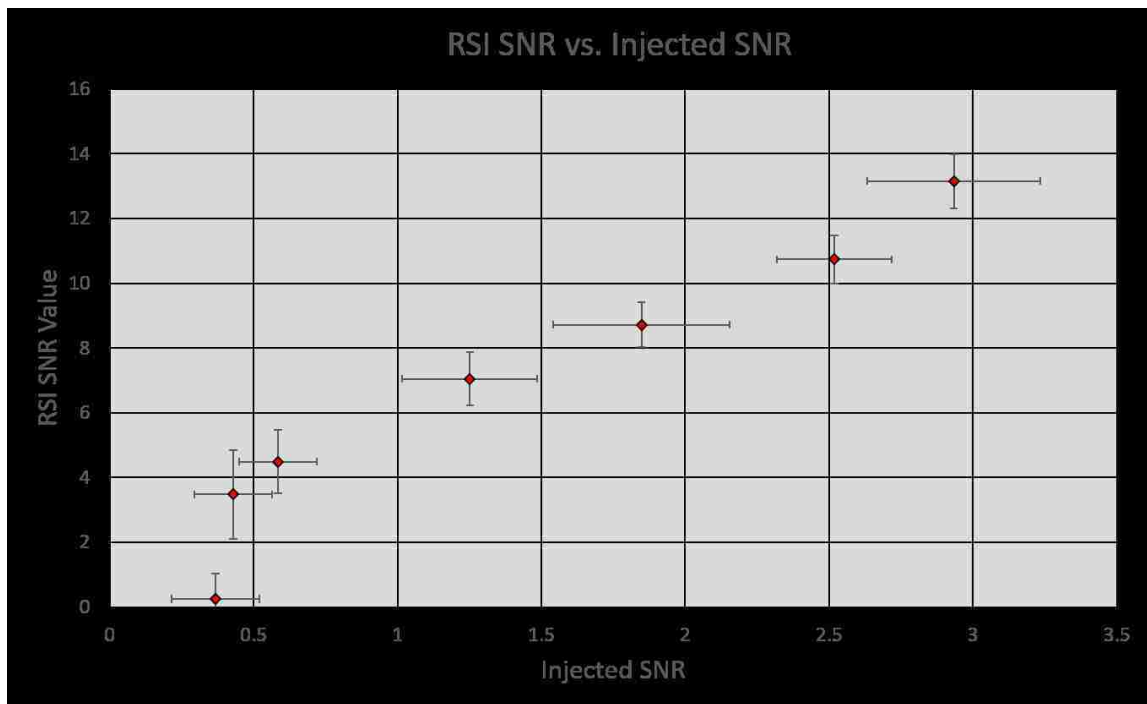


Figure 4.16: RSI algorithm output SNR vs. simulated injected SNR.

4.6 Assumptions and Limitations

The biggest limitation to the simulation tool, as it's currently implemented, is that for configurations other than a bare source, the shielding is assumed to be uniform in all directions. There is no mechanism in place to account for streaming paths or for varying path lengths through a shield. An example of how this limitation could impact the results was seen in the comparison of the source in vehicle drive by comparisons. If the shielding is fixed in relation to the detector array, then the flexibility of the cubic spline interpolation will be able to account for it.

In this case, the drive-by experiments identified the correct isotope 7 times out of 10 trials, but when the simulated results were fed into the RadAssist replay tool, this isotope was identified 0 out of 10 trials. It was determined that for the 7 experimental trials that correctly identified the isotope, all of the identifications came from one of the upper detectors. Looking back at the dwell measurement that was used to create the source primitive that was loaded into the simulation tool, it was noted that even though the solid angle to the upper detectors was less than the solid angle to the lower detectors, the upper detectors recorded more net counts in the photopeak than the lower detector. By changing the primitive spectrum from the spectrum measured with detector 1 to the spectrum measured with detector 2 (and correctly adjusting based on the ratio of one solid angle to the other), the simulated results produced an output that was identified 10 out of 10 trials. These results are summarized in Table 4.5. The reason for the difference is that in the vehicle that the source was placed, there was less shielding material in the path of the photons that were traveling to the upper detectors than there was in the path of the photons going to the lower detectors. Since a single source primitive is used to predict the detector response of all detectors in the simulation, there is no mechanism in place to account for different shielding material or thicknesses between the different detectors and the source.

Chapter 4. Results

Table 4.5: Effect of primitive used.

Measured Correct ID	Simulated Correct ID Using Lower Detector	Simulated Correct ID Using Upper Detector
7/10	0/10	10/10

A similar example that was not seen in the validation measurements that were made, but could easily be imagined is the impact of streaming paths. For instance, if a source were located inside of a container of some sort and placed directly behind something that did a good job of shielding photons, then the detector would not see the source when it is directly in line, but offsetting the detector slightly (or performing an in-motion measurement) might allow the source to be seen streaming past the edges of the shielding material, depending on the geometry of the configuration. The simulation tool does not have a mechanism to account for this type of streaming path situation. A diagram and anticipated detector response profile is shown in Figure 4.17.

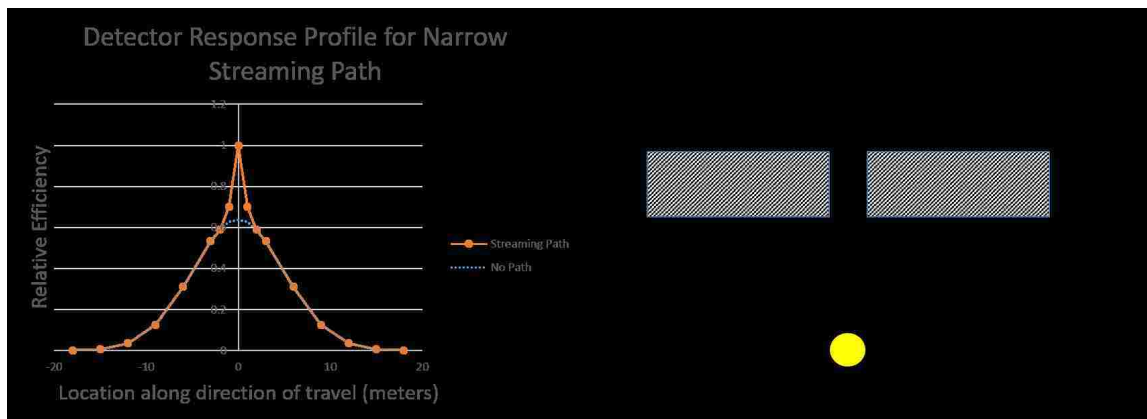


Figure 4.17: Illustration of detector response in the presence of a narrow streaming path.

For this thesis, a single “standard vehicle” was used to make the source in vehicle measurements and this limits the results to only being valid for a source in a Hyundai Sonata. Other vehicles that are similar in size may have different shielding material and/or thickness that would cause the detector response to vary significantly. The

Chapter 4. Results

Hyundai Sonata was chosen due to its availability to the author and the desire to include some results regarding the capability of simulating source in vehicle scenarios that may be encountered in real world situations, even if the validity of those results are limited to a single vehicle make and model.

The solid angle calculations only account for the front face of the detector and will under-predict the detector profile for configurations that have the source pass very close to the detector array (small source-to-detector distance). The solid angle contributions from the sides and top/bottom of the detector were left out of the simulation tool because they caused an over-prediction of the detector response profile for source-to-detector distances that are expected to be more commonly encountered ($\gtrsim 1.0$ m).

The simulation tool is intended to be used for determining the limits of detection for the detector system and therefore it is assumed that the effects of pulse pile-up and dead time losses will not have a significant impact on the simulated results and are ignored.

The simulation tool is currently limited to 25 sources with 10 configurations each. These values were chosen to encompass a reasonably large set of sources and configurations without having the application take up too much memory on the computer that is running the application.

Chapter 5

Conclusions

In this thesis work a simulation tool was created for sources in motion past detectors in a variety of realistic situations, with different background noise and shielding. The simulations were compared with real detector results. Both the simulation results and measured results were fed into a proprietary identification software to compare the software response in order to validate the simulations. We cannot make public the TIA results for each specific case, but we can compare results between simulated and experimental data for matching, though undisclosed, cases to show the goodness of the simulated data.

From the results presented, it can be seen that the simulation tool does a very good job at predicting the detector response for the sources used in this thesis. The majority of the validation measurement comparisons saw the simulated results agree with the measured data in both the ROI detector response profile and the Threat Identification Algorithm's identification ability. There were several cases that do not agree, and most of these discrepancies can be explained by uncertainty in the measurement setup, or limitations in the capability of the simulation tool to accurately model certain configurations such as very small source-to-detector distances,

Chapter 5. Conclusions

non-uniform shielding, streaming paths, and background suppression. The most likely cause is a significant uncertainty in the source-to-detector distances that was noted while driving the detector system past the sources for the in-motion validation measurements.

Of the 17 drive-by validation configurations, 10 had simulated data fall within the error bars of the measured data, with 5 of the 7 cases falling outside of this being source-in-vehicle trials. Source in vehicle results are expected to have the most uncertainty due to the non-uniform nature of the shielding that is encountered during a drive-by trial.

For the 8 gantry validation configurations, only 1 had agreement between the simulated and measured count rate ROI profiles, but this was due to background suppression that was caused by the flatbed trailer that the measurements were made on. By adjusting the measured profiles to compensate for the background suppression, 6 of the 8 configurations showed agreement between the simulated and measured results. Correctly modeling background suppression is a feature that will be addressed in future work.

When looking at the results for how the TIA performed between the simulated results and the measured results, there are two things that can be compared. The first is how many how many times the algorithm correctly identified the source for simulated vs. measured trials and the second is to compare the SNR value output from the TIA from simulated results to the SNR value output from the TIA of the measured data. For the correct identification rate, the algorithm correctly identified 114/130 from the measured data, and 107/130 for the simulated data. For many of the verification measurements, the source had a relatively high activity and it was quite easy for the algorithm to properly identify 10/10 trials for that configuration. In these cases, the comparison between measured and simulated results does not provide a lot of detail into how similar the spectra looked to the algorithm. Those

Chapter 5. Conclusions

identifications were performed using TIA recommended thresholds. Varying the thresholds to understand differences in results from simulated and measured data showed the correct number of identifications tracking fairly well between the sets. A much better metric to compare is the SNR value, which is a decimal value for how confident the algorithm is in a specific isotope. The value of the SNR was compared for all 130 verification measurements and the values from the simulated results track very well to the values of the measured data with the simulated results being slightly higher on average. The ratio of the SNR value from the simulated results to the measured results for all of the verification measurements is 1.07 ± 0.03 . Since the intended purpose of this simulation tool is to inform and reduce the effort required for a testing and evaluation campaign, 10-20% uncertainty is acceptable to provide useful information about what should or shouldn't be included a measurement campaign. The flexibility in the tool to be able to provide simulation results quickly and reliably for a large variety of configurations reduces its accuracy to some extent, but greatly increase its value to a program, such as the Office of Nuclear Smuggling Detection and Deterrence, that is interested in evaluating how a detector system will perform in a variety of environments and configurations.

Chapter 6

Future Work

Additional measurements should also be performed at greater speeds, non-uniform shielding, greater (and lesser) source-to-detector distances, and with varying source heights in order to gain additional information regarding how well the simulation tool can reproduce measured data under a greater variation of configuration parameters. In addition to this, it would be beneficial to investigate ways in which the uncertainty in the source primitives can be used to limit the scaling factors that are used in the simulation trials. By performing this sensitivity investigation, an estimate of the uncertainty for a given configuration can be made to better inform the user when they are attempting to simulate something that is beyond the capabilities of the tool.

The solid angle calculation is limited by the fact that it only takes into account the amount of the source emission that is “seen” by the detector and does not account for the energy deposition of the photons in the detector media. It should be investigated if the simulation results can be improved by replacing the solid angle calculations with an energy dependent function that accounts for the photon path length through the detector media, such as the method described by M. I. Abbas[30].

Chapter 6. Future Work

For a setup such as a radiation portal monitor that measures cargo containers, it is known that the background radiation is suppressed by as much as 20% or more which may have an impact in the alarm threshold[31]. If this simulation tool is going to be used to predict the detector response for a portal monitor situation where background suppression is expected, then there should be a mechanism built in to allow the accurate simulation of this phenomenon. The simplest way to achieve this is to apply a uniform reduction across the background component of the simulation run over a portion of the trial that corresponds to the cargo container. This could be done by taking advantage of the multitude of data that already exists for gross counting radiation portal monitors that are deployed around the world. The occupancy data could be analyzed to produce a distribution function of all of the background suppression that is encountered in the real world. A more realistic approach would be to make spectroscopic measurements of the background suppression and derive an energy-dependent function since the suppression likely impact the lower energy photons more than the higher energy photons.

For this thesis, only a single representative vehicle was used to determine the impact of shielding by placing a source at various locations within a vehicle. It would be more useful to characterize a set of small, medium, and large vehicles to better understand the variation in shielding and streaming paths that might be encountered in the real world. This would give the simulation tool more representative data for vehicles expected to be encountered in the real world.

References

- [1] William J Perry Project. Nuclear Nightmare: Washington D.C. <http://www.wjperryproject.org/notes-from-the-brink/nuclear-nightmare-dc>. Online, accessed 05-15-2018.
- [2] U.S. Department of Homeland Security. Domestic Nuclear Detection Office. <https://www.dhs.gov/domestic-nuclear-detection-office>. Online, accessed 05-10-2018.
- [3] U.S. Department of Energy. NNSA and Nuclear Smuggling Detection and Deterrence. <https://www.energy.gov/nnsa/nnsa-and-nuclear-smuggling-detection-and-deterrence>. Online, accessed 05-10-2018.
- [4] Australian Safeguards and Non-Proliferation Office (ASNO). ASNO Annual Report 20162017. <http://dfat.gov.au/about-us/publications/corporate/annual-reports/asno-annual-report-2016-17/html/section-4/output-11-national-safeguards-system.html>. Online, accessed 06-18-2018.
- [5] Bubble Technology Industries Inc. Vehicle Mounted RID. <http://bubbletech.ca/wp-content/uploads/2014/02/FlexSpec-Image-Copy.jpg>. Online, accessed 06-18-2018.
- [6] Southern Scientific Ltd. Vehicle Portal Radiation Monitors. <https://www.southernscientific.co.uk/data/image/e/a/ea19ff47bf3a435f42cddfa6c55479ca.1474186437.jpg>. Online, accessed 06-18-2018.
- [7] John Rennie, Jim Toevs, and Mark Abhold. Preliminary test for the mobile detection system specification. Technical Report LA-CP-15-20040, Los Alamos National Laboratory, Los Alamos, NM, January 2015.

References

- [8] American National Standards Institute. *American National Standard Data Format for Radiation Detectors Used for Homeland Security*. Institute of Electrical and Electronics Engineers, New York, NY, 2013.
- [9] C. J. Sullivan and J. Lu. Automated photopeak detection and analysis in low resolution gamma-ray spectra for isotope identification. In *2013 IEEE Nuclear Science Symposium and Medical Imaging Conference (2013 NSS/MIC)*, pages 1–6, Oct 2013.
- [10] Zhang jian Qin, Chuan Chen, Jun song Luo, Xing hong Xie, Liang quan Ge, and Qi fan Wu. Peak center and area estimation in gamma-ray energy spectra using a mexican-hat wavelet. *Nuclear Instruments and Methods in Physics Research Section A: Accelerators, Spectrometers, Detectors and Associated Equipment*, 858:22 – 29, 2017.
- [11] M. Alamaniotis, A. Heifetz, A. C. Raptis, and L. H. Tsoukalas. Fuzzy-logic radioisotope identifier for gamma spectroscopy in source search. *IEEE Transactions on Nuclear Science*, 60(4):3014–3024, Aug 2013.
- [12] R. J. Estep, B. A. Sapp, and W. Russ. Improved isotopic identification for nai spectroscopic portal monitors using the material basis set (mbs) method. In *2007 IEEE Conference on Technologies for Homeland Security*, pages 168–173, May 2007.
- [13] M. J. Neuer, K. Ruhnau, A. Ruhnau, R. Lentering, G. Pausch, F. Platte, and J. Stein. Surveillance of nuclear threats using multiple, autonomous detection units. In *2008 IEEE Nuclear Science Symposium Conference Record*, pages 3324–3329, Oct 2008.
- [14] R. C. Runkle, T. M. Mercier, K. K. Anderson, and D. K. Carlson. Point source detection and characterization for vehicle radiation portal monitors. *IEEE Transactions on Nuclear Science*, 52(6):3020–3025, Dec 2005.
- [15] United States Nuclear Regulatory Commission. Special Nuclear Material. <https://www.nrc.gov/materials/sp-nucmaterials.html>. Online, accessed 08-08-2018.
- [16] S. Levinson, B. Sarusi, A. Osovizky, V. Pushkarsky, U. German, E. Marcus, Y. Cohen, and I. Belaish. Synthetic gamma-ray spectra for homeland security radionuclides analysis. In *2009 IEEE Nuclear Science Symposium Conference Record (NSS/MIC)*, pages 504–508, Oct 2009.

References

- [17] A.N. Berlizov and K. Mayer. Fast and accurate approach to γ -spectrum modelling: A validation study with a shielded/unshielded voluminous uranium sample. *Applied Radiation and Isotopes*, 68(9):1822 – 1831, 2010.
- [18] A.N. Berlizov and R. Dreher. Web-accessible γ -spectrum simulator with on-line monte carlo for voluminous and shielded γ -sources: First results of experimental validation. *Nuclear Instruments and Methods in Physics Research Section A: Accelerators, Spectrometers, Detectors and Associated Equipment*, 609(1):19 – 23, 2009.
- [19] R. Arlt, K. Baird, J. Blackadar, C. Blessenger, D. Blumenthal, P. Chiaro, K. Frame, E. Mark, M. Mayorov, M. Milovidov, and R. York. Semi-empirical approach for performance evaluation of radionuclide identifiers. In *2009 IEEE Nuclear Science Symposium Conference Record (NSS/MIC)*, pages 990–994, Oct 2009.
- [20] A. Flynn, D. Boardman, and M.I. Reinhard. The validation of synthetic spectra used in the performance evaluation of radionuclide identifiers. *Applied Radiation and Isotopes*, 77:145 – 152, 2013.
- [21] G.F. Knoll. *Radiation Detection and Measurement*. Wiley, 2000.
- [22] Radiation Solutions Inc. RS-700 Mobile Radiation Monitoring System Datasheet. <http://www.radiationsolutions.ca/wp-content/uploads/2016/06/RS700.pdf>. Online, accessed 08-09-2018.
- [23] Dann C. Ward. *Sandia National Laboratories Results for the 2010 Criticality Accident Dosimetry Exercise, at the CALIBAN Reactor, CEA Valduc France, September 2010*. 2011.
- [24] Jim Toevs, Richard Greco, John Rennie, Darrin Wallace, Chris Lovejoy, and Mark Abhold. Rapiscan tsa md134 test report. Technical Report LA-CP-13-01091, Los Alamos National Laboratory, Los Alamos, NM, September 2013.
- [25] Jim Toevs, Richard Greco, John Rennie, Darrin Wallace, Chris Lovejoy, and Mark Abhold. Rapiscan tsa-md134 survey mode and virtual survey test report addendum to the mobile detection system (mds) final report. Technical Report LA-CP-13-01153, Los Alamos National Laboratory, Los Alamos, NM, September 2013.
- [26] William H. Press, Saul A. Teukolsky, William T. Vetterling, and Brian P. Flannery. *Numerical Recipes 3rd Edition: The Art of Scientific Computing*. Cambridge University Press, 2007.

References

- [27] H. GOTOH and H. YAGI. Solid angle subtended by a rectangular slit. *Nuclear Instruments and Methods*, 96:485–486, 10 1971.
- [28] Wolfram Research, Inc. Cubic Spline. <http://mathworld.wolfram.com/CubicSpline.html>. Online, accessed 08-15-2018.
- [29] Doug Jenkins. CSpline2.xlsb. <http://interactiveds.com.au/software/CSpline2.zip>. Online, accessed 03-10-2018.
- [30] Mahmoud I. Abbas. A direct mathematical method to calculate the efficiencies of a parallelepiped detector for an arbitrarily positioned point source. *Radiation Physics and Chemistry*, 60(1):3 – 9, 2001.
- [31] P.E. Fehlau, C. Garcia Jr., R. A. Payne, and E. R. Shunk. Vehicle monitors for domestic perimeter safeguards. Technical Report LA-9633-MS, Los Alamos National Laboratory, Los Alamos, NM, January 1983.

Appendices

A. N42 example file

113

Appendix A

N42 example file

Below is an example .n42 file for an in-motion scan with four virtual detectors. An .n42 file has the same structure as an .xml file and the same terminology of nodes, attributes, data, etc. can be used when describing the .n42 file. This particular file was produced with a sample rate of 200 ms; each <Measurement> node contains 0.2 seconds worth of data for each of the four virtual detectors, plus GPS coordinates and dose rate information for each of the four virtual detectors. For each virtual detector, the spectrum is presented in 1024 channel data as well as a 256 channel compressed version. For this example, the spectra have been replaced by [1024 channel data] or [256 channel compressed data]. Two 0.2 second samples are included in this example (normally there would be much more than this to capture the full measurement time), and following the measurements are information about energy calibration and then RadAssist version and threshold information.

```

<?xml version="1.0" encoding="UTF-8"?>
<N42InstrumentData
xmlns="http://physics.nist.gov/Divisions/Div846/Gp4/ANSIN4242/2005/ANSIN4242"
xmlns:xsi="http://www.w3.org/2001/XMLSchema-instance"
xmlns:rsin42o="http://www.radiationsolutions.ca/2010/rsin42o"
xsi:schemaLocation="http://physics.nist.gov/Divisions/Div846/Gp4/ANSIN4242/2005/ANSIN4242
http://physics.nist.gov/Divisions/Div846/Gp4/ANSIN4242/2005/ANSIN4242.xsd">

<!-- Produced by RadAssist - Radiation Solution Inc. -->

<Measurement>
  <InstrumentInformation>
    <InstrumentType>Spectrometer</InstrumentType>
    <Manufacturer>Radiation Solutions Inc.</Manufacturer>
    <InstrumentModel>RS-705</InstrumentModel>
    <InstrumentID>6045</InstrumentID>
  </InstrumentInformation>
  <MeasuredItemInformation>
    <MeasurementLocation>
      <Coordinates>35.10700 -106.57726 1583.99459</Coordinates>
    </MeasurementLocation>
  </MeasuredItemInformation>
  <DetectorData>
    <StartTime>2018-06-06T14:13:14Z</StartTime>
    <SampleRealTime>PT0.19992S</SampleRealTime>
    <DetectorMeasurement Detector="VD1" DetectorType="Gamma">
      <SpectrumMeasurement>
        <SpectrumAvailable>true</SpectrumAvailable>
        <Spectrum CalibrationIDs="LinEnCal">
          <RealTime>PT0.20002S</RealTime>
          <LiveTime>PT0.19992S</LiveTime>
          <SourceType>Item</SourceType>
          <ChannelData Compression="CountedZeroes">
            [1024 channel data]
          </ChannelData>
        </Spectrum>
        <Spectrum CalibrationIDs="CmpEnCal">
          <RealTime>PT0.20002S</RealTime>
          <LiveTime>PT0.19992S</LiveTime>
          <SourceType>Item</SourceType>
          <ChannelData Compression="CountedZeroes">
            [256 channel compressed data]
          </ChannelData>
        </Spectrum>
      </SpectrumMeasurement>
    </DetectorMeasurement>
    <DetectorMeasurement Detector="VD2" DetectorType="Gamma">
      <SpectrumMeasurement>
        <SpectrumAvailable>true</SpectrumAvailable>
        <Spectrum CalibrationIDs="LinEnCal">
          <RealTime>PT0.20002S</RealTime>
          <LiveTime>PT0.20002S</LiveTime>
          <SourceType>Item</SourceType>
          <ChannelData Compression="CountedZeroes">
            [1024 channel data]
          </ChannelData>
        </Spectrum>
      </SpectrumMeasurement>
    </DetectorMeasurement>
  </DetectorData>
</Measurement>

```

```
</Spectrum>
<Spectrum CalibrationIDs="CmpEnCal">
  <RealTime>PT0.20002S</RealTime>
  <LiveTime>PT0.20002S</LiveTime>
  <SourceType>Item</SourceType>
  <ChannelData Compression="CountedZeroes">
    [256 channel compressed data]
  </ChannelData>
</Spectrum>
</SpectrumMeasurement>
</DetectorMeasurement>
<DetectorMeasurement Detector="VD3" DetectorType="Gamma">
  <SpectrumMeasurement>
    <SpectrumAvailable>true</SpectrumAvailable>
    <Spectrum CalibrationIDs="LinEnCal">
      <RealTime>PT0.20002S</RealTime>
      <LiveTime>PT0.19972S</LiveTime>
      <SourceType>Item</SourceType>
      <ChannelData Compression="CountedZeroes">
        [1024 channel data]
      </ChannelData>
    </Spectrum>
    <Spectrum CalibrationIDs="CmpEnCal">
      <RealTime>PT0.20002S</RealTime>
      <LiveTime>PT0.19972S</LiveTime>
      <SourceType>Item</SourceType>
      <ChannelData Compression="CountedZeroes">
        [256 channel compressed data]
      </ChannelData>
    </Spectrum>
  </SpectrumMeasurement>
</DetectorMeasurement>
<DetectorMeasurement Detector="VD4" DetectorType="Gamma">
  <SpectrumMeasurement>
    <SpectrumAvailable>true</SpectrumAvailable>
    <Spectrum CalibrationIDs="LinEnCal">
      <RealTime>PT0.20002S</RealTime>
      <LiveTime>PT0.19982S</LiveTime>
      <SourceType>Item</SourceType>
      <ChannelData Compression="CountedZeroes">
        [1024 channel data]
      </ChannelData>
    </Spectrum>
    <Spectrum CalibrationIDs="CmpEnCal">
      <RealTime>PT0.20002S</RealTime>
      <LiveTime>PT0.19982S</LiveTime>
      <SourceType>Item</SourceType>
      <ChannelData Compression="CountedZeroes">
        [256 channel compressed data]
      </ChannelData>
    </Spectrum>
  </SpectrumMeasurement>
</DetectorMeasurement>
</DetectorData>
<CountDoseData Detector="VD1" DetectorType="Gamma">
  <StartTime>2018-06-06T14:13:14Z</StartTime>
  <SampleRealTime>PT0.20002S</SampleRealTime>
```

```
<AbsorbedDoseRate Units="uGy">0.04873</AbsorbedDoseRate>
</CountDoseData>
<CountDoseData Detector="VD2" DetectorType="Gamma">
  <StartTime>2018-06-06T14:13:14Z</StartTime>
  <SampleRealTime>PT0.20002S</SampleRealTime>
  <AbsorbedDoseRate Units="uGy">0.04510</AbsorbedDoseRate>
</CountDoseData>
<CountDoseData Detector="VD3" DetectorType="Gamma">
  <StartTime>2018-06-06T14:13:14Z</StartTime>
  <SampleRealTime>PT0.20002S</SampleRealTime>
  <AbsorbedDoseRate Units="uGy">0.04782</AbsorbedDoseRate>
</CountDoseData>
<CountDoseData Detector="VD4" DetectorType="Gamma">
  <StartTime>2018-06-06T14:13:14Z</StartTime>
  <SampleRealTime>PT0.20002S</SampleRealTime>
  <AbsorbedDoseRate Units="uGy">0.05123</AbsorbedDoseRate>
</CountDoseData>
<rsin42o:SampleEx>
  <rsin42o:ADC1>0.000000</rsin42o:ADC1>
  <rsin42o:ADC2>0.001221</rsin42o:ADC2>
</rsin42o:SampleEx>
</Measurement>
<Measurement>
  <InstrumentInformation>
    <InstrumentType>Spectrometer</InstrumentType>
    <Manufacturer>Radiation Solutions Inc.</Manufacturer>
    <InstrumentModel>RS-705</InstrumentModel>
    <InstrumentID>6045</InstrumentID>
  </InstrumentInformation>
  <MeasuredItemInformation>
    <MeasurementLocation>
      <Coordinates>35.10700 -106.57726 1583.99459</Coordinates>
    </MeasurementLocation>
  </MeasuredItemInformation>
  <DetectorData>
    <StartTime>2018-06-06T14:13:14Z</StartTime>
    <SampleRealTime>PT0.19982S</SampleRealTime>
    <DetectorMeasurement Detector="VD1" DetectorType="Gamma">
      <SpectrumMeasurement>
        <SpectrumAvailable>true</SpectrumAvailable>
        <Spectrum CalibrationIDs="LinEnCal">
          <RealTime>PT0.20002S</RealTime>
          <LiveTime>PT0.19982S</LiveTime>
          <SourceType>Item</SourceType>
          <ChannelData Compression="CountedZeroes">
            [1024 channel data]
          </ChannelData>
        </Spectrum>
        <Spectrum CalibrationIDs="CmpEnCal">
          <RealTime>PT0.20002S</RealTime>
          <LiveTime>PT0.19982S</LiveTime>
          <SourceType>Item</SourceType>
          <ChannelData Compression="CountedZeroes">
            [256 channel compressed data]
          </ChannelData>
        </Spectrum>
      </DetectorMeasurement>
    </DetectorData>
  </Measurement>
</Measurement>
```

```
</DetectorMeasurement>
<DetectorMeasurement Detector="VD2" DetectorType="Gamma">
  <SpectrumMeasurement>
    <SpectrumAvailable>true</SpectrumAvailable>
    <Spectrum CalibrationIDs="LinEnCal">
      <RealTime>PT0.20002S</RealTime>
      <LiveTime>PT0.19982S</LiveTime>
      <SourceType>Item</SourceType>
      <ChannelData Compression="CountedZeroes">
        [1024 channel data]
      </ChannelData>
    </Spectrum>
    <Spectrum CalibrationIDs="CmpEnCal">
      <RealTime>PT0.20002S</RealTime>
      <LiveTime>PT0.19982S</LiveTime>
      <SourceType>Item</SourceType>
      <ChannelData Compression="CountedZeroes">
        [256 channel compressed data]
      </ChannelData>
    </Spectrum>
  </SpectrumMeasurement>
</DetectorMeasurement>
<DetectorMeasurement Detector="VD3" DetectorType="Gamma">
  <SpectrumMeasurement>
    <SpectrumAvailable>true</SpectrumAvailable>
    <Spectrum CalibrationIDs="LinEnCal">
      <RealTime>PT0.20002S</RealTime>
      <LiveTime>PT0.20002S</LiveTime>
      <SourceType>Item</SourceType>
      <ChannelData Compression="CountedZeroes">
        [1024 channel data]
      </ChannelData>
    </Spectrum>
    <Spectrum CalibrationIDs="CmpEnCal">
      <RealTime>PT0.20002S</RealTime>
      <LiveTime>PT0.20002S</LiveTime>
      <SourceType>Item</SourceType>
      <ChannelData Compression="CountedZeroes">
        [256 channel compressed data]
      </ChannelData>
    </Spectrum>
  </SpectrumMeasurement>
</DetectorMeasurement>
<DetectorMeasurement Detector="VD4" DetectorType="Gamma">
  <SpectrumMeasurement>
    <SpectrumAvailable>true</SpectrumAvailable>
    <Spectrum CalibrationIDs="LinEnCal">
      <RealTime>PT0.20002S</RealTime>
      <LiveTime>PT0.19992S</LiveTime>
      <SourceType>Item</SourceType>
      <ChannelData Compression="CountedZeroes">
        [1024 channel data]
      </ChannelData>
    </Spectrum>
    <Spectrum CalibrationIDs="CmpEnCal">
      <RealTime>PT0.20002S</RealTime>
      <LiveTime>PT0.19992S</LiveTime>
```

```

        <SourceType>Item</SourceType>
        <ChannelData Compression="CountedZeroes">
            [256 channel compressed data]
        </ChannelData>
    </Spectrum>
</SpectrumMeasurement>
</DetectorMeasurement>
</DetectorData>
<CountDoseData Detector="VD1" DetectorType="Gamma">
    <StartTime>2018-06-06T14:13:14Z</StartTime>
    <SampleRealTime>PT0.20002S</SampleRealTime>
    <AbsorbedDoseRate Units="uGy">0.04819</AbsorbedDoseRate>
</CountDoseData>
<CountDoseData Detector="VD2" DetectorType="Gamma">
    <StartTime>2018-06-06T14:13:14Z</StartTime>
    <SampleRealTime>PT0.20002S</SampleRealTime>
    <AbsorbedDoseRate Units="uGy">0.05613</AbsorbedDoseRate>
</CountDoseData>
<CountDoseData Detector="VD3" DetectorType="Gamma">
    <StartTime>2018-06-06T14:13:14Z</StartTime>
    <SampleRealTime>PT0.20002S</SampleRealTime>
    <AbsorbedDoseRate Units="uGy">0.04702</AbsorbedDoseRate>
</CountDoseData>
<CountDoseData Detector="VD4" DetectorType="Gamma">
    <StartTime>2018-06-06T14:13:14Z</StartTime>
    <SampleRealTime>PT0.20002S</SampleRealTime>
    <AbsorbedDoseRate Units="uGy">0.04732</AbsorbedDoseRate>
</CountDoseData>
<rsin42o:SampleEx>
    <rsin42o:ADC1>0.000000</rsin42o:ADC1>
    <rsin42o:ADC2>0.001221</rsin42o:ADC2>
</rsin42o:SampleEx>
</Measurement>
<Calibration Type="Energy" EnergyUnits="keV" ID="LinEnCal">
    <Equation Model="Polynomial">
        <Coefficients>0 3</Coefficients>
    </Equation>
</Calibration>
<Calibration Type="Energy" EnergyUnits="keV" ID="CmpEnCal">
    <Equation Model="Polynomial">
        <Coefficients>0 0 0.046136</Coefficients>
    </Equation>
</Calibration>
<rsin42o:RsiMeasurement>
    <rsin42o:AppName>RadAssist</rsin42o:AppName>
    <rsin42o:AppVers>5.7.1.0</rsin42o:AppVers>
    <rsin42o:TemplLibVers>12.80.0.0</rsin42o:TemplLibVers>
    <rsin42o:SpAnDllVers>4.3.0.0</rsin42o:SpAnDllVers>
    <rsin42o:DeviceName>LANL</rsin42o:DeviceName>
    <rsin42o:DocGenTime>2018-06-06T08:31:17-06:00</rsin42o:DocGenTime>
    <rsin42o:PseudoStartTime>2018-06-06T08:29:55</rsin42o:PseudoStartTime>
    <rsin42o:SpanTemplate>
        <rsin42o:IsoTemplate Name="Uranium" Used="1"
Threshold=["value"]>1</rsin42o:IsoTemplate>
        <rsin42o:IsoTemplate Name="Plutonium" Used="1"
Threshold=["value"]>2</rsin42o:IsoTemplate>
        <rsin42o:IsoTemplate Name="Americium" Used="1"

```

```
Threshold="[value]">3</rsin42o:IsoTemplate>
  <rsin42o:IsoTemplate Name="Barium" Used="1"
Threshold="[value]">4</rsin42o:IsoTemplate>
  <rsin42o:IsoTemplate Name="Cobalt" Used="1"
Threshold="[value]">5</rsin42o:IsoTemplate>
  <rsin42o:IsoTemplate Name="Cobalt" Used="1"
Threshold="[value]">6</rsin42o:IsoTemplate>
  <rsin42o:IsoTemplate Name="Cesium" Used="1"
Threshold="[value]">7</rsin42o:IsoTemplate>
  <rsin42o:IsoTemplate Name="Sodium" Used="1"
Threshold="[value]">8</rsin42o:IsoTemplate>
  <rsin42o:IsoTemplate Name="Neptunium" Used="1"
Threshold="[value]">9</rsin42o:IsoTemplate>
  <rsin42o:IsoTemplate Name="Radium" Used="1"
Threshold="[value]">10</rsin42o:IsoTemplate>
  <rsin42o:IsoTemplate Name="Thorium" Used="1"
Threshold="[value]">11</rsin42o:IsoTemplate>
  <rsin42o:IsoTemplate Name="Technetium" Used="1"
Threshold="[value]">12</rsin42o:IsoTemplate>
  <rsin42o:IsoTemplate Name="Gallium" Used="1"
Threshold="[value]">13</rsin42o:IsoTemplate>
  <rsin42o:IsoTemplate Name="Iodine" Used="1"
Threshold="[value]">14</rsin42o:IsoTemplate>
  <rsin42o:IsoTemplate Name="Thallium" Used="1"
Threshold="[value]">15</rsin42o:IsoTemplate>
  <rsin42o:IsoTemplate Name="Thorium" Used="1"
Threshold="[value]">16</rsin42o:IsoTemplate>
  <rsin42o:IsoTemplate Name="Potassium" Used="1"
Threshold="[value]">17</rsin42o:IsoTemplate>
  <rsin42o:IsoTemplate Name="DU" Used="1"
Threshold="[value]">18</rsin42o:IsoTemplate>
  <rsin42o:IsoTemplate Name="Ir" Used="1"
Threshold="[value]">19</rsin42o:IsoTemplate>
  <rsin42o:IsoTemplate Name="Cr" Used="1"
Threshold="[value]">20</rsin42o:IsoTemplate>
  <rsin42o:IsoTemplate Name="In" Used="1"
Threshold="[value]">21</rsin42o:IsoTemplate>
  <rsin42o:IsoTemplate Name="Sm" Used="1"
Threshold="[value]">22</rsin42o:IsoTemplate>
  <rsin42o:IsoTemplate Name="Mo" Used="1"
Threshold="[value]">23</rsin42o:IsoTemplate>
  <rsin42o:IsoTemplate Name="Ge" Used="1"
Threshold="[value]">24</rsin42o:IsoTemplate>
  <rsin42o:IsoTemplate Name="Cosm" Used="1"
Threshold="[value]">25</rsin42o:IsoTemplate>
  <rsin42o:IsoTemplate Name="Eu" Used="1"
Threshold="[value]">26</rsin42o:IsoTemplate>
  <rsin42o:IsoTemplate Name="F" Used="1"
Threshold="[value]">27</rsin42o:IsoTemplate>
  </rsin42o:SpanTemplate>
</rsin42o:RsiMeasurement>
</N42InstrumentData>
```